MARINE ICING SENSOR ARRAY FOR MEASURING ICE THICKNESS

By

©Abdulrazak H.Elzaidi

A thesis submitted to the School of Graduate Studies in partial fulfilment of the requirements for the degree of Doctor of Philosophy

Electrical and Computer Engineering Department

Faculty of Engineering and Applied Science

Memorial University of Newfoundland

St. John's, NL.

12 Nov 2021

Abstract

Marine Icing is the process of ice accumulation on ships and other offshore structures in cold regions that can create serious working conditions besides the adverse effects to the offshore operations efficiency. Monitoring of icing conditions together with a number of de-icing strategies is therefore important in decreasing the safety hazards and increase the working effectiveness. Detection of the ice accretion rate on the offshore structures is a challenge due to the harsh environment and the multiphase property of the ice.

This thesis is focused on developing a low cost array sensor for the ice accretion detection applicable to the harsh marine environments. We utilized a stray-capacitance technique that encodes a layered multiphase icing accretion uniquely. Capacitive sensors are popular in diverse industrial settings due to their relative simplicity, robustness and low cost. The sensor transducers are compatible with the printed circuit board technology which made this research time effective.

The thesis is based on three distinct publications, two journal papers (IEEE, MDPI) and one peer-reviewed conference paper (IEEE), each in a separate chapter. All publications include a theoretical background, simulations, and experimental validation. The underlying novel approach that is more or less shared in all applications is the use of linearly independent sensor array for unique multiphase ice detection. The first two papers utilize a different inter-electrode spacing array but a different signal conditioning algorithm. The third paper then uses an array of constant spacing but different dielectric layer height.

As stated above, the main objective of this work is to measure the multiphase icing accretion which consists of water above ice, the real situation which has not been addressed to date. A number of different techniques have been developed over the last two decades mainly as a response to the rapidly expanding offshore oil&gas in northern regions, offshore wind power generation, or shipping across or fishing in arctic waters. This thesis outlines three methods that can be directly

applied to these industries.

Acknowledgements

This thesis is dedicated to Almighty ALLAH for giving me the blessings and the opportunity to complete this thesis. Further, I would like to dedicate this work to the souls of my mom and my dad. This work won't be possible without support, patience and love of my wife and three children, and all my extended family members who this work is also dedicated to.

I would like to express my deep gratitude to my supervisor Dr. Vlastimil Masek for his continued support, encouragement, and patience with me throughout my Ph.D. journey. I can't thank him enough, it has been an honour working alongside with him. I also extend my gratitude to my supervisory committee members Dr.Stephen Bruneau and Dr.Tariq Iqbal for their motivation, valuable suggestions and financial support during my study at the Memorial University of Newfoundland.

Last but not least, I would like to express utmost gratitude to the Libyan Ministry of High Education for providing me with the necessary financial support to complete my Ph.D. study at Memorial University. Many thanks also go to the Machine Shop Supervisor David Snook, Electronic Design and Development Supervisor Bill Maloney, and to the electrical technicians Greg O'Leary for helping me in getting the essential components and laboratory supplies for my experiments. I also would like to thank my friends and colleagues in LAB1037 for their great ideas and suggestions.

Co-authorship Statement and A List of Publications

Abdulrazak Elzaidi is the main author of all three papers. Dr.Vlastimil Masek, Dr.Stephen Bruneau, and Dr. Yuri Muzychka are co-authors who provided valuable guidance and financial support with the publication. The peer-reviewed manuscripts included in this thesis are listed as follows:

1. A. Elzaidi, V. Masek and Y. Muzychka, "Phase Discrimination in Marine Icing Using a Coplanar Capacitive Array," in IEEE Sensors Journal. doi: 10.1109/JSEN.2019.2935616

2. Elzaidi, A.; Masek, V.; Bruneau, S., "Water and Ice Detection in Marine Icing by Capacitive Sensor Array and the Artificial Neural Network Model", In Proceedings of the 2019 IEEE 10th Annual Information Technology, Electronics and Mobile Communication Conference (IEMCON), Vancouver, BC, Canada, 17–19 October 2019.

3. Elzaidi, A. Masek, V. Bruneau, "Water and Ice Detection in Marine Icing by Capacitive Sensor Array and the Artificial Neural Network Model with different Activation Functions", presented at The 28th Annual Newfoundland Electrical and Computer Engineering Conference (IEEE NECEC 2019) was held Nov. 19, 2019 in St. John's, Newfoundland and Labrador, Canada.

4. Elzaidi, A., Masek, V. and Bruneau, S., "Marine Icing Sensor with Phase Discrimination". MDPI Sensors, 2021, 21(2), p.612.

Abdulrazak Elzaidi

November 2021

Contents

List of Tables

List of Figures

List of Abbreviations and Symbols

ANN Artificial Neural Network

CNC Computer Numerical Control

DAQ Data Acquisition Card

EM Electro Magnetic

FDC Frequency-to-Digital Converter

FEM Finite Element Method

FN False Negative

FP False Positive

IR Infra Red

LPF Low pass filter

LSQ Least Square Method

NOR Normalize

PCB Printed Circuit Board

PCI Programing Counter/Timer

PET Polyethylene Terephthalate

TTL Transistor-Transistor Logic

TN True Negative

TP True Positive

$\boldsymbol{E}$ Electric Field

$\boldsymbol{Q}$ Charge[coulomb]

$\boldsymbol{\sigma}$ Charge Density

$\boldsymbol{\varepsilon}$ Relative Permittivity

$\boldsymbol{\varepsilon}_0$ Relative Permittivity of the Air

$\boldsymbol{h}$ Height[mm]

$\boldsymbol{C}$ Mmeasured Capacitance[pF]

$\hat{\boldsymbol{C}}$ Normalized Capacitance[pF]

$\bar{\boldsymbol{C}}$ Nominal Capacitance[pF]

$\boldsymbol{k_1}, \boldsymbol{k_2}$ constant coefficients

$\boldsymbol{Bi}$ Input Biases

$\boldsymbol{Bo}$ Output Biases

$\boldsymbol{Wi}$ Input Weights

$\boldsymbol{Wo}$ Output Weights

$\boldsymbol{pi}$ Probability of the Class

Chapter 1

Introduction and Overview

1.1 Introduction

Marine icing is a natural and complex phenomena due to its non-homogenous composition. Marine icing is also an unwanted phenomena because it poses a severe safety hazard for which many polar expeditions of the past either failed or had to retreat to warmer latitudes. However, due to natural resources depletion and the fierce global competition, many projects in the harsh Arctic region are currently being operated or developed as a result. Marine icing is one of the main problems the offshore industry faces in these cold climate regions.

Our task is to provide an accurate icing monitoring tool that will inform the operators about the accretion rate and to enable them to make an informed decision about the icing management. In this chapter, we first describe the effects of marine icing and then review all existing methods known to us that have been developed or some of them commercialized for the ice detection. Many of these sensors were developed for the terestrial markets and were never tested in the marine conditions, others were designed for the marine icing applicatons but without consideration for the multiphase composition. While onshore shown some success in ice accumulation detection. This is the gap we try to close by proposing our unique sensor array system.

1.2 Marine Icing

Marine icing is created in low air temperatures when water spray brakes off from ocean waves or upon impact with offshore structures such as ship bows, oil & gas platforms or wind power towers. Figure 1.1 shows the marine icing process [5]. The marine ice accretion is created when the airborne supercooled water spray droplets pound on mostly steel structures and freeze there before the droplets have time to run off from the stucture. This happens under particular environmen-

tal conditions that involve low temperature (ambient & structure), water salinity, water flux, water droplet size, relative humidity, wind speed and wind direction [1], [2]. There are two methods used to measure marine icing: the direct method and the indirect method. Monitoring marine icing in the indirect manner is complex as it relies on measurements of atmospheric conditions and weather pattern historical data. Such systems are used for example in icing forecasting for electric power distribution or wind power generation [3], [4].

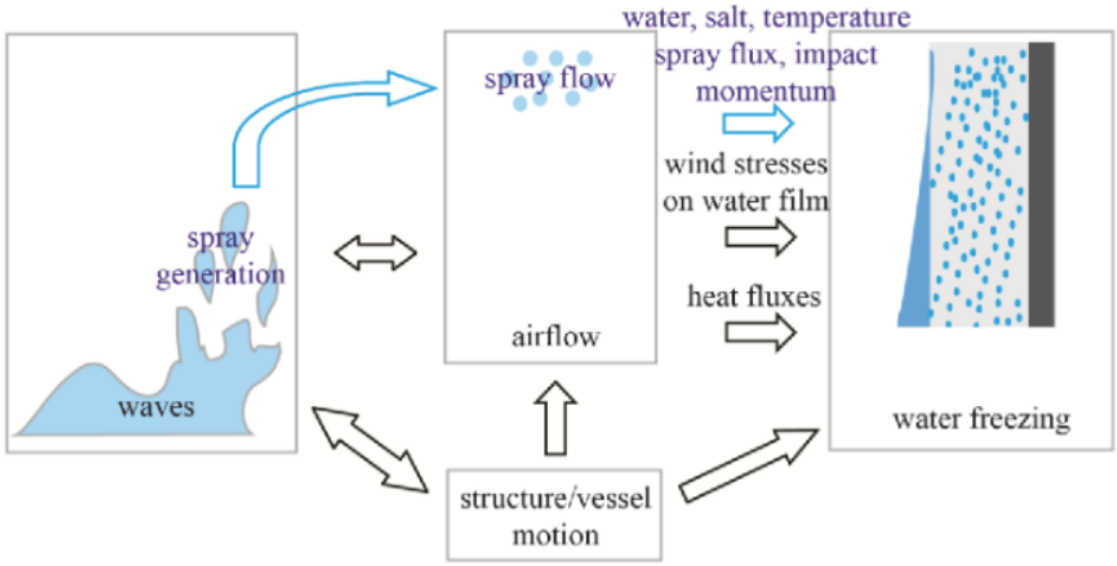

Figure 1.1: Marine Icing Process [5]

Marine Icing differs from the other icing types like the Atmospheric Icing or precipitation Icing. Atmospheric ice also called as clouding ice occurs when atmospheric moisture results in ice or snow crystals being accumulated on a supercooled surface such as power distrubution cables, communication towers or air plane wings. Figure 1.2 shows such conditions.

Precipitation icing is on the other hand created by a saturated freezing drizzle or freezing rain being accummulated on a supercooled structure [6]. This happens when freezing rain or wet snow

Figure 1.2: Examples of Icing conditions

falls on a surface with a temperature below 0 C [3].

Marine icing process is similar to the Precipitation icing in the sense that it creates a layered media with the liquid phase on top, but differs in water salinity levels naturally. It has been a surprising discovery that many monitoring systems on the market today do not consider the two layer composition at all. The majority of the products we reviewed consider a homogenous single-phase ice layer. Only the resonance or weight based systems can measure the total accretion height but there is no data to further refine the information on how much ice and how much water there is. Our proposed system aims at providing this information about the ice and the water layer simultaneously.

1.3 Common principles in Ice detection

The measurement of marine icing is necessary for offshore operations, since ice can create unsafe conditions for the service personnel. Vessels operating in the Arctic waters during winter are likely to experience the marine icing on exposed areas such as decks, stairs, handrails or parts of the hull. Apart from posing a danger to those on board, marine icing can seriously affect the vessel's manoeuvrability and speed. Ice loads are one of the most influential factors in ship dynamics and maneuvering ability because the center of gravity is moved up. Some smaller transport vessels can

even overturn due to ice load that is unevenly distributed around the vessel.

Marine icing can also represent a serious challenge to offshore wind farms, not just in terms of a decreased performance by alternation of the airfoil parameters. The more severe challenges relate to the dynamic rotor unbalance which often results in very costly repairs or replacement. [3].

A number of R&D or commercial concepts is listed below. We analyze them in terms of their abilities to detect the multiphase phenomena present in Marine or Precipitation icing conditions.

1.3.1 Ultrasonic Method

This sensor considers transmitter and receiver [7]. A transmitter is a source of an ultrasonic wave generator and receiver that detects changes in the resonant frequency and through time intervals can detect ice thickness in one place. The water phase adversely affects the measurement as the acoustic impedance between ice and air differs significantly when the water layer is present.

1.3.2 Infrared Beam

The main idea in this method relies on measuring the reflection of an infrared beam from the ice surface [8]. This method is not designed to consider the presence of the water layer on the ice surface as well.

1.3.3 Strain / Stress Principles

This type of ice measurements is based on measuring the weight of a sample structure using a load cell [9]. This method can potentially perform well in an offshore application however the dynamic nature of a floating platform would advesely affect the measurement. In addition, we can only know the cummulative effect of ice and water, not each separately.

1.3.4 Capacitance Method

Electrical capacitance and ice accretion are in a proportional relationship because the ice dielectric properties are significantly different from the air dielectric properties [10], [11]. We adopted this principle but unlike the cited methods, we created a linearly independent array to encode the ice dielectric and the water dielectric separately in a unique way that can be decoded unambiguously.

1.4 Survey of Commercial Products

1.4.1 Labkotec LID-3300IP Ice Detector

The theory of operation the Labkotec LID-3300IP ice sensor is based on ultrasonic vibrations of a wire wrapped around a flat oval aluminum surface as depicted in Figure 1.3. As the ice forms on the wire, the amplitude of the wire's ultrasonic vibrations is reduced [7]. The critical level of icing is detected when the amplitude of the ultrasound signal falls below a pre set threshold. After this phase a reconditioning phase starts in which the ice is thawed by the heating applied. When the signal hits a stop limit, and the heating reaches a predetermined temperature, the heating is then shut off. The user can set the cut off temperature, ice warning amplitude, and heating power. The sensor's detector detects ice most effectively when the wind direction is perpendicular to the sensor's surface. No testing in marine icing conditions were reported to this day.

1.4.2 Combitech Ice Monitor

The Combitech's ice monitor sensor was developed for monitoring the icing conditions on power lines [9]. It is one of the most common icing sensor systems on the market since it simply measures the mass of ice that has formed on a surface by the force of gravity. The sensor has a very low power consumption and is designed as a freely rotating steel cylinder pivoting on a rod mounted on load cells as shown in Figure 1.4. This system cannot be used in the marine environment due to the

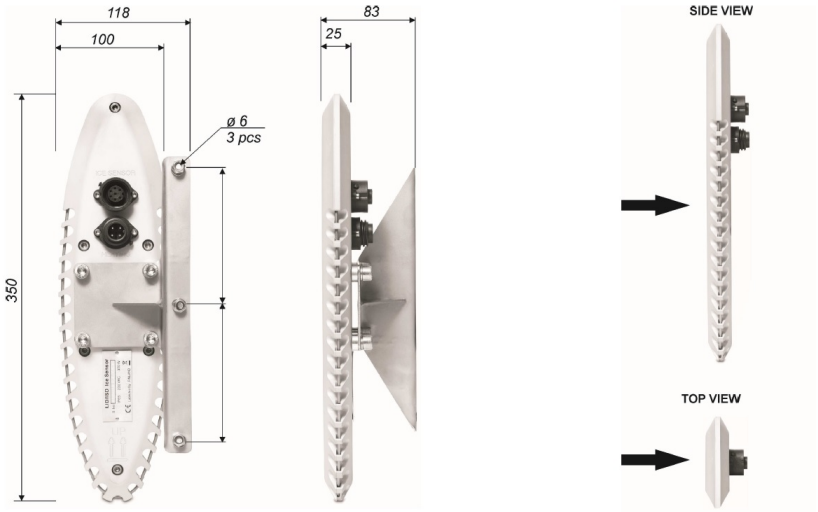

Figure 1.3: Labkotec LID-3300IP Ice Detector

dynamic forces present on a floating platform and the omnidirectional nature of the water droplets flow.

Figure 1.4: Combitech Ice Monitor

1.4.3 HoloOptics T40 Series

Figure 1.5 shows the HoloOptics T40 series ice detector built from four curved arms. The arms carry infrared transmitters, receivers and a heating system inside the ice probe detector. The ice thickness is measured by the amount of light that reflects back to the probe. The ice absorbs some of the infrared light that is reflected by a reflector [8]. The ice accumulates gradually on the surface of the probe, and the reflected infrared signal will decrease until it reaches the ice thickness set point. This system is designed to monitor a single phase ice accretion and therefore the water 'glaze' layer present in marine icing would negatively impact the accuracy of the IR based system.

Figure 1.5: HoloOptics T40-series icing rate sensors

1.4.4 The Ice Meister

The Ice Meister sensor is designed to detect ice in aviation and in a wide variety of industrial applications as shown in Figure 1.6. The sensor monitors the optical properties of ice that comes into contact with the probe's acrylic surfaces [12]. The output signal obtained by the sensor indicates the existence of the ice and that is about it. The system is therefore similar to a dew point temperature

measurement where only the presence of the other phase is monitored, not its properties like the accretion rate.

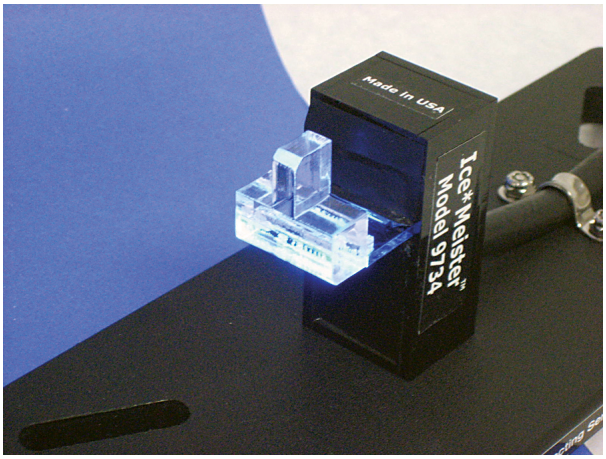

Figure 1.6: The Ice Meister

1.4.5 The EAG 200

The EAG 200 icing sensor shown in Figure 1.7 is used to detect ice loads by measuring the weight of the ice accretion on a PVC pole. The diameter of the PVC pole is 32 mm, and the length is from 0.5 m to 1 m. The EAG 200 employs an electromechanical scale operating in the range from 0 to 10kg with an accuracy up to ± 50 g [3]. Due to the structural vibrations and intense wind gusts on a marine platform this sensor cannot be used.

Figure 1.7: The EAG 200

1.4.6 The Goodrich ice detector

In the aviation industry, the Goodrich ice detector sensor type 0871LH1 is commonly used. Figure 1.8 shows the detector. The sensor detects icing accumulation on probes by measuring the frequency changes as the mass of ice on the surface increases over time [13]. When the probe's resonance frequency approaches or exceeds the preset level, the deicing mode is triggered for a specified period of time to melt the icing on the probes. One of the sensor's drawbacks is that it can't tell the difference between ice and water. The Goodrich ice detector can only reliably measure very thin ice, according to tests carried out by the company.

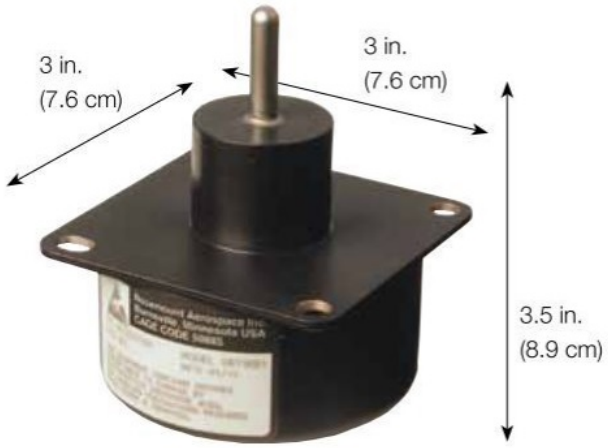

Figure 1.8: The Goodrich ice detector

1.4.7 Ice detection method using cylindrical probes

Kwadwo [14] used two aluminum cylinders to make a capacitive sensor probe and conducted several experiments. The presence of ice disrupts the fringing electric field between two electrically charged cylindrical probes, raising the probe mutual capacitance and reducing the resistance. The super cooled water droplets are travelling toward the probes that are positioned vertically to electric field

lines as seen in Figure 1.9. The ice accretion on the probes is then determined by the capacitance measurement as well as the resistance measurement. The resistance is largely correlated with the conductivity of the water phase. In marine environments the water salinity makes this phase many times more conductive than the athmospheric water precipitation making this system unsuitable for such applications.

Figure 1.9: Ice detection method using cylindrical probes

1.5 Commercial Systems Summary & Motivation & Problem Statement

An effective icing accretion monitoring system is needed to manage and reduce potential icing hazards. The above presented commercial systems are all specified for use in terestrial applications (athmospheric/precipitation icing) or in avionics. In the ideal scenario, we would source each such system and subject it to the marine conditions offshore. This research work did not have such capacity and mandate. The goal was, based on the theoretical and already reported shortcomings of the current systems, to propose a simple system that operates under the two-phase icing conditions, ice and water. We have developed three methods presented in this thesis. Each method was subjected to in-lab validation with promissing results.

The underlying principle of all three methods is based on fringing field capacitive sensor array. Capacitive sensors are found in many applications in almost all industrial fields. Some are modulated by dimensional changes of the electrodes or the gap between them, some utilize a change in electric permittivity of the dielectric layer between or above the electrodes.

Our problem is complicated by the presence of two dielectric materials above the electrodes, the ice phase and the water phase. We approched this problem by applying an array of capacitive sensing elements each of varying parameters to modulate the correlation with the multiphase dielectric uniquely. Only then it is possible to discriminate between the individual phases.

1.6 Thesis Organization

Chapter 1 presents the background information, the literature survey and the problem statement.

Chapter 2 covers the fundamental physics of capacitive sensors with fringing field dielectrics in particular.

Chapter 3 is paper published in IEEE Sensors Journal (Volume: 19, Issue: 23, Dec.1, 1 2019), DOI: 10.1109/JSEN.2019.2935616

Chapter 4 is paper published in 2019 IEEE 10th Annual Information Technology, Electronics and Mobile Communication Conference (IEMCON), DOI: 10.1109/IEMCON.2019.8936232

Chapter 5 is paper published in MDPI Sensors — An Open Access Journal from MDPI Sensors, 17 January 2021, Communication Article, Remote Sensing, Sensors 2021, 21(2), 612; https://doi.org/10.3390/s21020612

Chapter 6 summarizes the research contribution and speculates about the direction of the future work.

Appendices include the datasheets for the key electronic components and the local conference paper (IEEE NECEC 2019).

Chapter 2

Capacitive Sensors

2.1 Introduction

Capacitive sensors are used in many industrial applications, such as proximity sensors in plants to detect specific products. They have been developed to replace manual or mechanical monitoring systems in various applications. The capacitive sensing method can be used for sensing water, ice, moisture, or speed and acceleration. Capacitive sensors can also detect chemical gas composition and send alerts in the presence of dangerous gases (e.g. carbon monoxide sensors). In the field of ice monitoring and detection a number of commercial systems have been developed on the basis of capacitive sensors as listed in the previous chapter. In summary, capacitive sensors

1. are easy to assemble and modify, and typically less costly,
2. do not include any mechanical parts that rotate, vibrate or move which minimize the performance or even damage the system after some wear and tear,
3. typically use very low power electronics in its overall design,
4. are robust even in harsh environments and require minimal maintenance or recalibration,
5. work well in low or high temperatures as long as the thermal compensation is well addressed,
6. are easy to install and deploy in the field like on offshore vessels and rigs.

There are some shortcomings of capacitive sensors which are listed below.

1. The capacitive sensors are sensitive to alterations in environmental conditions for instance humidity, temperature, etc.
2. The output impedance relies on the frequency.
3. The capacitance measurement might get changed by dust matter.

The capacitive sensors have two electrodes, the exciting electrode and the sensing electrode with a dielectric in between them or above them as is the case in this study. The following section discusses the capacitance modulation and measurement and illustrates the fundamental physics and concepts behind dielectrics and the capacitance.

2.2 Dielectrics Materials and Capacitance

Capacitors are electrical passive components that can hold electric charges, which results in a potential difference between the positive and negative electrodes that make up a capacitor. The most basic capacitor is made up of two non-contact parallel electrodes of known metal materials separated by an insulator, the dielectric media like air, oil, gas, etc. Capacitors are available on the market in a wide range of dimensions and formats, depending on voltage rating and the application for which they are made; however, the basic internal configuration remains the same. The basic structure of a capacitor sensor is shown in Figure 2.1, which consists of two conductors holding equal but opposite charges, and the electric field interaction often begins on the positive electrode and ends on the negative electrode [14].

The charge state and the uncharged state are the two states of a capacitor. The charge on both of the conductors is zero in the uncharged state, which means that no electrons pass from the positive electrode to the negative electrode in this state. When a direct current is applied across the capacitive electrodes, a charging process occurs. During the charging process, a charge (Q) is transferred from one conductor to the other, with the charged conductor becoming positive (+Q) and the uncharged conductor becoming negative (-Q).

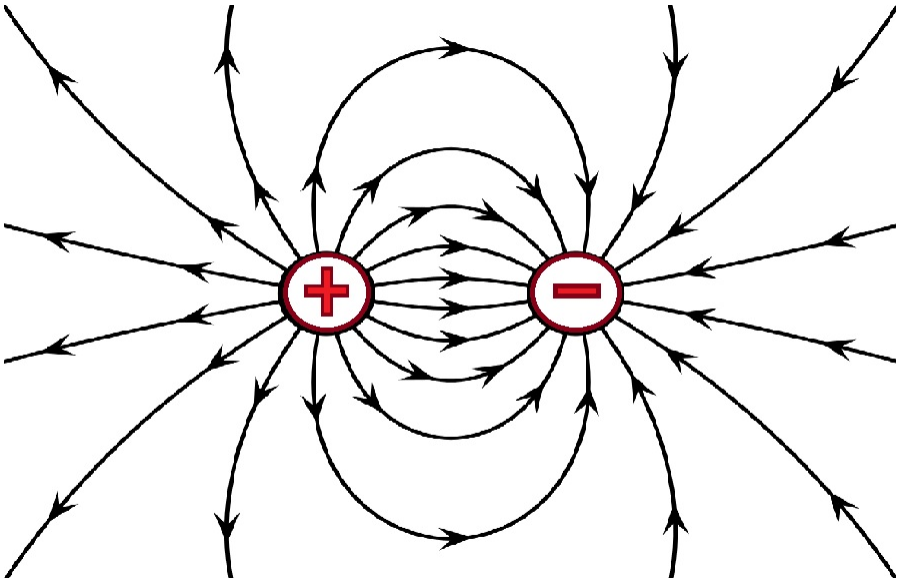

Figure 2.1: Electric Charges

The potential difference is generated between the electrodes during this process; the positively charged electrode is called the ”higher potential” while the negatively charged electrode is called the ”lower potential”. The insulating layer’s resistance controls the DC current flowing through the capacitor; the charge exchange process produces a voltage across the electrodes in the form of an electrical charge, which the capacitor “stores” [15].

When a steady DC current is present, the capacitive electrodes keep charging until the capacitor arrives at its steady state status, during which time the charge increases as the voltage rise.

2.3 Electrostatic Field Intensity

The type of dielectric materials in between the electrodes affects the electric field; the electric field effect is always related to the capacitance of a capacitor sensor. The surfaces generate an electric field when a voltage is applied to one of the sensing electrodes. These electric field lines determine the capacitance between a pair of conductors in a rather complicated way. The electric field should

be enclosed in the space between the sensing electrodes and the target substance in the ideal situation. The dielectric is presumed to be a vacuum in the case of an ideal capacitor, allowing the materials to be detected based on their dielectric characteristics as they split the electric field lines.

Figure 2.2 depicts a simple two parallel electrode capacitor with a gap having area A and distance D. The capacitance value can be calculated by assuming that one electrode has a charge +Q and the other electrode has a charge –Q, and that all field lines produced at the positively charged electrode end at the negatively charged electrode [16]. The following equation describes the relationship between the electric field lines and the area density:

$$E = \frac{\sigma}{\varepsilon * \varepsilon_0} \tag{2.1}$$

The area A and the charge Q are both associated by charge density.

$$\sigma = \frac{Q}{A} \tag{2.2}$$

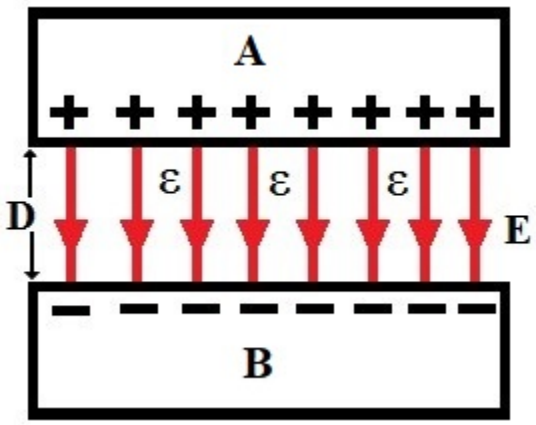

Figure 2.2: Parallel capacitor

In the case of a uniform electric field, the orientation of the electric field approximates that of electrodes with large dimensions compared to their disconnection [16].

The voltage difference V_{AB} between the two electrodes is frequently described in terms of work done on a single charge moving from the positive electrode to the negative electrode. The work done on this charge is :

$$V_{AB} = \frac{F * D}{Q} = E * D \tag{2.3}$$

The capacitance is a term for measuring the capacity to store charge and is denoted by C. It is defined as the ratio of the amount charge stored to the charge-produced potential difference between the two electrodes.

$$C = \frac{Q}{V_{AB}} \tag{2.4}$$

An ideal storage capacitor has a high work done per charge and a large capacitance; thus, capacitance can be expressed as follows using equations (2.3) and (2.4) :

$$C = \frac{Q}{E * D} \tag{2.5}$$

(2.1) in (2.5) gives the following formula for capacitance.

$$C = \frac{Q * \varepsilon * \varepsilon_0}{\sigma * D} = \frac{Q * A * \varepsilon * \varepsilon_0}{Q * D} = \frac{A * \varepsilon * \varepsilon_0}{D} \tag{2.6}$$

Furthermore, an increment in capacitance causes an increase in charge contained in the capacitor, which results in an increment in the potential difference between the electrodes, as shown by the equation above. According to equation (2.5), it will result in an increment in the electric field.

This thesis is primarily focussed on the correlation of different dielectric materials with the capacitance. K is known as the dielectric constant.

$$E_{(Dielectric)} = \frac{E_0}{K} \tag{2.7}$$

$$V_{(Dielectric)} = \frac{V_0}{K} \tag{2.8}$$

The potential difference across free space is larger than the potential difference across a real dielectric, as shown in equation (2.3)

$$C = \frac{Q}{V_{AB}} = K * \frac{Q}{V_{AB}} = K * C_0 \tag{2.9}$$

2.4 Summary

The capacitance increases with dielectric of higher permeability at the same size and spatial distribution. Here we consider a single dielectric material. Our sensing method hinges on these principles. However, the model is more complex as two dielectric materials are present in varying composition and spatial distribution. How can we effectively decode this multidimensional situation? Well, the answer is provided in the following three chapters. We employ an array of capacitive sensors that vary in some parameters. Chapter 3 and 4 are utilizing varying gap array whereas Chapter 5 is based on a sensor array of constant gap spacing but varying insulation layer on top of the electrodes. This way we decople individual effects of each phase making the multi phase sensing problem feasible.

Chapter 3

Phase Discrimination in Marine Icing Using a Coplanar Capacitive Array

Abdulrazak Elzaidi, Vlastimil Masek, Yuri Muzychka

A version of this chapter was published in:

IEEE Sensors Journal (Volume: 19, Issue: 23, Dec.1, 1 2019)

DOI: 10.1109/JSEN.2019.2935616

3.1 Abstract

This paper describes the development of an array of coplanar capacitive sensors applied to marine icing. Current atmospheric icing monitoring systems consider single phase conditions in their operation. Marine icing conditions present a unique environment where the liquid water phase effects cannot be neglected and require a novel approach. We have conducted an initial proof of concept and propose a new icing monitoring system which can distinguish between the individual phases. A numerical model confirmed our initial hypothesis of the system's ability to discriminate the multiphase domains based on the array of geometrically dissimilar capacitive sensors. In addition, we also developed a novel experimental technique based on a comparative study under constant conditions to eliminate the need for an independent ice accretion monitoring system normally required in sensor development. The new approach promises a better characteristic in marine icing monitoring systems or in similar applications where multiphase dielectric is present.

Index Terms — Capacitive sensors, multiphase dielectric material, coplanar electrodes, finite element analysis, capacitance-to frequency conversion, linearly independent characteristics, least squares equations, offshore industry, wind power generation, marine icing.

3.2 Introduction

New methodology for monitoring marine icing phenomena in arctic offshore environments is being proposed. Marine icing is created by a combination of low air temperatures and water spray and can severely affect ships or offshore platforms [3]. Offshore wind farms can face a reduced efficiency due to the ice accretion. For example, the icing can lead to the rotor imbalance which can lead to the system being permanently damaged [4]. The ice layer in marine icing is formed when super-cooled water spray droplets freeze on parts of the structure before the water runoff time elapses [1, 2]. A number of laboratory derived methods to monitor the icing has been proposed recently such as the

systems based on image processing in visible or IR light in [20–23]. These are complex systems and require an unobstructed view, artificial ambient lighting, possibly camera vibration damping besides other requirements which makes their deployment in the harsh marine environment challenging and maintenance costly.

Sensors of low cost characteristic, robust performance and low maintenance are preferred by the industry. The need for expert installation or field re-calibration is additional factor considered in this research. Deployment on a curved rotor blade requires a low weight characteristic and ability of being integrated on a curved surface. Battery operation in wirelessly connected systems require low power characteristics. We have considered a number of existing techniques with these requirements in mind and developed a new method along a proof-of-concept prototype for experimental validation. A range of ideas was adopted in our development at an individual sensor level before we combined an array of dissimilar geometry capacitive sensors to decode two layers of ice and water uniquely. We developed a novel data analysis based on least squares equations to generate a formula of signal-to-measurand mapping. A comparative study without the need for an expensive experimental setup with an independent ice monitoring system proved the new concept's feasibility. This presented research work outlines the first step in our icing sensor development and provides a level of confidence needed for the further study.

The next Section 3.3 outlines the background information in the field of icing sensing in general and capacitance, followed by Section 3.4 which describes a theoretical approach to pre-validate the new concept. Section 3.5 explains the hardware setup to conduct the experimental work with results in 3.6. Conclusions are drawn in Section 3.7

3.3 Previous Work

A large proportion of the current literature on icing sensing systems considers atmospheric icing phenomena on land that also causes severe operational and safety hazards to personnel or equipment like power distribution systems, wind power generation systems, cable cars, transportation or communication towers. A comprehensive survey of current commercial systems is presented in [4].

A research team from Graz Technical University [24] describes their latest work on using a capacitive array applied to atmospheric icing on high voltage power lines. The objectives are somewhat similar, however the sensor array composition and the signal processing methods are different. Their method is using a larger size array with a constant spacing and constant spatial distribution which enables a computer tomography type analysis to assess irregularities in ice accretion across the sensed area. Our system considers a relatively small size array to monitor a localized area. Similarly to our work, Graz team considered the two phase phenomena, ice and water. What makes our independent research largely different is the location of the water domains. We focus more on the surface water layer above the ice while the referenced work considers water domains trapped in the ice layer once the ice starts forming. The lack of common experimental data (marine vs atmospheric) makes it difficult to compare both methods.

On the commercial side, Combitech IceMonitor [9] measures the ice mass on a rotating rod by a load cell. One of the best systems on the market for terestrial applications there is a need for keeping the rotating parts such as bearings free of ice in case of severe conditions. The system provides accuracy of $\pm 50g$ and is not used for measuring light icing events. The system requires a stationary installation which could challenge a potential use in marine/offshore applications due to the dynamic forces, vibration, wind gusts or dynamic water splashes. Long term stability issues have been addressed in [4].

The Goodrich 0871LH1 ice detectors [13] use an axially vibrating probe to detect the presence of icing conditions. In an icing environment, ice collects on the sensing probe, causing the resonance frequency of the sensing probe (~ 40 kHz) to decrease. The ice load depends linearly on the induced frequency shift. When the ice accretion increases beyond a predefined threshold, the probe is de-iced until the frequency rises back to the normal conditions. Goodrich ice detector is designed for thin ice layer applications like avionics and to the date no reports of detecting the ice under the water phase presence has been released.

HoloOptics T42 [8] employs IR signal passed through the medium between the emitter and the detector. In heavy intensity rain or dew the probe may saturate, resulting in a false indication. The manufacturer recommends using an external rain detector together with the sensor to eliminate the sources of false indications. No testing in marine icing conditions was conducted with the T42.

The Ice Meister Model 9734-SYSTEM industrial ice detector [12] monitors the optical characteristics of the substance which is in contact with the optical surfaces of the probe. The parameters measured are opacity and optical refraction. This sensor has no specified accuracy, and is not intended to be used as an analog measuring instrument of any kind. It only recognizes whether air, water or ice is present. This concept is somewhat similar to chilled mirror dew point sensor which often employs the optical reflectivity.

IDS-20 system [25] measures the complex impedance of the icing medium using capacitive plates hermetically sealed. The sensor can distinguish between water and ice as the above sensor, however not in a combined multiphase state.

Zhi et al. [10] conducted recently an experimental research using capacitive sensors to measure ice growth in real time. The developed system has also been patented [26] but the authors conclude the water layer formation has to be prevented in order to maintain the accuracy. Ezeoru [11] conducted a similar research using the same capacitive technique with interdigitated comb-style

electrodes. Both works experienced the transformation from liquid state to solid state which has been reflected in a ramp capacitance profile in time. However, no one has tried to quantify the transitional multiphase period.

3.3.1 Capacitive Sensing

Capacitive sensors are widely used in many industrial and scientific applications due to their simplicity, low cost, high reliability, long term stability and simple signal conditioning [16]. In our application, the sensor features a low profile design that can be attached to flat or curved surfaces. In addition, a simple de-icing mechanism can be conveniently integrated on the same substrate like in a car windshield defogging system. The capacitive probe is usually lightweight, making the sensor suitable for placement on dynamic systems or moving parts.

A capacitor in a charged state creates an electric field that is modulated by the presence of a dielectric material in its proximity. In many applications, the electric field is distributed across the measured dielectric material while being confined between two sensing plates of a regular shape. Most frequently, the field equipotential lines are parallel or concentric with the electrodes in which case an analytical modeling in a curvilinear coordinate system can be very accurate.

Our method exploits the concept of fringing fields set by a coplanar pair of electrodes. Planar capacitors can take many different shapes and forms like interdigitated (comb fingers), rectangular or circular spirals etc. [11], Go [26], Arshak [27] used the interdigitated electrodes while Gong [28] and [29] used spiral electrodes. Whichever form the planar capacitor takes, the common key parameter is the dimension of the gap along the interfacial line between the two electrodes. As long as the covered sensing area is the same, all geometries are equivalent and it is only the matter of a personal choice.

Capacitive sensors are however prone to undesired effects of parasitic and offset capacitances as well as the dielectric loss in the form of a conductance. Our capacitive array is spin coated to form an insulation layer to significantly suppress the effect of the conductance and a simple capacitance to frequency conversion is being employed. However, more advanced and very accurate conversion methods have been recently developed like the research of Malik et al. [30] where the maximum error due to parasitic capacitance is found to be within $\pm 0.05\%$.

Our method also operates on a differential principle in which four capacitances are compared by an algorithm. This concept can be viewed as a multidimensional Wheatstone bridge. In general the comparative or differential methods are very effective to deal with the offset and parasitic capacitance as long as they drift consistently, in most cases due to temperature effects. A brief analysis of the drift effects is presented in the Results section.

The work of Alex Risos [31–34] on interdigitated capacitive sensors employs the differential principle in which the reference sensor is thermally coupled with the transformer oil sensing probe. He also uses a four wire bridge measurement technique which significantly suppresses the effect of lead wire impedance. Risos et al also points out another potential issue surrounding the capacitive sensors which is a noise source by charged particles in the dielectric medium being analyzed. To eliminate the effect of such charges and the parasitic capacitance, he introduced a liquid permeable Faraday cage above the sensor plain plus inserted a tiny deflector electrode between the sensing electrodes. The deflective electrode is held at the GND potential but is not connected to GND. Unfortunately we cannot use this method as any cage in front of the sensor would be subject to the icing phenomena. Heating the Faraday cage would not be effective either as the thermodynamic balance would be negatively affected. In our research however, we do not anticipate any charged particles in the dielectric medium since each conductive droplet arriving at the sensor plain originates from the ocean wave breaking off the ship bow which are in fact the GND reference. To our knowledge there is also no mechanism of acquiring a charge during the flight through moist atmosphere above

the ocean. In terms of the deflector electrode, we may introduce this technique in the future work. Currently our sensor array is using a variation in the gap between the electrodes which prohibits the deflector electrode use without a modified approach.

Figure 3.1 shows experimental data acquired by Ezeoru [11] at a rate of 16 samples per second, or $\sim$ 1000 samples per 1 minute. The graph describes ice forming in three transitional steps (water to ice), tap water on top and sea water below. Each step starts by wetting the sensor plane and waiting for the water to turn into ice at a constant $-20^{\circ}C$. One can observe that the sea water of 3.5% salinity (by mass) takes much longer to turn into ice. The ice accretion was determined by weight measurement.

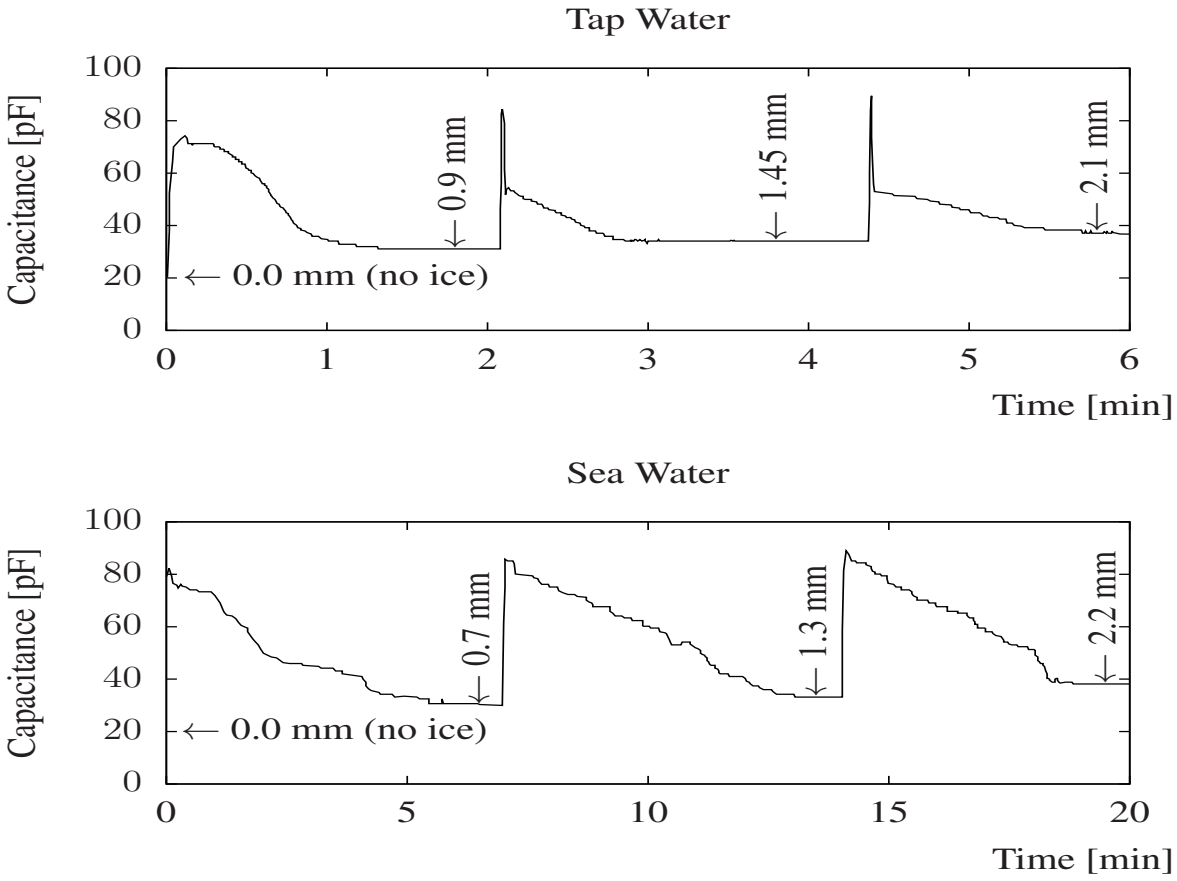

Figure 3.1: Experiment for Sensor Calibration, Ezeoru 2016 [11]

From [11] we extracted four pairs of data as indicated by arrows in Figure 3.1 in order to derive the calibration characteristics for low ice accretion levels shown in Figure 3.2.

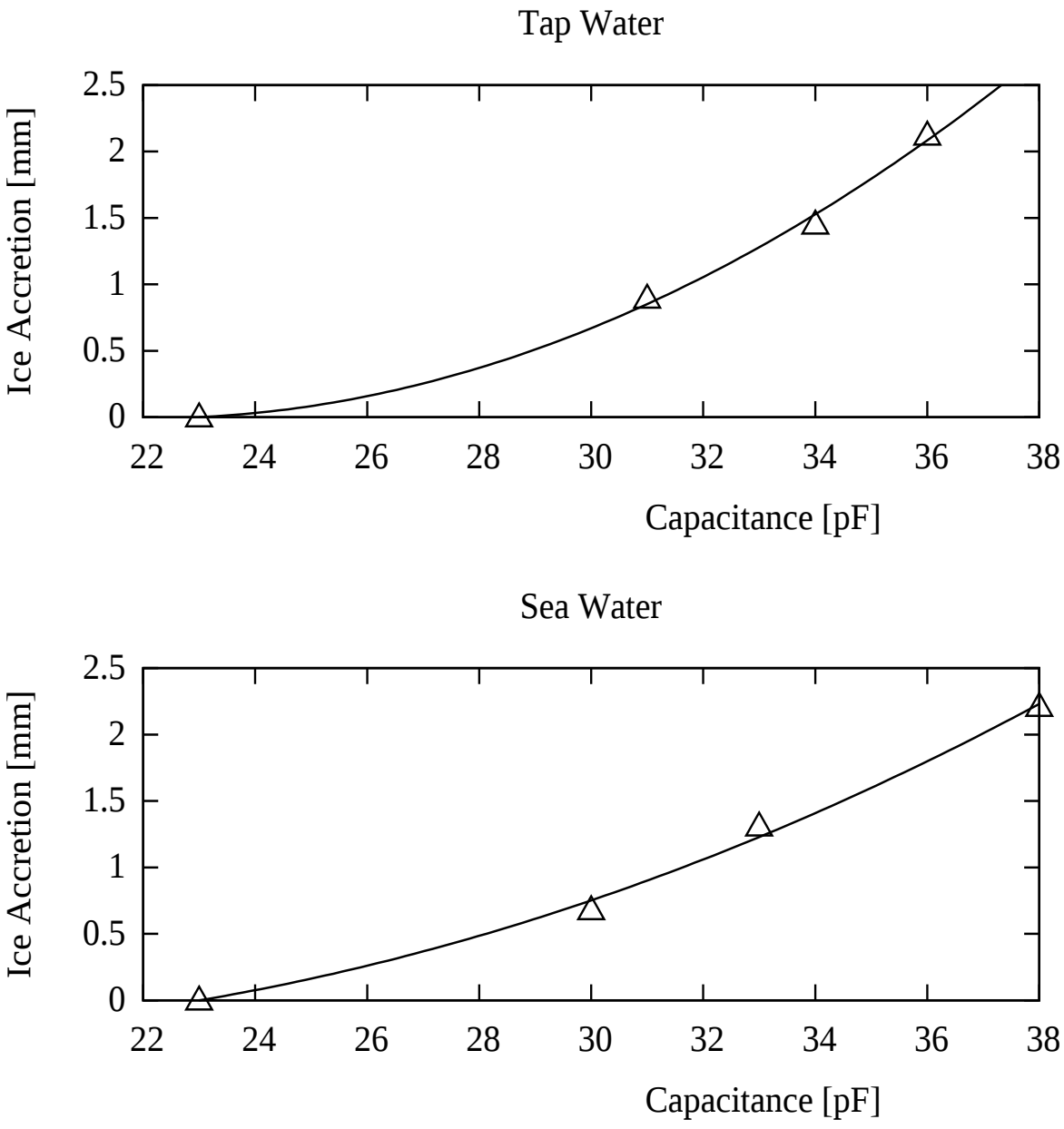

Figure 3.2: Ice Accretion vs Capacitance

The capacitance data were first normalized according to (3.1) and then utilized in least squares fitting of a quadratic characteristic (3.2) as depicted in Figure 3.2. The fitting was derived with the final sum of squares of residuals of 0.00869474 as compared to 0.146793 in a liner characteristic fit (tap water case).

Applying the single phase icing sensor characteristic to the original two-phase conditions during the transients we generated Figure3.3. The grey segments are subject to errors of the order of magnitude which limits the sensor's application in two-phase marine icing conditions.

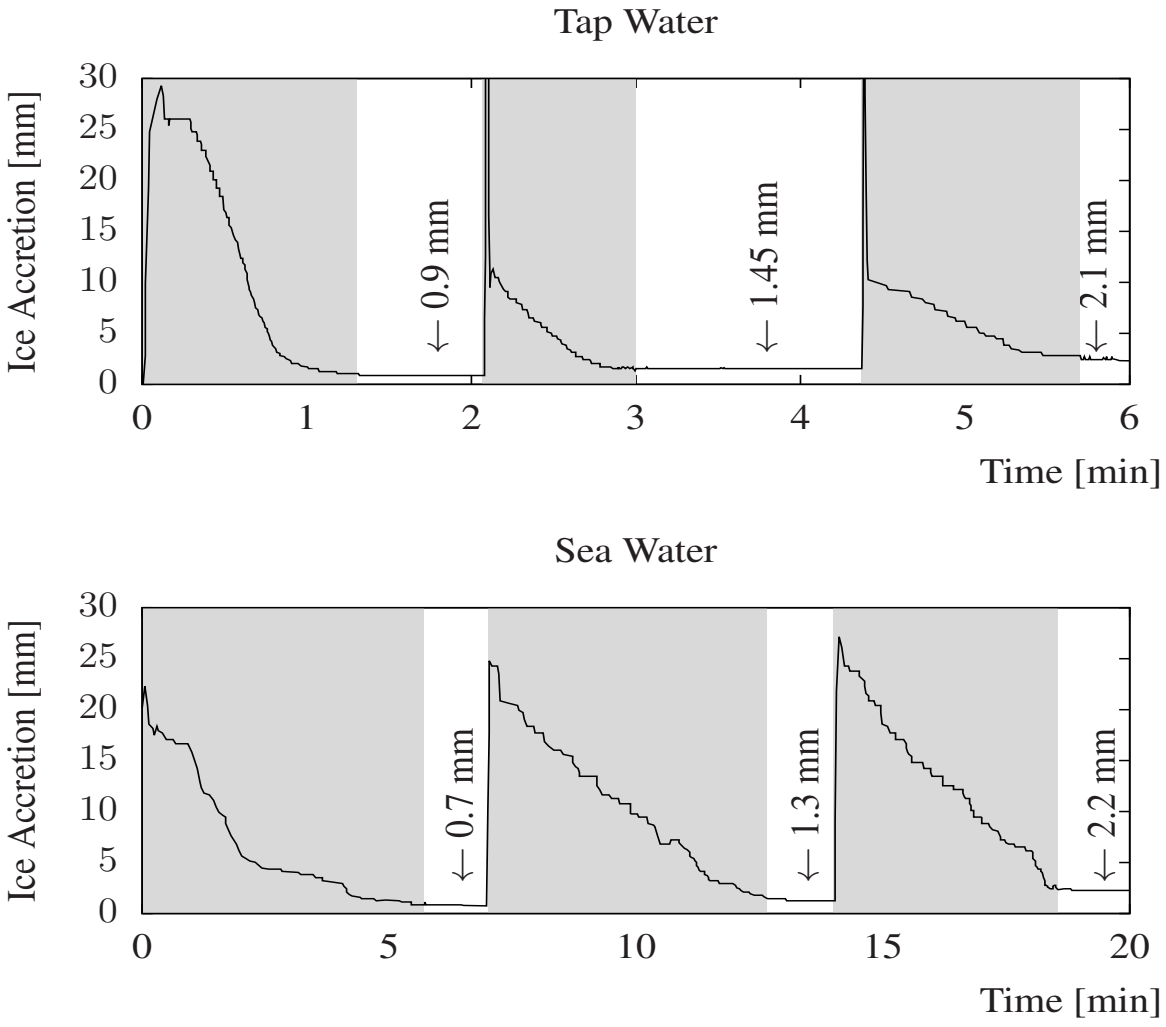

Figure 3.3: Faulty Measurement Results under Two-Phase Conditions

Applying this technique to marine icing would require a human operator to extract the bottom envelope of the measurement data and disregard the multiphase transients that provide faulty ice accretion reading. This is feasible in a lab derived data however real marine icing conditions make this human intervention task difficult as there may never be a period of single phase icing for a period of time when the sensor is constantly exposed to icy waters. Also applying a low pass filter with a low corner frequency would smooth the transients at the cost of raising the bias making the data unreliable again. Therefore, unless single phase conditions can be guaranteed, we need to consider the effects of both water and ice together.

$$\hat{C} = \left(\frac{C - \bar{C}}{\bar{C}} \right) \tag{3.1}$$

$$h = k_1 \hat{C} + k_2 \hat{C}^2 \tag{3.2}$$

h	[mm]	ice accretion
$\hat{C}$	[1]	normalized capacitance
C	[pF]	measured capacitance
$\bar{C}$	[pF]	nominal capacitance
k_1, k_2	[mm]	constant coefficients

3.4 FEM Simulation

The marine icing phenomena as described above consists of both the solid phase (ice) and the liquid phase (water) with a different proportion at different times. Except [24], all known methods

assume only the ice phase which makes it inaccurate if the water phase is present as there is a large discrepancy in the dielectric constant between the ice and water ($\sim 20\times$).

We adopted a concept of modulating the sensor's depth of penetration by changing the air gap between two spiral electrodes, [29, 35]. Two different electrode separation sensors uniquely modulate the electric field above the XY plane of each sensor. The resulting capacitances must therefore be linearly independent of each other making it possible to discriminate between the two phases.

In order to verify the above statement, we first conducted a finite element simulation using two concentric electrode probes of 1mm and 2mm electrode separation in a similar way as described in [29, 35]. The problem was modeled in Maxwell software developed by Ansys using axisymmetrical coordinates in RZ plane. Table 3.1 lists all domains in the model and their corresponding parameters.

Table 3.1: ANSYS Maxwell Model Parameters

tag	object	material	ε_r	sources	matrix
Ⓐ	background	air	1.0006		
Ⓑ	balloon			voltage	
Ⓒ	object2	water-fresh	81		
Ⓓ	object1	ice	4.2		
Ⓔ	electrode-gnd	copper		0V	GND
Ⓕ	electrode-sig	copper		1V	Signal
Ⓖ	dielectric	epoxy-Kevlar-xy	3.6		
Ⓗ	PCB-backing	epoxy-Kevlar-xy	3.6		

The capacitance is calculated from the total field energy W across the modeling domain using 3.3 where V represents the applied voltage, conveniently set to 1V for easier result validation.

$$C = \frac{2W}{V^2} \tag{3.3}$$

The field for the sensor geometry having 2mm electrode separation and r = 9mm & R = 15mm is depicted in Figure 3.4. The second geometry has 1mm separation and r = 10mm & R = 15mm. When two characteristics are linearly independent, a common solution can be derived from their intersection point.

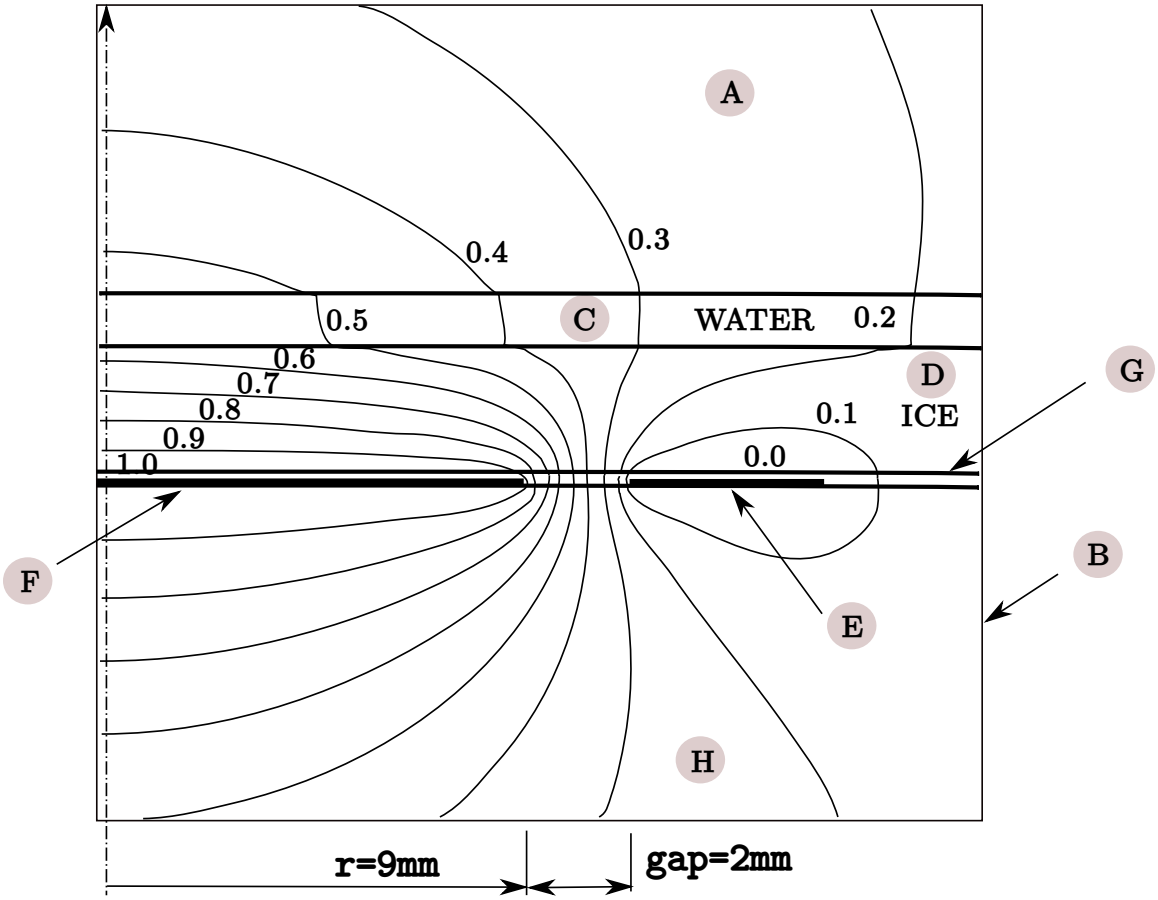

Figure 3.4: Equipotential Lines of Electric Field for 2.5mm Ice&1mm Water

Figure 3.5 demonstrates this concept using contours of constant capacitance for the two sensor geometries combined in one plane, 1mm sensor contours depicted by solid lines and 2mm sensor contours by dashed lines. One particular solution is highlighted for 1mm gap sensor at 6.5pF capacitance and 2mm gap sensor at 5.0pF capacitance having a common intersection point at 0.75mm ice layer and 0.35mm water layer above. The larger the angle of intersection between any two contours the more robust solution is derived. This type of analysis was conducted by Ortiz [36].

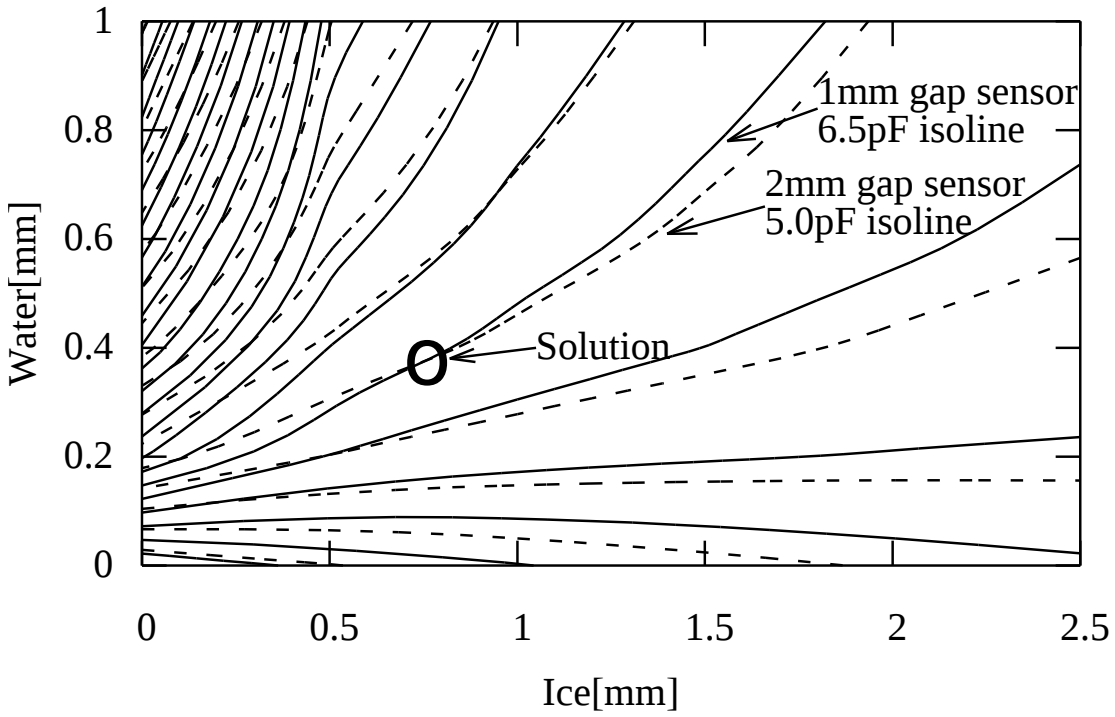

Figure 3.5: Contours of Constant Capacitance for Both Sensor Geometries

In summary, the FEM simulations have proven in theory that an array of coplanar sensors of different electrode spacing characteristics can uniquely map the presence of the water phase and use this information in deriving the ice accretion level with more accuracy and confidence.

3.5 Experimental Setup

Chen and Bowler [29, 35] used a simple PCB layout software approximating the spiral electrodes by arc segments of varying radii creating a small discontinuity whenever two 180° arc segments of different radii are connected. Our array of capacitive probes was manufactured on a printed circuit board (PCB) with the spiral electrodes modeled by OpenSCAD software as true Archimedes spirals ensuring a constant spacing between each electrode pair.

The PCB was spin coated with a thin layer of dielectric lacquer to eliminate the effect of conductivity between the individual electrodes. A similar process is widely used in many commercial systems such as tactile/touch sensor from Texas Instruments [37].

Each probe is conditioned by a capacitance-to-frequency converter which utilizes FET Hartley oscillator (Figure 3.6). The air-core coil is provided with a center tap and was made using a *basket weave* technique to suppress a parasitic capacitance and a magnetic coupling via the proximity effect. We have subjected each channel to two extreme conditions, one with air dielectric and the other with 5 mm of tap water layer to assess the oscillations are sustained between the two limits.

In order to interface the oscillator to a PC data acquisition card, the harmonic signal of 13 to 16 MHz generated by each oscillator was first converted to a square wave signal by utilizing a fast comparator MAX 912 and then divided by 8 using a 74LS163 counter to meet the data acquisition card's input frequency range (Advantech PCI-1780 8-ch Counter/Timer Card).

The LC filters are required to prevent any coupling among the oscillators through the common power supply. The array of six oscillators is enclosed in a Faraday cage enclosure each made of mild steel sheet and grounded. This arrangement shields any undesired EM interference between oscillators. The harmonic signal was converted to TTL signal using dual, high-speed comparators with differential input and consequently six TTL counters were used as 8x frequency dividers. The signal processing part of the system was shrink wrapped to prevent any humidity entering

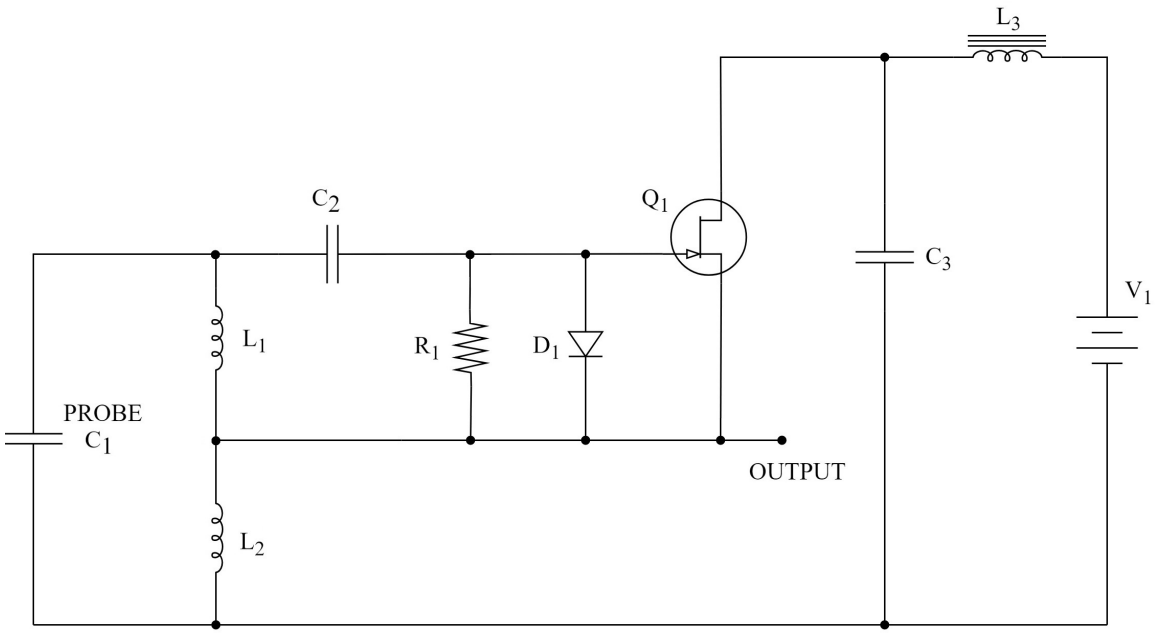

Figure 3.6: Hartley Oscillator as Capacitance-to-Frequency Converter

the oscillators, comparators and frequency dividers and the capacitive array PCB was leveled in a deep freezer at $-20°C$ using a custom built frame shown in Figure 3.7. A flat ribbon cable 1m long interconnected the sensors with the PC and external power supply, and folded flat under the freezer's cover lid.

Our experiments assumed that all capacitive probes in the array face the same conditions, i.e. ice layer and water layer of the same height. In case of a small size array this assumption is valid however a sufficient border area around the array should be provided to eliminate potential irregularities due to leading edge or trailing edge boundary effects in certain wind conditions.

To assure a uniform icing buildup, we modified the experimental procedure from [11] and used a paint roller instead of a spray bottle. Three runs were conducted to ensure the uniformity of the ice accretion. The sensor system was tempered at $-20°C$ for two hours before starting the experiment.

Figure 3.7: Sensor Leveling prior to the Experiment

3.6 Results

The experimental setup described above provided data in Figure 3.8. When the transient response started to settle down, a new wetting cycle was initiated with a total of three cycles. The sharp trough in data plot provides a time reference for each wetting phase which closely corresponds to the work in [11] with a difference of inverted sign characteristics due to the fact that frequency is being plotted instead of the capacitance; i.e the higher the capacitance, the lower the frequency.

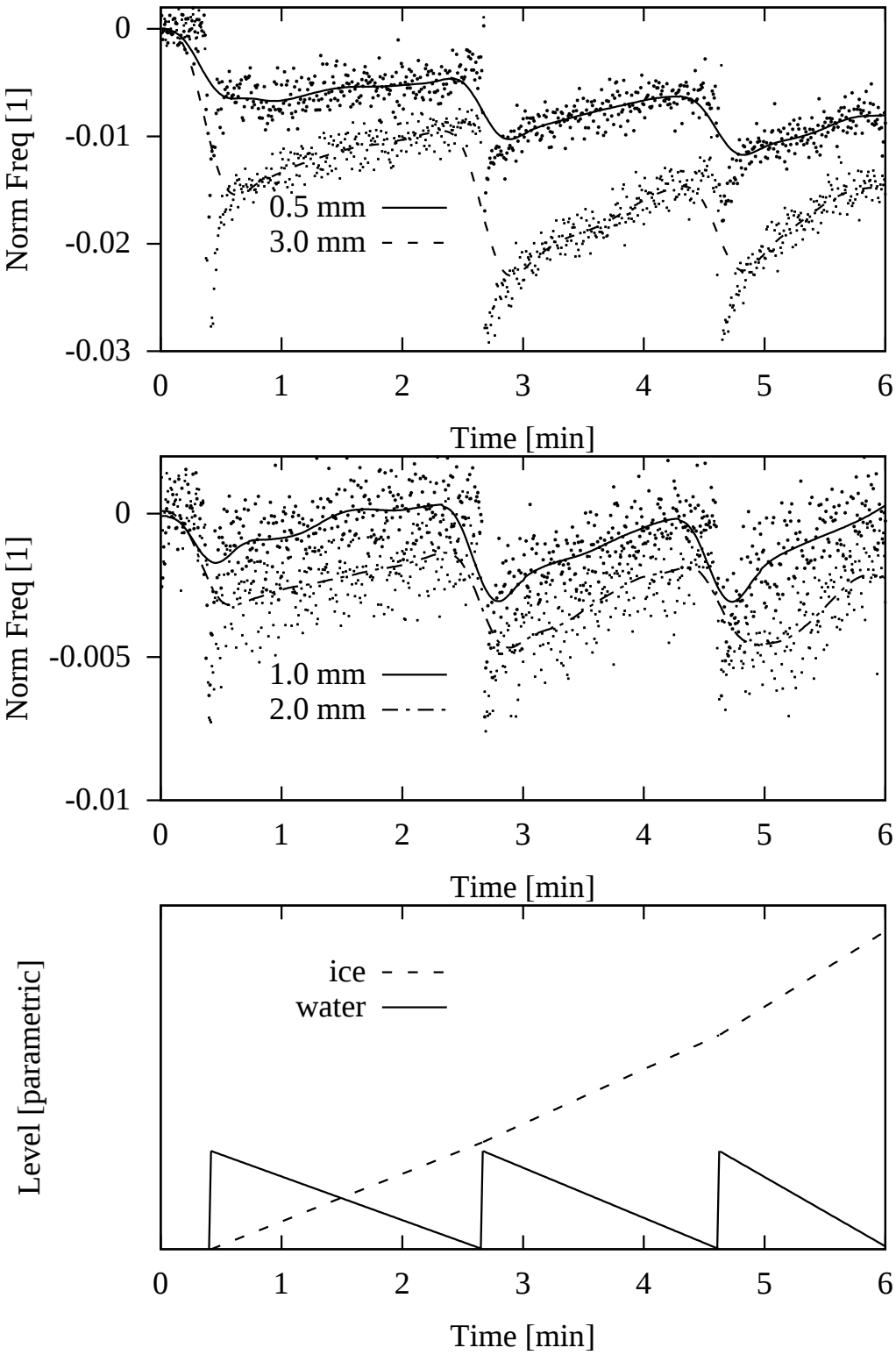

Figure 3.8: Back-Shifted Filter Signal Synchronized with the Process

In line with the above assumption of having all probes facing the same conditions at any time, we introduce a second assumption about the conditions time profile. In this work the icing phenomena is considered to follow a linear time profile for the sake of proof of concept. Other characteristics such as a first-order dynamic response can be used, however, without an accurate real-time ice and water level monitoring system in place, the uncertainty will remain. The objective of our work is not the accuracy or quantitative indicators of ice accretion measurement. In this study, we only assume that each wetting cycle creates a consistent layer of water film across the array. The ice level accounts for 9% increase in the volume. Each consecutive cycle also gets shorter time to settle attributed to the thermal inertia of the accumulated ice layer underneath.

In order to compare and align the data from four oscillators, each frequency was normalized using nominal frequencies acquired when no ice nor water was present. Table 3.2 lists the four nominal frequencies along the original frequency and normalized frequency for#100^{th} sample. The normalization process can be viewed as the sampled data being shifted up or down along the frequency axis and then scaled, the operations that do not affect the linear independence of individual characteristics.

gap width	0.5mm	1mm	2mm	3mm
	f_1	f_2	f_3	f_4
Nominal	1.686 MHz	1.976 MHz	1.907 MHz	1.595 MHz
Measured	1.674 MHz	1.975 MHz	1.899 MHz	1.572 MHz
Normalized	-0.006826	-0.0002940	-0.003981	-0.01406

Table 3.2: Nominal Frequencies & Normalization, sample # 100

The frequency data were sampled at a rate of 2 samples per second using a DAQ card and the noise was filtered off-line in Matlab using a Butterworth low pass filter with a medium delay of 40 samples. Due to the low sampling frequency we are not confident about the noise origin, however, the lab environment had a large refrigeration equipment running in the vicinity of our setup which suggest a potential 60Hz noise. The signals were also sampled sequentially making the analysis of raw data more challenging, nevertheless, we do include the raw data analysis at the end.

The resulting filtered data sets were then backshifted by 40 samples to align with the original raw data only for the demonstration purposes as illustrated in Figure3.8.

To verify the initial hypothesis that an array of planar probes of different spacing parameters can uniquely determine the multiphase phenomena, we propose to use a linear combination of the measured frequencies and their squares similar to the earlier quadratic fit depicted in Figure 3.1, [11]. Equation (3.7) reviews this concept including the coefficients $k_1,\ldots,k_8$. One set of eight coefficients is used for determining the ice level ($k_{1i},\ldots,k_{8i}$.) and another set for the water level $k_{1w},\ldots,k_{8w}$.

The eight unknown coefficients in (3.7) can be determined from eight linearly independent equations that correspond to different sample instances. The challenge is to find a set of eight representative samples that will form the eight equations. We took a different approach by using all available samples.

Instead of finding the vector of coefficients **k** from eight linearly independent equations **Fk=h**, we searched for the vector **k** such that **Fk** is as close as possible to h, as measured by the square of the Euclidean norm in (3.4).

$$\begin{aligned} ||\mathbf{Fk}-\mathbf{h}||_2^2 &= (Fk-h)^T(Fk-h) \\ &= k^TF^TFk-2h^TFk+h^Th \end{aligned} \tag{3.4}$$

Taking the gradient with respect to **k** we obtain (3.5).

$$\begin{aligned} &\nabla_k(k^T F^T F k - 2h^T F k + h^T h) = \\ &\nabla_k k^T F^T F k - \nabla_k 2h^T F k + \nabla_k h^T h = \\ &2F^T F k - 2F^T h \end{aligned} \tag{3.5}$$

Setting the gradient expression equal to zero and solving for **k** provides the normal equations in (3.6).

$$k = \left(F^T F\right)^{-1} F^T h \tag{3.6}$$

This approach shares some similarities with Artificial Neural Network (ANN) training process, where a training set of input data (frequencies) is presented to ANN along with the desired output (ice layer height and water level height). The difference is that ANN training follows an iterative process of training whereas Least Squares method is not. The solution convergence can be also an issue in ANN's.

We used Matlab to process the Least Squares computations according to (**??**) and once the coefficients **k** were determined, a test run by evaluating (3.7) for all samples was performed ((j = sample #). The resulting data for both water and ice phase are plotted in Figure 3.9.

$$h_j = \sum_{N=1}^{4} (f_{jN})\, k_{jN} + \sum_{N=1}^{4} (f_{jN})^{\mathbf{2}}\, k_{j(N+4)} \tag{3.7}$$

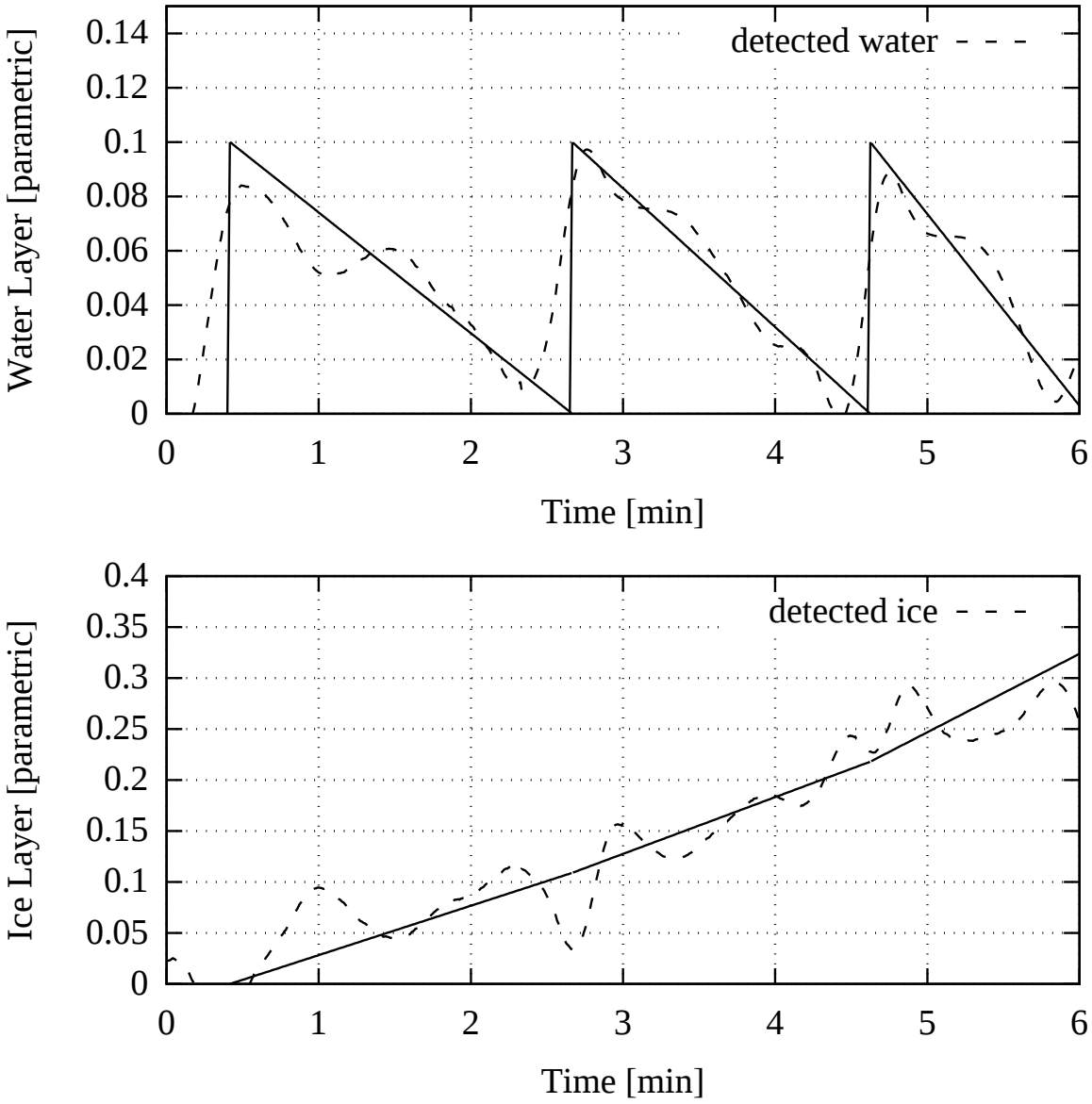

Figure 3.9: Detected Ice & Water vs Predictions using Filtered Data

As a result, the ice accretion *measurement* in not significantly impacted by the water phase as was the case of calibrating a sensor using the ice only data. Relatively small deviations are still present in our results, however, these are mainly concentrated around the time when the water layer is being applied to the sensor plane using a paint roller which does not exist in the real world.

We also present a plot on the effects of drifts in offset & parasitic capacitance and dielectric loss (Figure 3.10). The most common are drifts due to temperature changes or aging. We have subjected the normalized frequency data to a constant offset of 1×10^{-3}, 2×10^{-3} and 3×10^{-3} which represents nearly half of the total frequency range in '1mm' and '2mm' sensors. Yet the effect on the output is found insignificant in view of the other inaccuracies. A more detailed analysis would be needed in the future research including both absolute and relative data drifts.

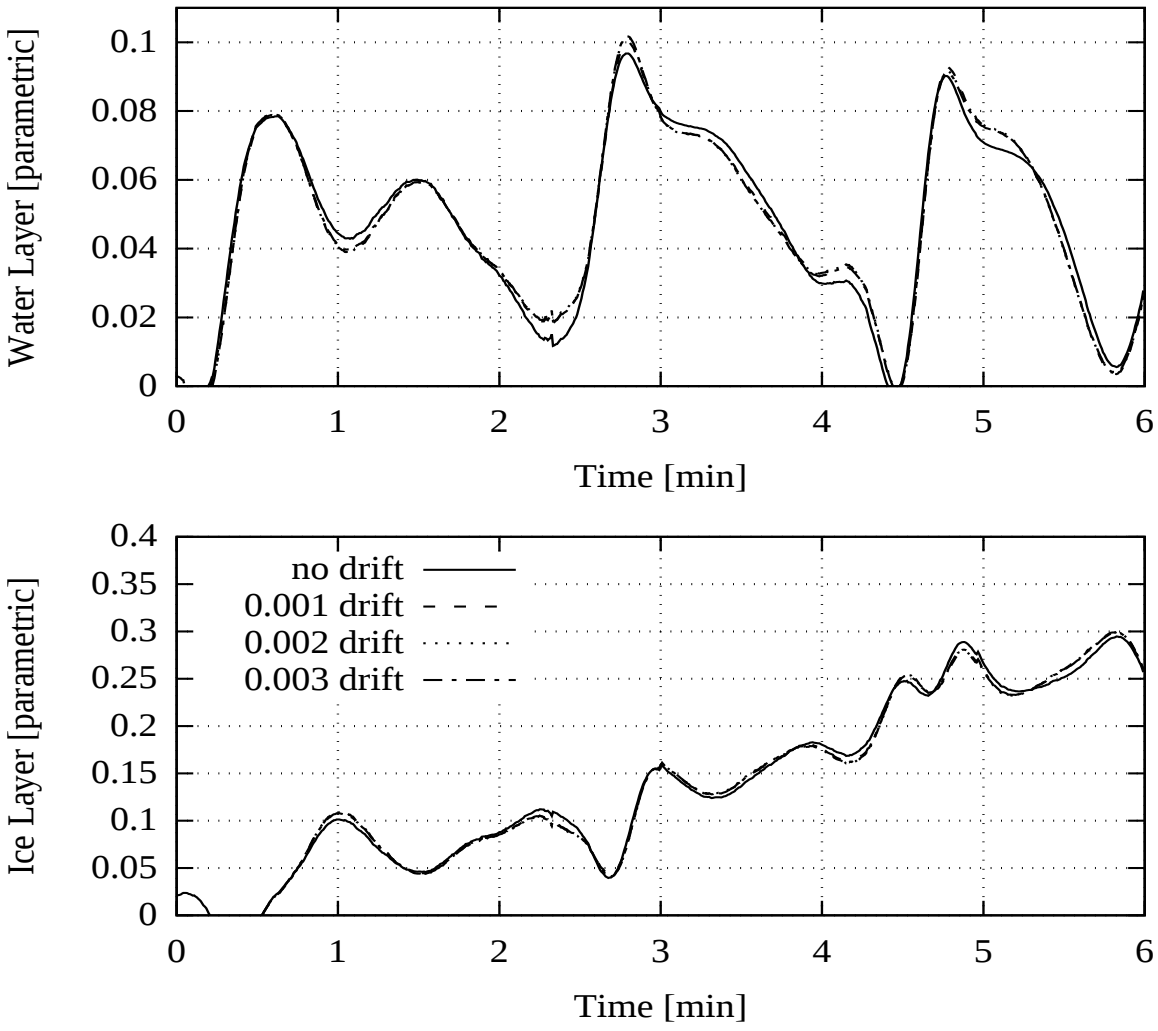

Figure 3.10: Detected Ice & Water under Presence of Frequency Drifting

The raw data analysis results are plotted in Figure 3.11 for completeness. The water and ice detection is not as close to the predicted profiles obtained in the filtered data analysis showed, however the approximate tendencies are clear without the order of magnitude errors we experienced before.

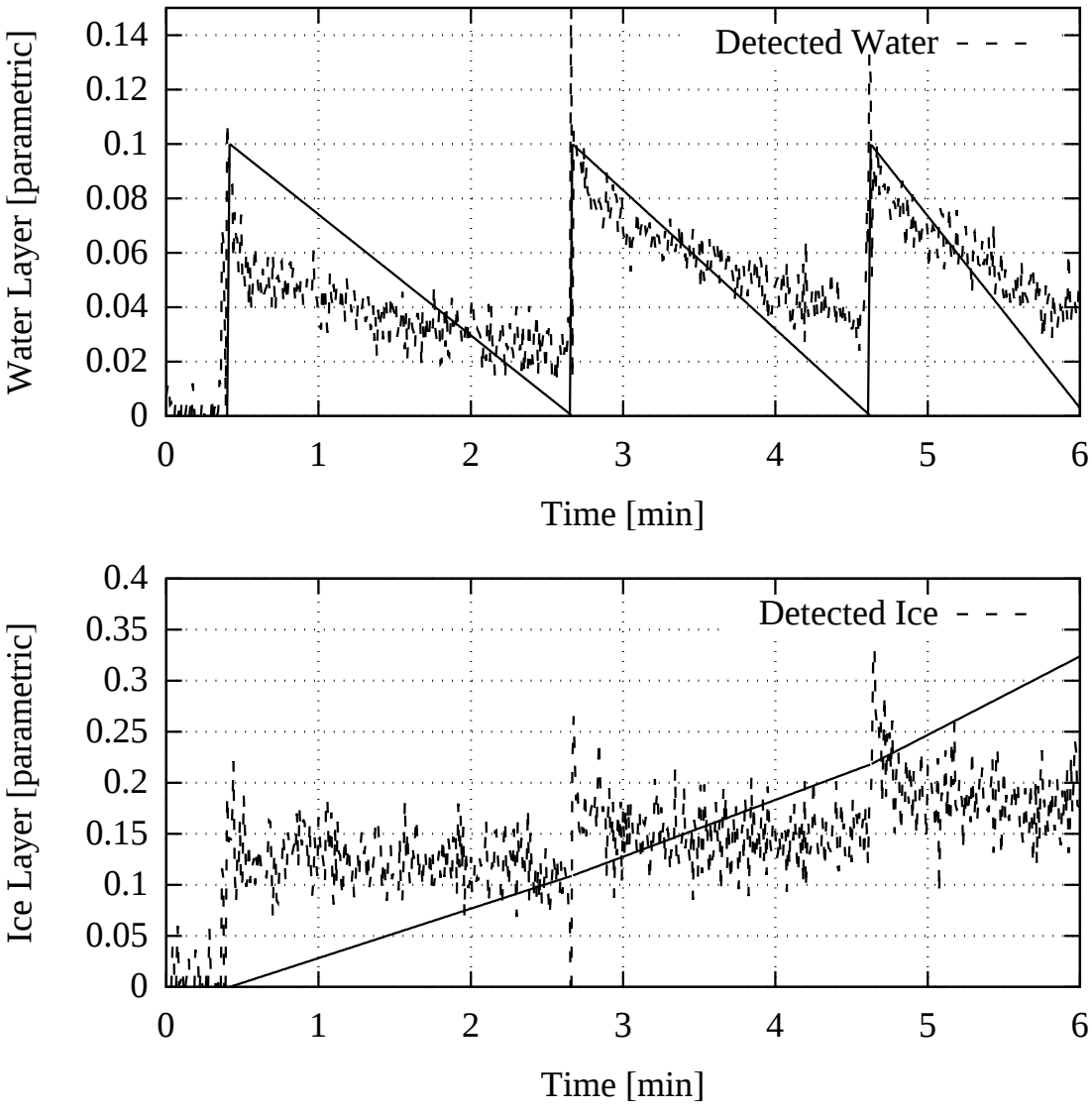

Figure 3.11: Detected Ice & Water vs Predictions using Raw Data

This scope-limited study also revealed where we need to focus in the future development. As the next step, this reaserch will incorporate a calibration system that will quantify the sensitivity and robustness of our system. A more robust drift-free signal conversion techniques will also be studied.

3.7 Conclusion

The presented work focused on development of a marine icing monitoring system under the real conditions of multiphase phenomena as the current monitoring systems do not consider the unique conditions. We have developed a novel method of utilizing an array of capacitive probes of different aspect ratio and thus a different penetration depth to be a candidate for multiphase phenomena sensing. FEM analysis was conducted to provide a theoretical proof of the novel approach. Then an experimental setup was developed to validate the proposed approach. The objective of our experiments was to prove the ability of our system to recognize the multiphase phenomena.

Instead of the traditional 'quantitative calibration' we selected a 'qualitative calibration' approach which only assumed three *identical & uniform* layers of water film applied to the sensor plane at each wetting cycle. Least Squares equations were solved to find a correlation among the array capacitances (measured as frequency) and the water & ice layer height represented parametrically. The experimental results confirmed our predictions which gives our novel approach the necessary backing to be developed further.

Chapter 4

Water and Ice Detection in Marine Icing by Capacitive Sensor Array and the Artificial Neural Network Model

Abdulrazak Elzaidi, Vlastimil Masek, Stephen Bruneau

A version of this chapter was published in:

2019 IEEE 10th Annual Information Technology, Electronics and Mobile Communication Conference (IEMCON)

DOI: 10.1109/IEMCON.2019.8936232

4.1 Abstract

This work describes a capacitive sensor array for the measurement of marine ice accretion. Currently, all commercial icing detectors only track the ice phase disregarding the water phase. This approach is acceptable in many applications, mostly in the atmospheric icing domain however in the case of marine icing, the water phase creates a significant component of the measurement signal. The water phase cannot be disregarded and requires a novel methodology that takes into account the water-ice conditions simultaneously. A neural network approach is used to implement the signal-to-measurand mapping. Compared to the previous least-squares based mapping, the neural network method is more accurate and therefore becomes a preferred method of signal processing in capacitive array based marine icing sensing.

Index Terms — Marine icing, Capacitive sensors, Coplanar PCB electrodes, Artificial Neural Network (ANN), Capacitance-tofrequency conversion, Multiphase Dielectrics.

4.2 Introduction

Marine icing monitoring provides the ice accumulation data in on/off-shore applications. Heavy icing conditions can cause severe operational challenges or can lead to severe safety hazards. Our main motivation is to develop a monitoring system which protects workers on vessels or ships [40]. Marine icing forms on a surface when the supercooled water turns into ice before the runoff time elapses. Chokmani [41], Zhi [42], and Ezeoru [11] developed a marine icing accretion monitoring system based on single phase assumption. Similarly, Sommer Messtechnik [25] is based on ice phase monitoring alone. Neumayer [43] and this work is focused on ice-water composition with a difference in the arrangement of the capacitive sensors.

Coplanar capacitive sensors are surface electrode structures which can be easily manufactured using a printed circuit board technology. Capacitive touch sensors replacing mechanical push but-

tons commonly used these days often employ this technology. The capacitance can be detected by numerous methods, however capacitance to time or frequency conversion gains wide popularity due to its digital nature and simple interface. Time or frequency signals are also less prone to interference. Neumayer [43] utilizes a capacitive array of constant spacing characteristics and applies Computer Tomography algorithm to detect the multiphase domains.

In our research, we utilize an array of capacitive elements of varying spacing dimension, the inter-electrode gap. Each element features a different depth of 'penetration' and in the combination, the system provides linearly independent signals that can uniquely encode the ice accretion and water layer depth.

4.3 Experimental Platform

Our previous work [44] describes the experimental platform in more detail. Figure 4.1 & Figure 4.2 show the capacitive elements of varying spacing (3.5 mm, 3 mm, 2.5 mm, 2 mm, 1 mm, and 0.5 mm). A thin layer of insulation was also deposited on top of the PCB to insulate the electrodes from the external environment. This is a common practice in capacitance sensors to prevent the conductance to influence the measurement unless it is the part of the measurement method.

Hartley oscillator is used to detect the capacitance of each element. A comparator MAX 912 is used to convert the harmonic sine wave signals generated from the oscillator to square wave signals and consequently a counter 74LS163 divides the frequency 8x.

Prior to the experiment, the PCB was leveled in a deep cooler at $-20°C$. We used a paint roller to deposit a water layer over the PCB. A wet roller was rolled over the sensor plane in three runs separated by a few minutes each as shown in the data plot below. We assumed the entire PCB surface experiencing the same conditions and that each wetting cycle deposited an equal layer of water.

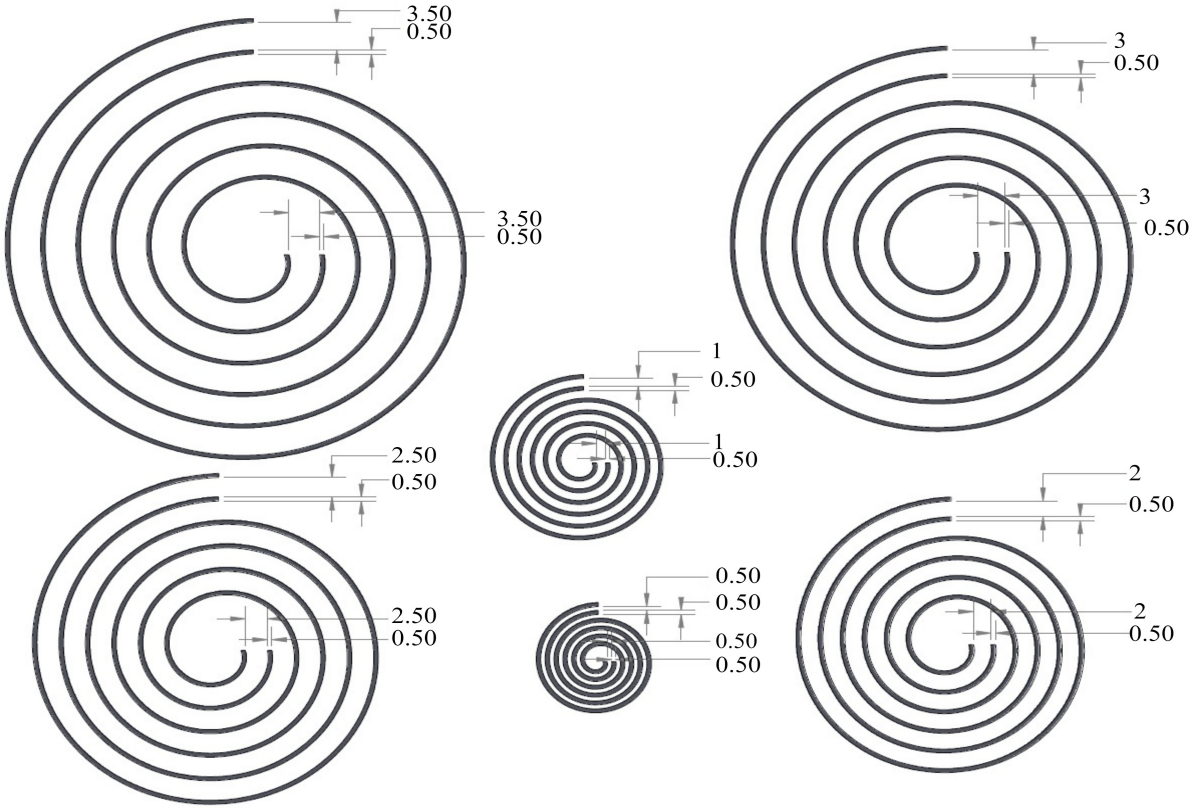

Figure 4.1: Design of coplanar spiral electrodes of different air-gap spacing

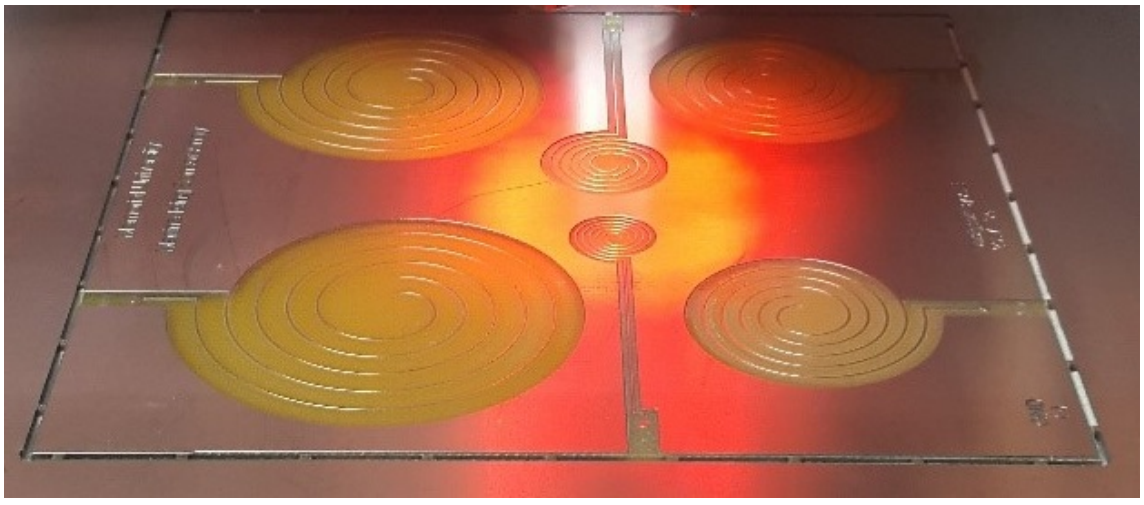

Figure 4.2: Capacitive Sensor Array

4.4 Signal Processing

Consistent water layers were created using a wet paint roller, and three wet cycles were applied across the sensor array PCB surface. The measured frequencies are shown in Figure 4.3. The plotted frequencies differed in a constant term as well as amplitude. Here the constant term corresponds to the case when no ice nor water is present, the initial condition.

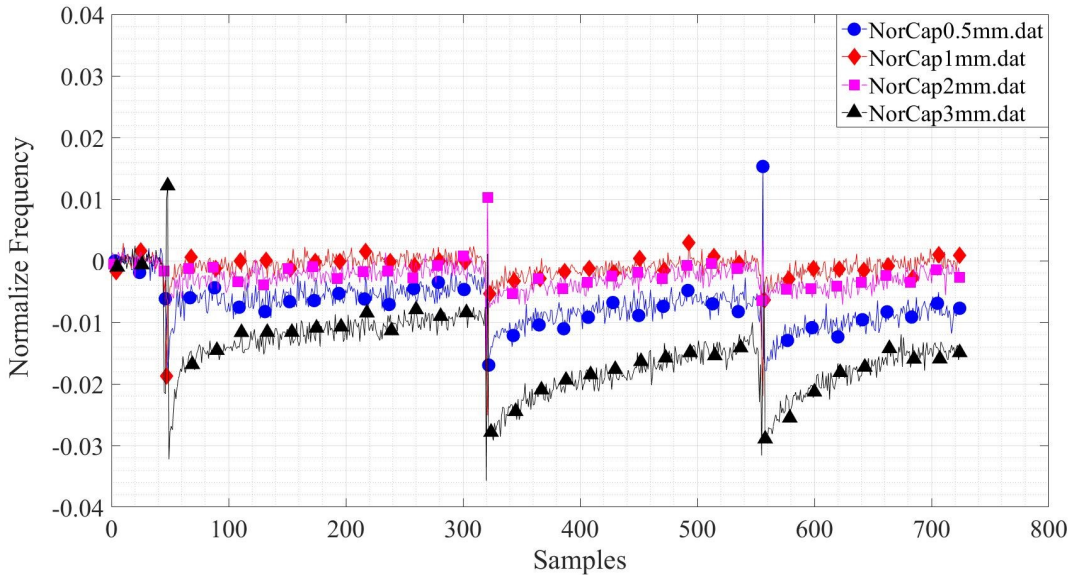

Figure 4.3: Normalize Frequencies from Four Oscillators

While maintaining their linear independence, we normalized the acquired frequencies by the constant (initial) term in order to present them in one graph for comparative reasons. Figure 4.3 includes data for four elements with a slightly differnt duration of each wetting cycle. The cycles are getting shorter as thermal inertia of the built up ice is growing.

The frequency data were sampled at a rate of two samples per second using a DAQ card and Matlab was used to filter the noise off-line by Butterworth filter, Figure 4.4. Figure 4.5 shows the filtered data shifted back by 40 samples to align the characteristics with each wetting cycle instead of delaying the ice and water profiles by the filter's delay.

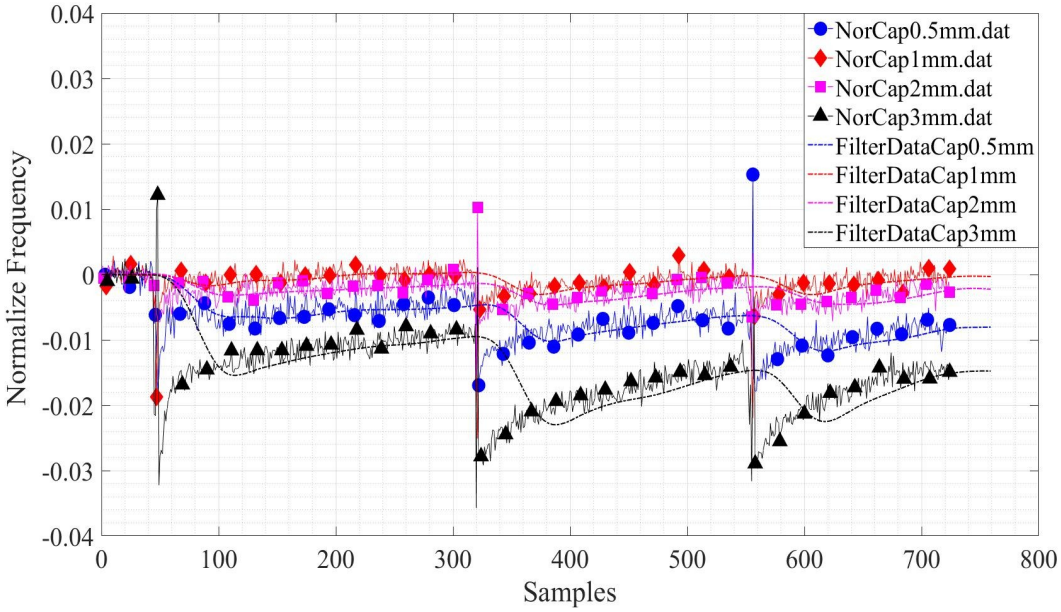

Figure 4.4: Filter Data and Normalized Data for 0.5, 1.0, 2.0, and 3.0-mm Gap Sensors

Again we assume that each wetting cycle creates a uniform water film layer over the PCB. Figure 4.6 illustrates this assumption in a time profile for water and ice accretion. The profiles are piecewise linear and their amplitude is not a concern in this study. In order to also determine the amplitudes, a more complex sensor calibration setup would be necessary where ice and water layer has to be measured accurately.

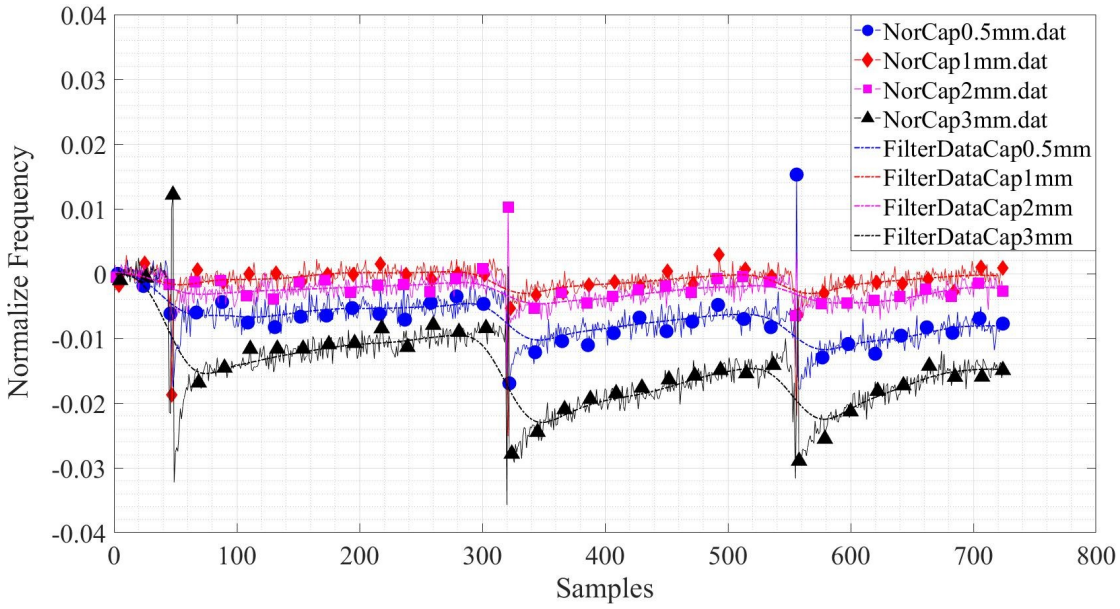

Figure 4.5: Removed Delay Shift from Filter Data

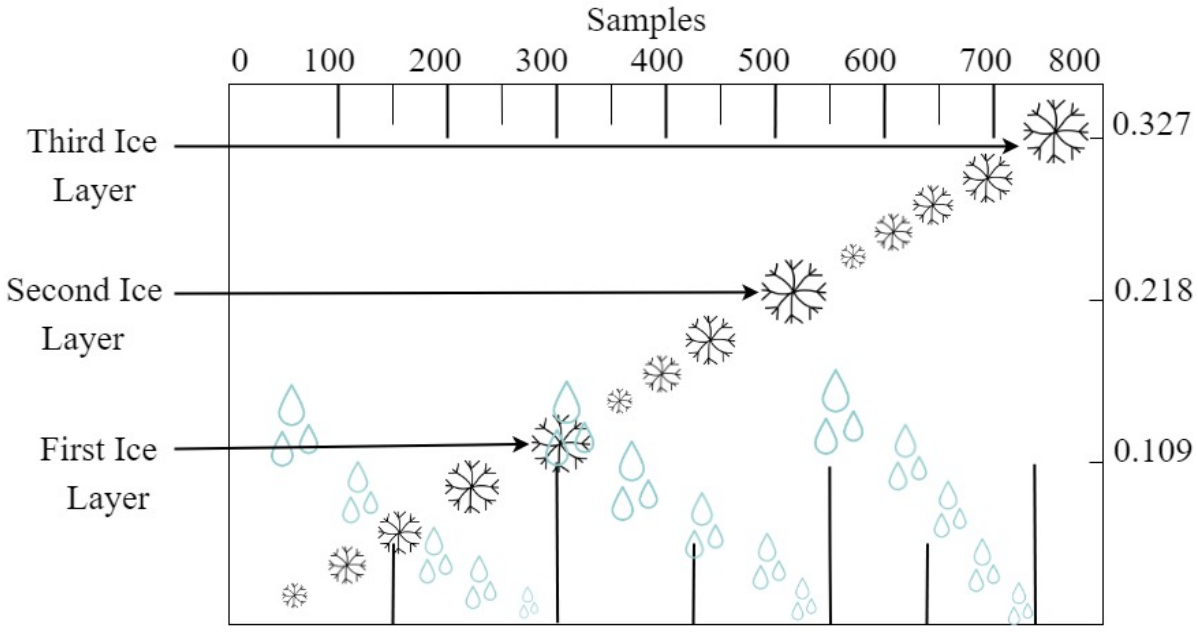

Figure 4.6: Main Idea for the Model of Ice and Water Experiment Data

4.5 Neural Network Mapping

Our previous work confirmed that an array of coplanar sensors of various spacing parameters has the ability to determine the ice phase and water phase individually. In this work we utilized an artificial neural network (ANN) to map the frequencies input to the ice accretion and water layer depth output. This is a novel method also used in other studies by McComber [45], Larouche et al [46], and Ohta [47]. For example ANN was used to predict the icing condition based on the temperature, wind speed, and precipitation rate. Gantasala [48] used two parameter frequencies and wind speeds to determine ice mass through the ANN.

In this research, capacitive sensor frequencies were used as input and the water-ice profile as output. Input-Output training data set was then created across 740 time samples. Figure 4.7 shows the architecture of the used ANN model, which has four neurons in the input layer for the four frequencies, twenty neurons in the hidden layer and two neurons in the output layer for ice and water.

The ANN processes the input information in the following manner:

$$\begin{aligned}
\mathbf{h_1} &= f1 * Wi1_1 + f2 * Wi2_1 + f3 * Wi3_1 \\
&\quad + f4 * Wi4_1 + Bi_1 \\
&\vdots \\
\mathbf{h_{20}} &= f1 * Wi1_{20} + f2 * Wi2_{20} + f3 * Wi3_{20} \\
&\quad + f4 * Wi4_{20} + Bi_{20} \\
\mathbf{h_n} &= f1 * Wi1_n + f2 * Wi2_n + f3 * Wi3_n + \\
&\quad f4 * Wi4_n + Bi_n
\end{aligned} \tag{4.1}$$

Wi, ***Wo***, ***Bi***, and ***Bo*** represent input weights, output weights, input biases, and output biases respectively.

The ANN output can be calculated by applying the output function from the net input and based on ***h*** values from hidden layers.

$$\begin{aligned} \mathbf{O_{Water}} &= (h_1 * Wo1_1) + (h_2 * Wo2_1) \\ &+ ..... + (h_{20} * Wo20_1) + Bo_1 \end{aligned} \tag{4.2}$$

$$\begin{aligned} \mathbf{O_{Ice}} &= (h_1 * Wo1_2) + (h_2 * Wo2_2) \\ &+ ..... + (h_{20} * Wo20_2) + Bo_2 \end{aligned} \tag{4.3}$$

$$\mathbf{O_j} = \sum_{j=1}^{2} \sum_{k=1}^{20} [[h_k * Wok_j] + Bo_j] \tag{4.4}$$

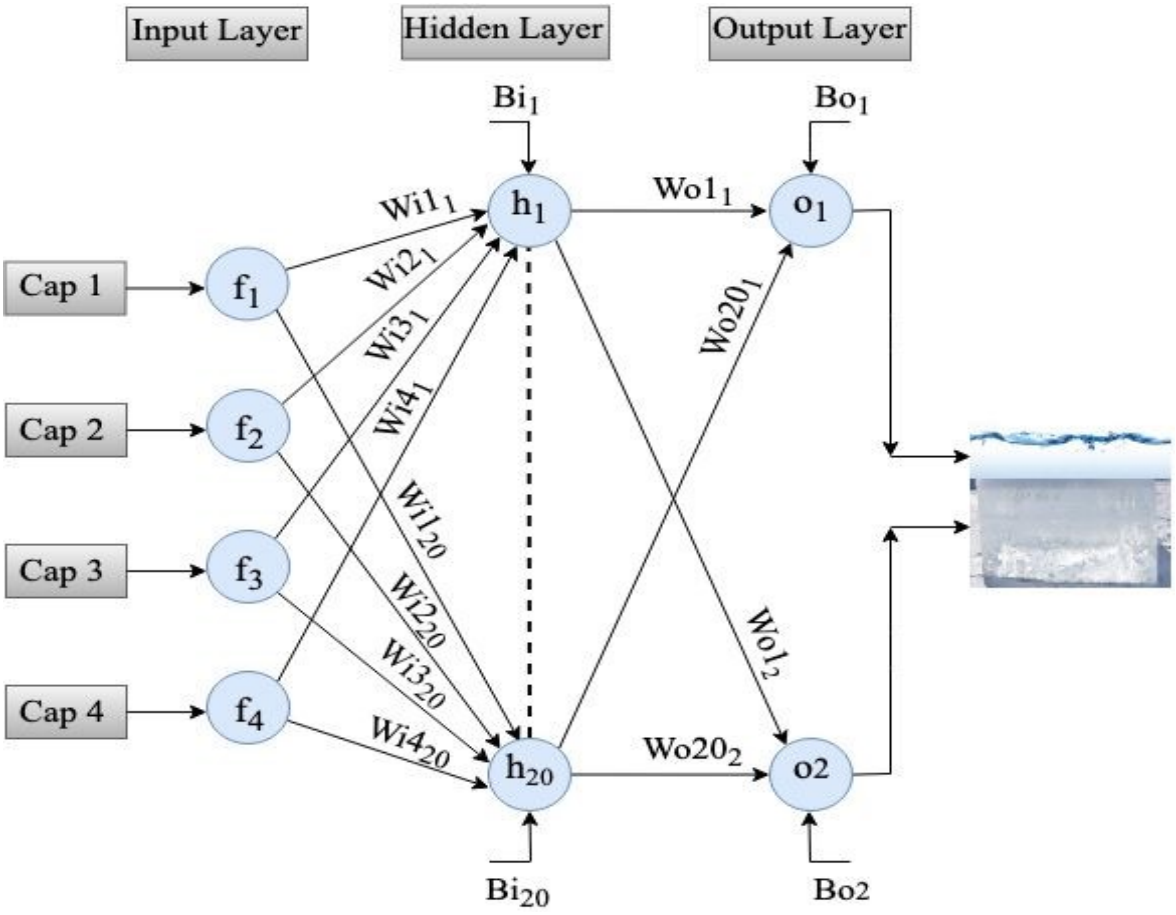

Figure 4.7: Neural Network Prediction Model

Figures 4.8 & 4.9 show the results from the ANN signal processing. Comparing this result to [44] repeated in Figure 4.10 without any detailed error analysis, one can observe the superiority of ANN algorithm over the least squares method in [44]. The nonlinear nature of tangent sigmoid neuron firing function in combination with the constant biases occurs to be a better fit to process the signals from linearly independent frequency data. Therefore we propose to use ANN over the least squares.

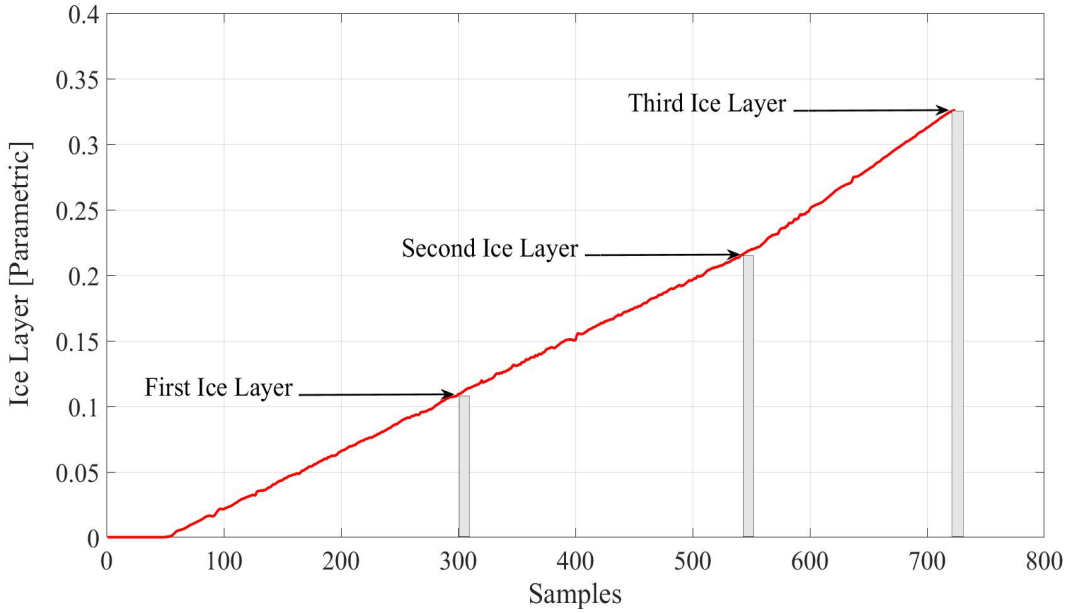

Figure 4.8: Ice Layers Predicted by the ANN Model

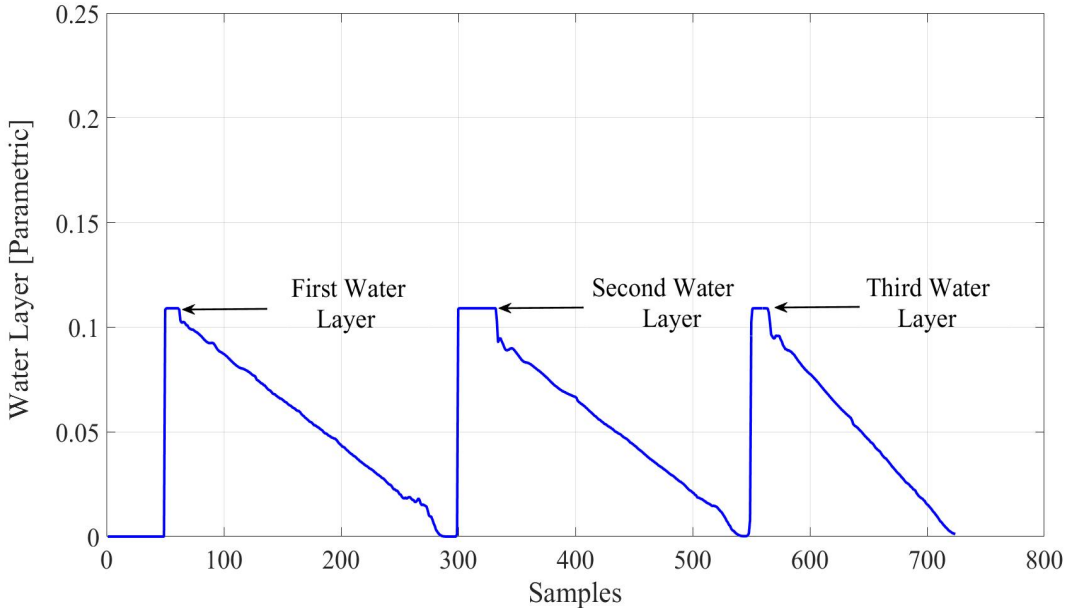

Figure 4.9: Water Levels Predicted by the ANN Model

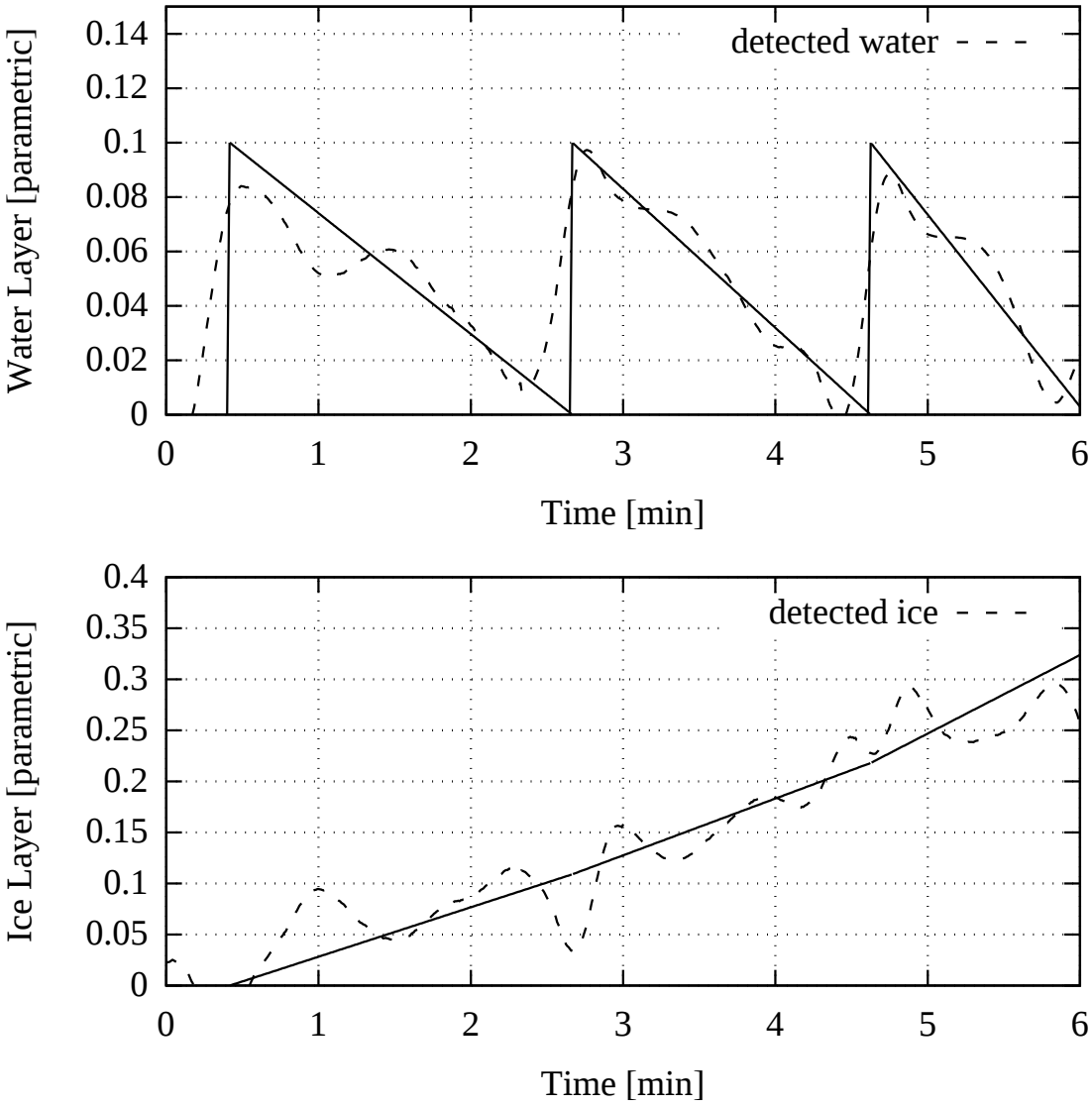

Figure 4.10: Water and Ice Levels Predicted by Least-Squares method in [44]

4.6 Conclusion

Our previous research revealed that an array of coplanar capacitive sensors on a PCB surface can detect the ice accretion rate in presence of a significant water layer. This work followed up in the research and proposed using an artificial neural network for signal processing instead of previously used least-squares method. We adopted a three layer ANN to process frequencies from four sensors, previously normalized and low pass filtered. As a result, the accuracy of ANN derived ice accretion and water layer is superior to the least squares method. However more work is needed to validate the method's robustness under a presence of signal drifting or a low frequency noise.

Chapter 5

Marine Icing Sensor with Phase Discrimination

Abdulrazak Elzaidi, Vlastimil Masek, Stephen Bruneau

A version of this chapter was published in:

MDPI Sensors — An Open Access Journal from MDPI Sensors, 17 January 2021, Communication Article, Remote Sensing

Sensors 2021, 21(2), 612; https://doi.org/10.3390/s21020612

5.1 Abstract

In this paper, a novel approach is presented to the measurement of marine icing phenomena under the presence of a two-phase condition. We have developed a sensor consisting of an electrostatic array and a signal processing based on a decision tree method. A three-element electrostatic array is employed to derive signals having linearly decoupled characteristics from which two key parameters, ice and water accretion layer dimension, can be determined for the purpose of environmental monitoring. The quantified characteristics revealed a correlation with the ice layer thickness in spite of the strong influence from the top water phase layer. The decision tree model established a relationship between the signal characteristics and the two accretion thickness parameters of water and ice layer. Through experimental verification, it has been observed that our sensor array in combination with the decision tree model based signal processing provides a simple practical solution to the challenging field of a two phase composition measurement such as in the marine icing considered in this study

keyword—electrostatic sensor Array; decision Tree Method; marine Icing.

5.2 Introduction

Marine Icing is an adverse phenomena affecting offshore vessels and other structures like wind farms [50] or oil and gas platforms [51]. Icing in general, including the atmospheric icing on airplane wings or transmission lines, poses a great deal of difficulties to many operations and can also be hazardous to personnel in the area especially the operators. The knowledge about the rate of ice growth besides the total accumulation would enable managing these hazardous conditions. One way to mitigate the challenging levels of icing is to heat trace the critical infrastructure or shutting down the operations.

Graz Technical University [24] applied a capacitive tomography to atmospheric icing on high voltage power lines. Graz team considered the two phase phenomena, ice and water, however, due to the focus on the atmospheric icing, the water phase was considered finely dispersed and embedded in the ice phase. We focus on marine icing with a significant water layer on top of the ice.

Combitech IceMonitor [9] measures the ice mass on a rotating rod by a load cell. The system requires a stationary installation which prevents this system being applied to ships and other marine structures due to the dynamic forces, vibration, wind gusts or dynamic water splashes.

The Goodrich 0871LH1 ice detectors [13] use an axially vibrating probe to detect the presence of light icing conditions. Goodrich ice detector is designed for thin ice layer applications like avionics and to the date no reports of detecting the ice under the water phase presence has been released.

HoloOptics T42 [8] employs IR signal passed through the medium and an external rain detector to eliminate the sources of false indications by water phase. No testing in marine icing conditions was conducted with the T42.

The Ice Meister Model 9734-SYSTEM industrial ice detector [12] monitors opacity and optical refraction of the ice along the contact with the probe surface. It only recognizes whether air, water or ice is present. This concept is somewhat similar to chilled mirror dew point sensor which often employs the optical reflectivity.

IDS-20 system [25] measures the complex impedance of the icing medium using capacitive plates hermetically sealed. The sensor can distinguish between water, however not in a combined multiphase state.

Jeung Sang Go with Xiang Zhi [10] employed capacitive sensors to measure ice growth in real time. The developed system has also been patented [26], however the authors conclude the water layer formation has to be prevented in order to maintain the accuracy. Charles Ezeoru [11]

conducted a similar research using the same capacitive technique with interdigitated comb-style electrodes. Both approaches experienced the transformation from liquid state to solid state which has been reflected in a ramp capacitance profile in time. Unfortunately, no one has tried to quantify the transitional multiphase period.

We have developed a sensor array that allows a flexibility to be applied on curved surfaces such as wind turbine wings. Our earlier work described in [52] utilized a planar array of electrostatic sensors of different spacing that have been instrumented by a custom circuitry based on LC oscillator. Here we report on using a constant-spacing electrostatic sensor array interfaced and conditioned by a commercial four-channel capacitive pickup board by Texas Instruments.

Previously we processed the array signals by a multidimensional least squares method [52] and in another approach by artificial neural networks [53]. In this work, we applied a machine learning strategy centered around a decision tree method.

Machine learning algorithms are being used in many applications ranging from flood prediction [54], solar radiation [55], to wind generator blade monitoring [56, 57]. Machine learning based on a decision tree method has been used in internet security systems [58] as well as in detecting stability of a power system voltage [59] or in classification tasks [60, 61].

The ice can take different formations described in [62], however, the dielectric properties remain nearly constant which is being exploited in this research work. The problem of marine icing detection is however complicated through the presence of a water phase on top of the ice layer since water's dielectric constant, the relative permittivity, is significantly larger than that of ice. The decision tree method has been found to meet our needs in recognizing and classifying the multiphase situations and provide a more accurate ice accretion measurement. This method translates the acquired signal data to a regression and classification model to determine the thickness of both layers of ice and water simultaneously.

5.3 Methodology

Our research into sensing and detecting the marine icing as a two phase phenomena has been initially founded on the principles of linearly decoupled array of electrostatic sensors of variable electrode gap spacing. The experimental verification confirmed our hypothesis of dissimilar gap spacing being capable to encode the stray electrostatic field above the sensor plane in a unique and linearly independent way. This phenomena was utilized in discriminating each individual phase, ice and water. Our team developed a multi-dimensional least-squares-method [52] to map the measured data to the measurands. The least-squares method was later substituted by a more robust and more accurate technique based on artificial neural networks method [53].

In this paper, we modified our earlier methods in four ways, (1) at the transducer array level (*constant gap spacing, variable insulator height*), (2) at the signal pick up circuitry (*commercial 4ch converter*), (3) at the signal processing algorithm level (*decision tree method*) and (4) at the spacial adaptation to curved surfaces (*structural flexibility*). Our earlier setup resulted in a large variation of capacitance range which required a custom build circuitry for capacitance to frequency conversion. In this work, we adapted an off-the-shelf signal detection board FDC2214EVM from Texas Instruments [63] which features four independent channels simultaneously scanned and a simple interfacing (Figure 5.1). FDC2214EVM module features 4-ch 28 bit capacitance-to-digital signal converters (FDC). The manufacturer also provides a software enabling the data streaming into a PC. In order to keep all array elements within a consistent accuracy range, we have built a new three element array of uniform elements (uniform spacing) that was attached to a curved surface of 80 mm radius (Figure 5.2).

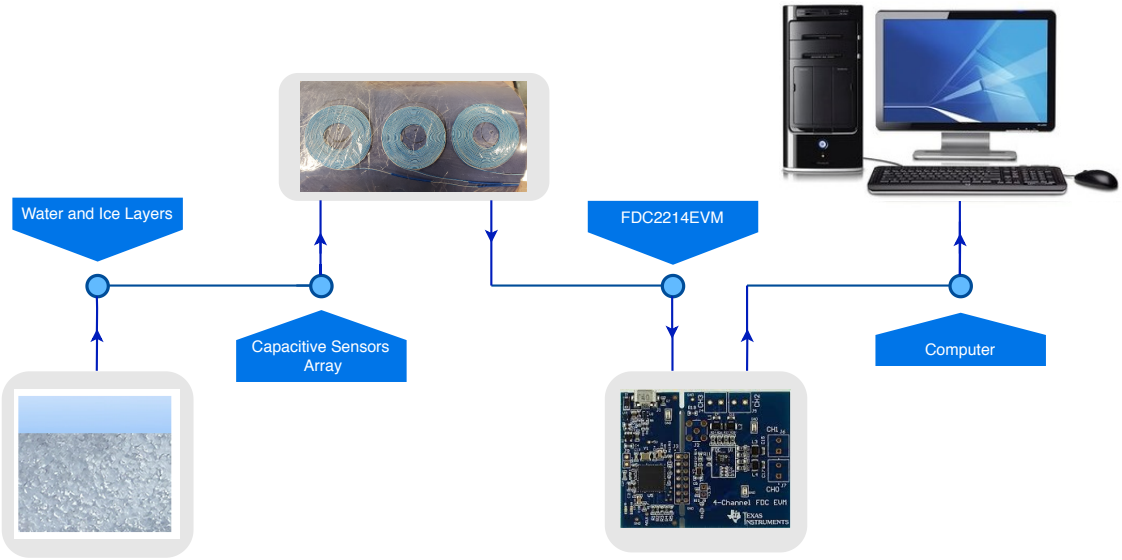

Figure 5.1: Interfacing Curved Capacitive Sensors Array with Computer by using FDC2214EVM.

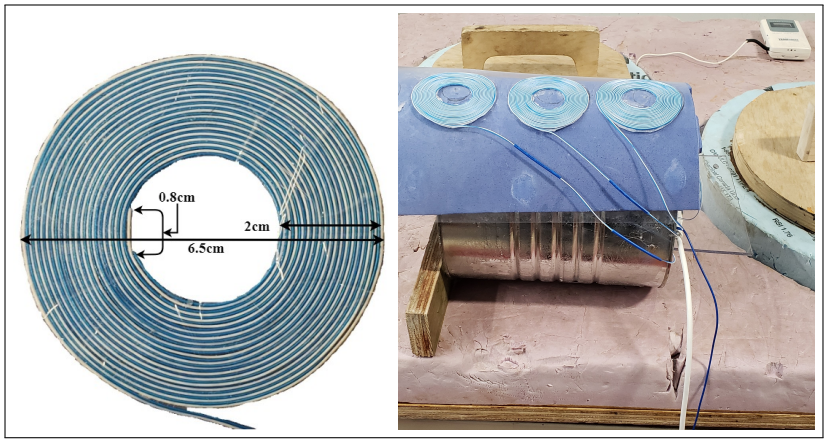

Figure 5.2: Spiral Capacitive Sensor Element.

In order to linearly decouple the measured capacitance across the array, we introduced three different dielectric layer heights. The capacitance of two elements was analyzed by a finite element method (FEM) using Ansys Maxwell software (Figure 5.3). The solid line characteristics represent the capacitance for an element having 0.25 mm coating of PET, plotted as constant capacitance contours across a range of ice and water accretion levels. The dotted line corresponds to 0.35 mm

dielectric coating layer. The graph demonstrates a linear independence in a similar way to the gap variation analysis in [52] though not as profoundly. The FEM parameters are listed in Table 5.1.

Material	ε_r
air	1.0006
water	81
ice	4.2
PET	3.6

Table 5.1: FEM Model Parameters

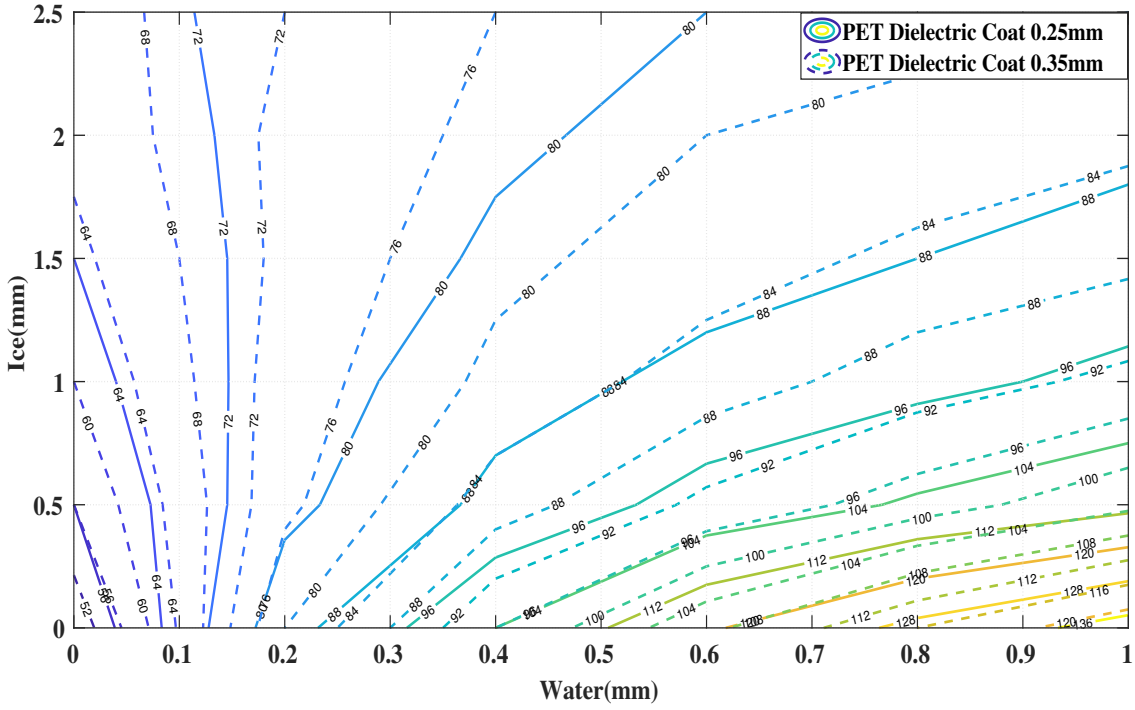

Figure 5.3: Contours of Constant Capacitance for Sensor Geometries 0.25 mm and 0.35 mm.

Any traditional insulation material that is not permeable to water will provide the function of eliminating the conductance (real part) from the impedance measurement. PET sheets were readily available to us and their dielectric constant is similar to the epoxy resin used in the past. The critical part in obtaining the linearly independent characteristics across the array is in a different number of stacked layers of PET sheets above each array element.

5.4 Experimental Validation

We have conducted a series of ice layer deposition experiments in a similar way described in [52] using a water saturated roller. The system was placed in a deep freezer at -20 °C and was initially tempered for 1 h. Then, over a period of two hours, we have periodically rolled a water layer onto the sensor surface which is illustrated in Figure 5.4. Each peak corresponds to a new wetting cycle during which the capacitance rises sharply. If we were to consider only the ice layer as a number of previously developed sensors were based upon, the reported ice layer accretion would follow the same sharp increase causing a large discrepancy from the real situation. A low pass filter could be applied to remedy these time limited deviations however the water phase could also be present at all times in situations of icy waters constantly battering the place of interest.

Figure 5.4 shows six transitional cycles where each cycle starts with a fresh water layer that gradually solidifies into a new ice layer. Each cycle took approximately fifteen minutes to settle. Our experimental approach is based on an assumption that each deposited layer is consistent with all the other layers without the need for knowing its exact dimensions which constitutes a parametric approach.

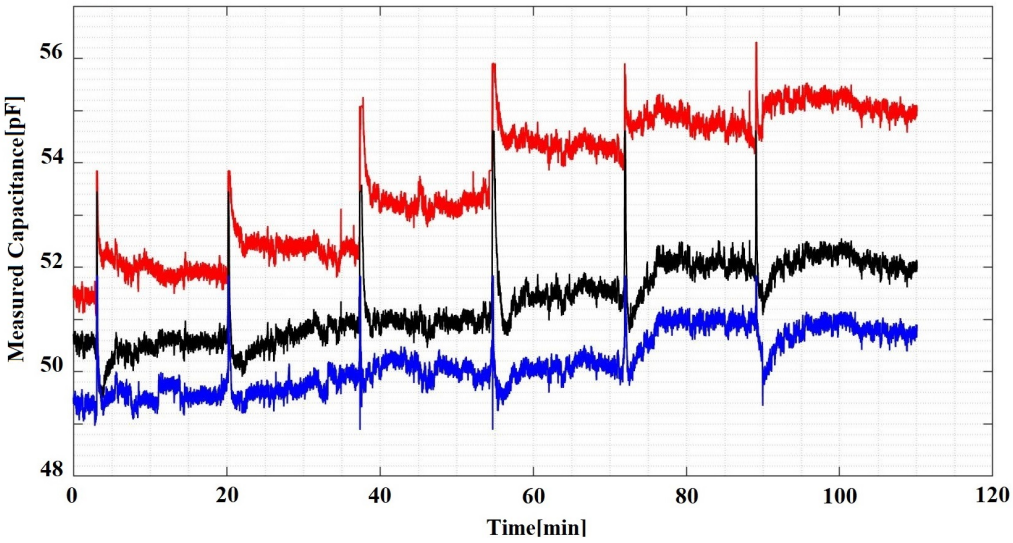

Figure 5.4: Experimental Data from Curved Capacitive Sensors Array.

5.5 Signal Processing

The Decision tree model is constructed from the main root branches consisting of the interior nodes and the final nodes also called the decision nodes [64]. The tree represents a mapping characteristic between the signal data and the target parameter, the ice accretion besides the water phase information as a byproduct.

We have split the acquired signal data and the corresponding ice and water accretion estimate into the training data set and the test data set. The training data is used to derive the decision tree parameters during the training phase. Figure 5.5 shows both the training and the testing processes. The training data set consists of 50% of data points from all the acquired data (odd rows in a column vector). Once the relationship between input data and the measurand was established, the testing phase has been conducted on the test data (even rows).

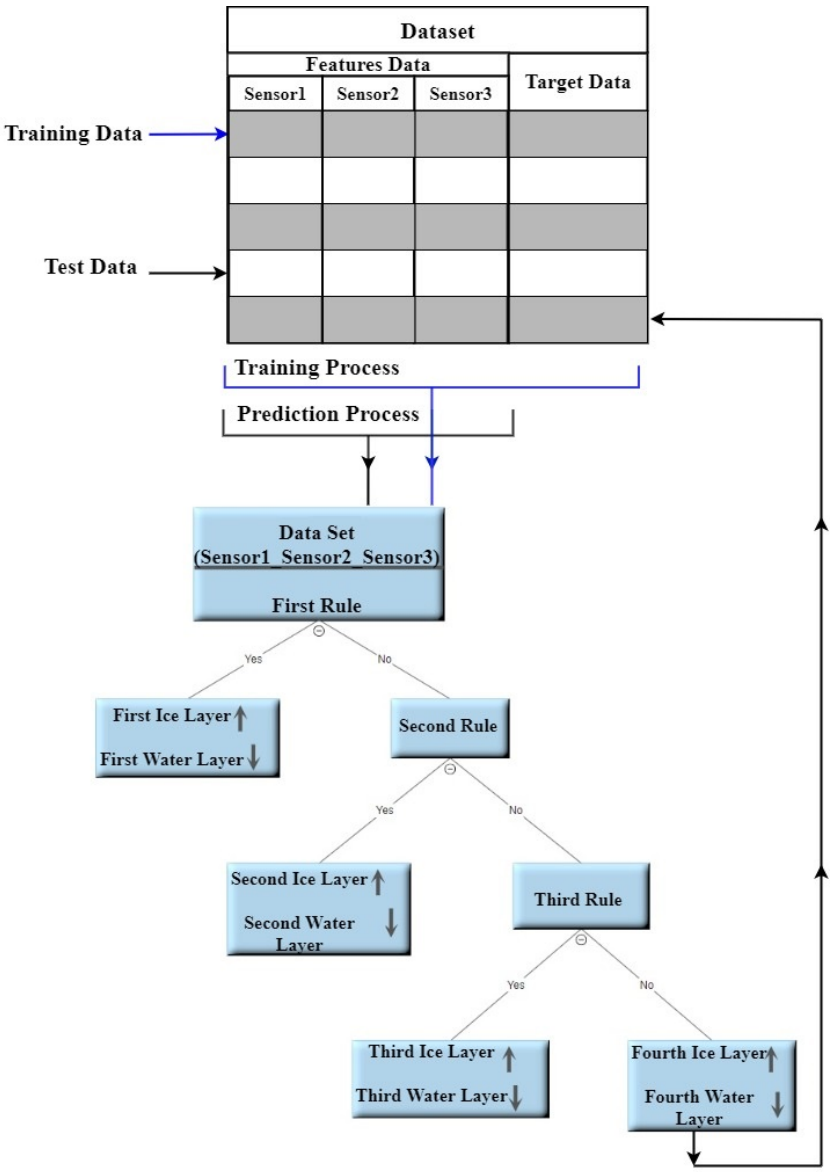

Figure 5.5: The Decision Tree Processes.

Figure 5.6 shows the 'pairplot' data set illustrating the relationship and its weight between the sensor data and the output classes. Our decision tree implementation is based on the Entropy rule described in [65].

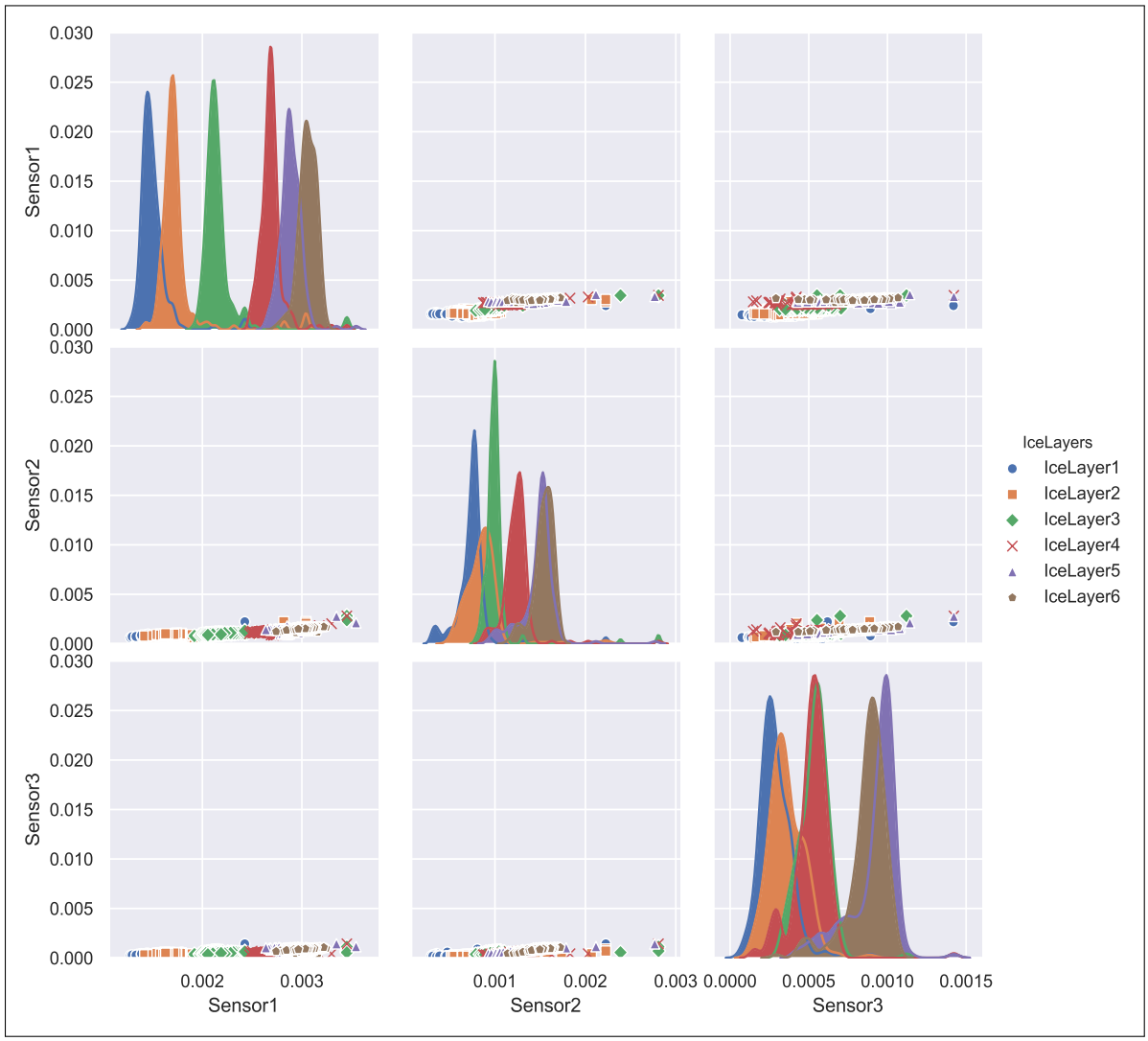

Figure 5.6: Pairplot data set for curved capacitive sensors array.

In comparison to other models like the Gini rule, the entropy model performed better in our specific application. Both rules are characterized in Equation (5.1) with p_i being the entropy measure.

$$\textbf{Gini} = 1 - \sum_{i=1}^{c} (p_i)^2$$

$$\textbf{Entropy} = \sum_{i=1}^{c} - p_i log_2(p_i) \tag{5.1}$$

Figure 5.7 shows our assumption in the time profile of our anticipated data of ice accretion (dotted line) and the water level height (solid line) [52]. At the end of each cycle, the water layer is completely converted into the ice.

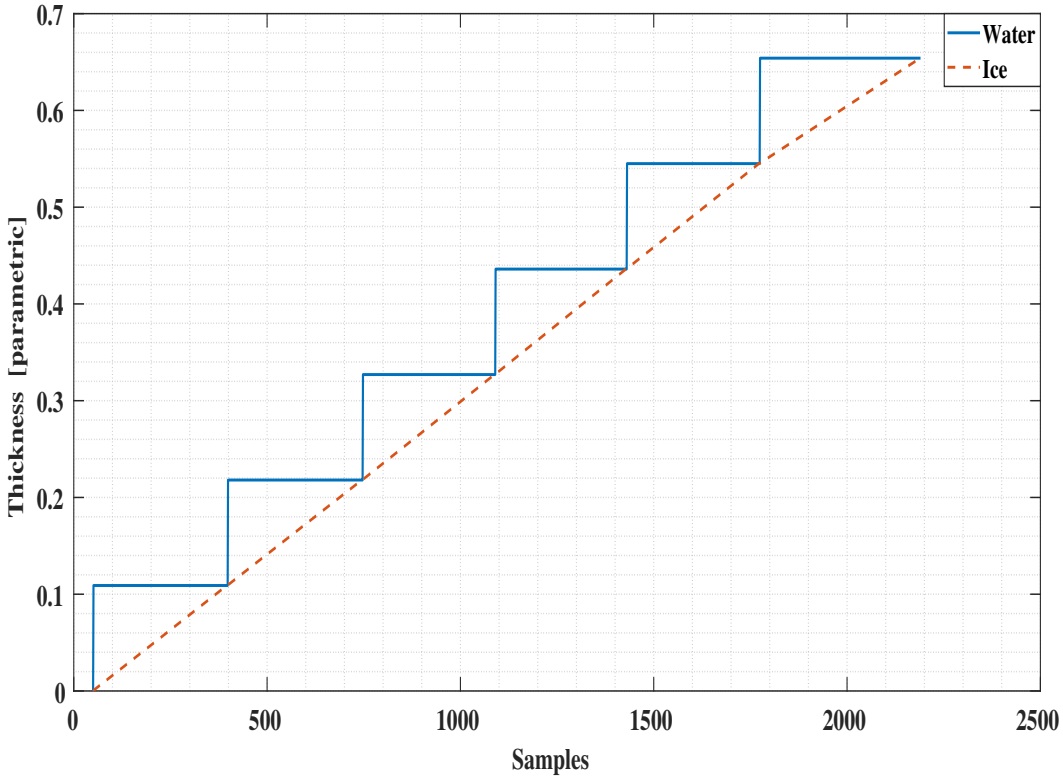

Figure 5.7: Ice and Water accretion in time during the experiment.

5.6 Results

We implemented a twelve level deep decision tree processes the measured data based on entropy value where a low entropy value leads to the best leaf node in terms of purity. Applying the trained decision tree model to the test data results in the ice accretion estimate depicted in Figure 5.8 and the water layer estimate depicted in Figure 5.9. Both profiles show a significant improvement over the earlier results reported in [52] and a corresponding results to the ANN approach in terms of the ice accretion [53].

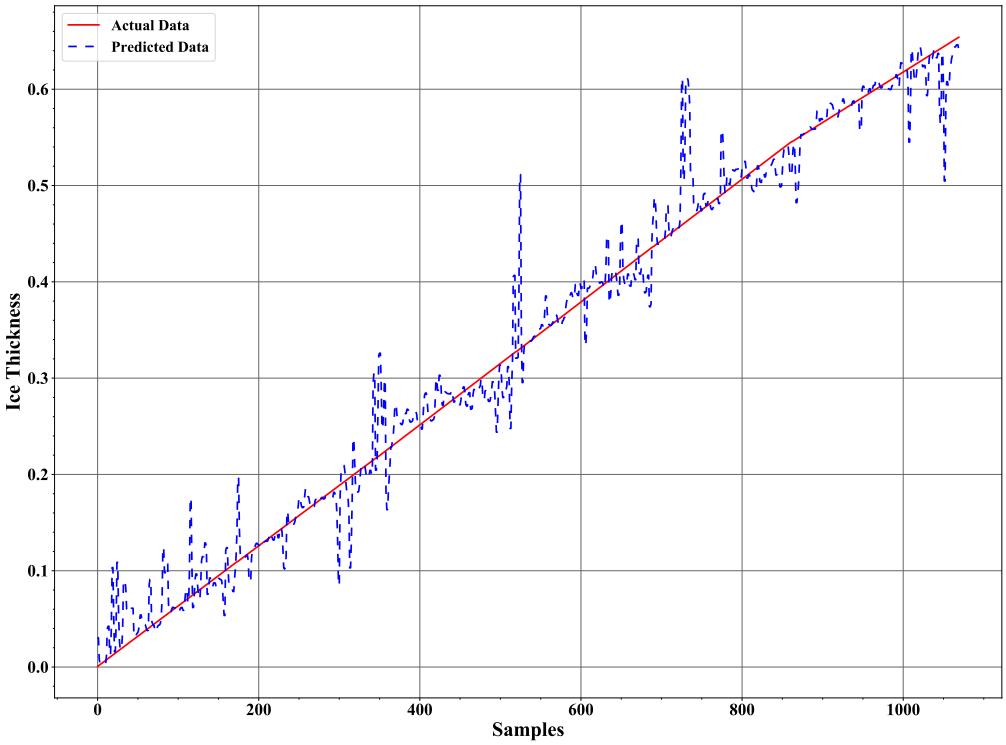

Figure 5.8: The ice accretion estimate in comparison to the assumed data characteristic.

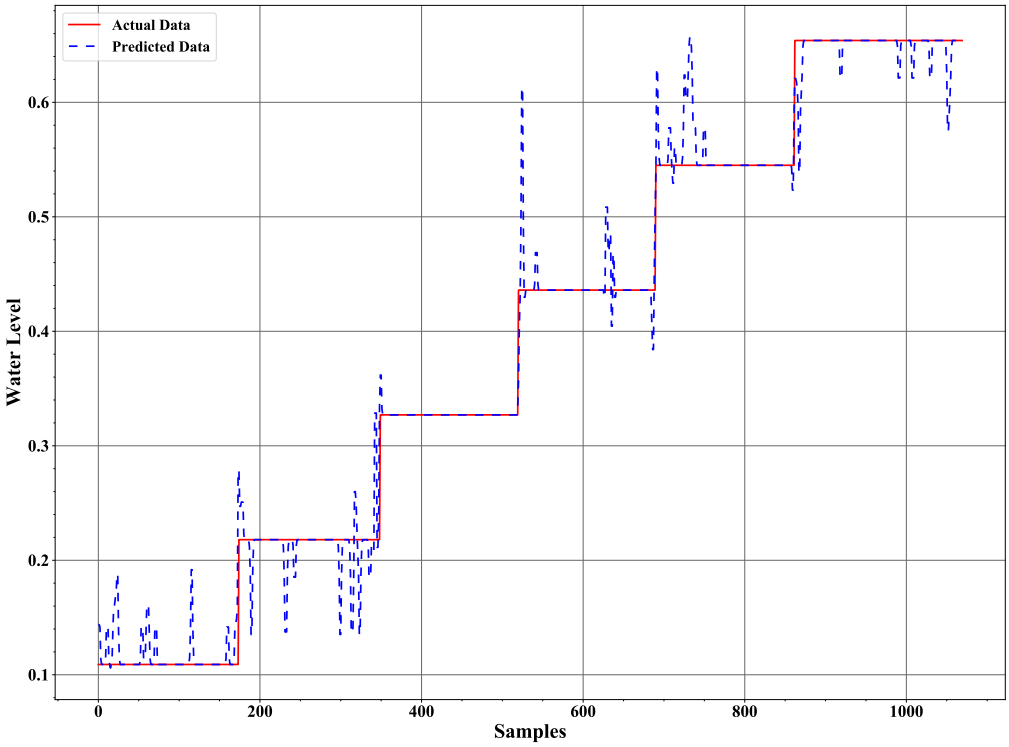

Figure 5.9: The water layer estimate in comparison to the assumed data characteristic.

The Precision, Recall, F-Measure and Accuracy are commonly used for evaluating classification methods in Machine learning [66]. Precision is the ratio between the correct positive predicted classes for a layer and the total number that includes the correct and incorrect positive classes predicted for the same layer. Recall is the ratio between the correct positive predicted classes for a layer and the total number of the correct and incorrect negative classes predicted for the same layer. F-Measure makes a harmonic relation between Precision and Recall. These parameters were calculated as follows:

$$\begin{aligned} \text{Precision} &= \frac{TP}{TP+FP} \\ \text{Recall} &= \frac{TP}{TP+FN} \\ \text{F-Measure} &= \frac{2 \times \text{Precision} \times \text{Recall}}{\text{Precision} + \text{Recall}} \end{aligned} \tag{5.2}$$

True Positive (TP) is a classification method outcome where the decision tree method generates a correct positive class layer. Likewise, True Negative (TN) is a classification method outcome where the decision tree method generates a correct negative class layer. False Positive(FP) and False Negative (FP) are a classification method outcome where the decision tree method generates incorrect positive and negative class, respectively.

The Confusion-matrix yields the most ideal suite of metrics for evaluating the performance of a classification algorithm. Gupta [67] provides a detailed description on the confusion matrix as a measure of determining the accuracy of the decision tree classification model. The confusion matrix for ice and water classifier is a 6x6 matrix illustrated in Figure 5.10 with the elements along the diagonal representing 'True Predicted' data. The overall accuracy for the prediction model of Ice and Water Classifier recorded accuracy of 92.8%.

The conventional method of using the least squares method to our experimental data as reported in [52] is presented in Figures 5.11 and 5.12. Comparing these results with the decision tree results clearly indicate the level of improvement by using the new signal processing method. A comparison with the ANN method applied to the same data(Figures 5.13 and 5.14) reveals a similar error characteristic in the ice accretion. The comparison analysis is quantitatively summarized by a root mean squares error analysis presented in Table 5.2. Both the decision tree and the ANN methods are equivalent in terms of the ice accretion measurement estimation, however, the current tree approach offers more lightweight implementation suitable for a microcontroller based system.

Method	Medium	Root Mean Square Error	Mean Absolute Error
Decision Tree	water	0.0231	0.0082
	ice	0.0291	0.01704
Least Squares [52]	water	0.0453	0.0336
	ice	0.0556	0.0424
Neural Network [53]	water	0.0144	0.0072
	ice	0.0214	0.01702

Table 5.2: Error Analysis

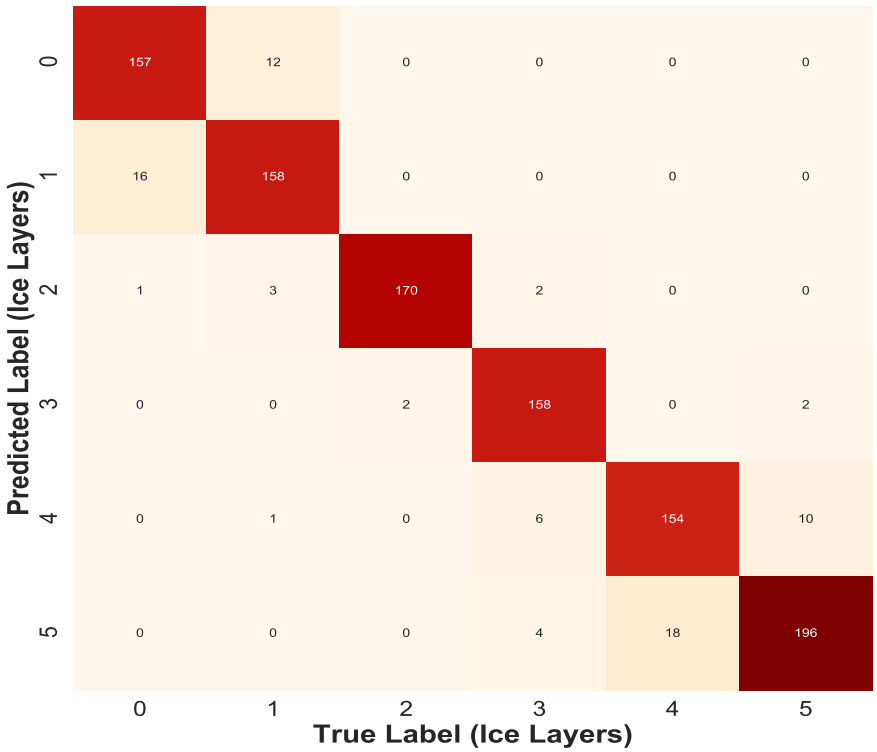

Figure 5.10: Confusion Matrix for Decision Tree Ice Classifier.

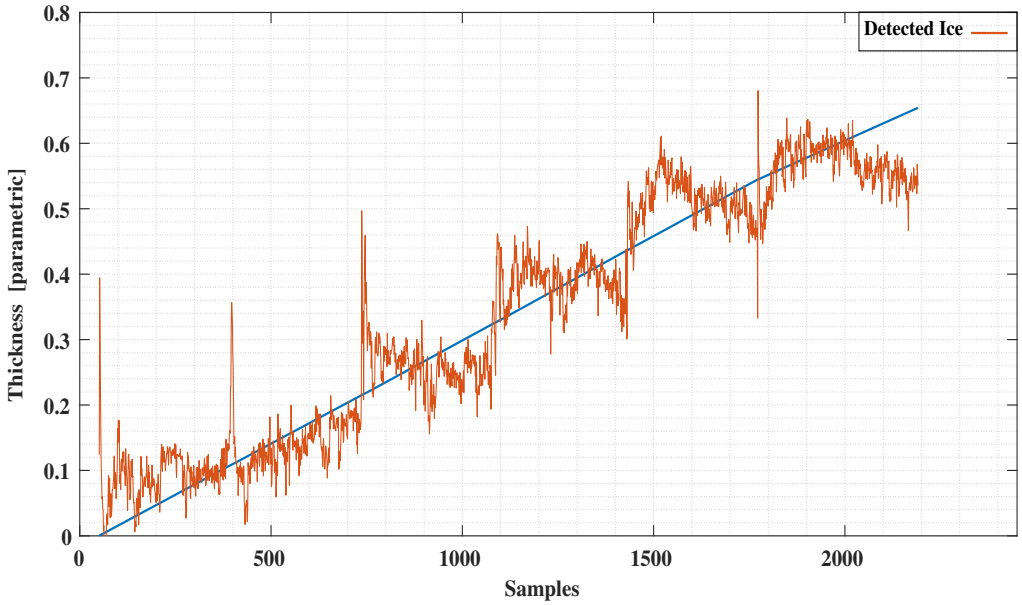

Figure 5.11: Detected Ice vs. Predictions using Least Squares.

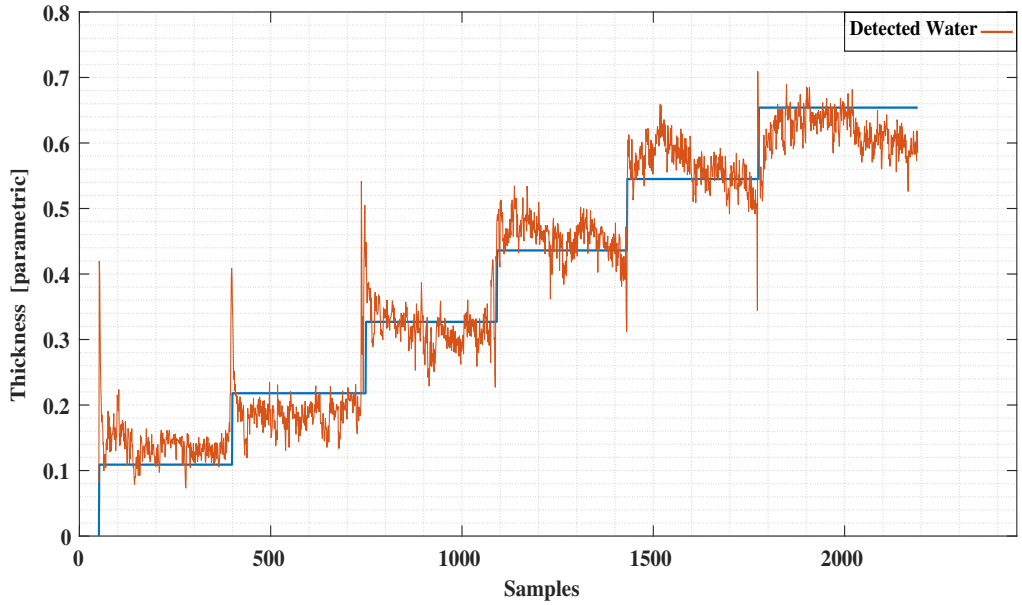

Figure 5.12: Detected Water vs. Predictions using Least Squares.

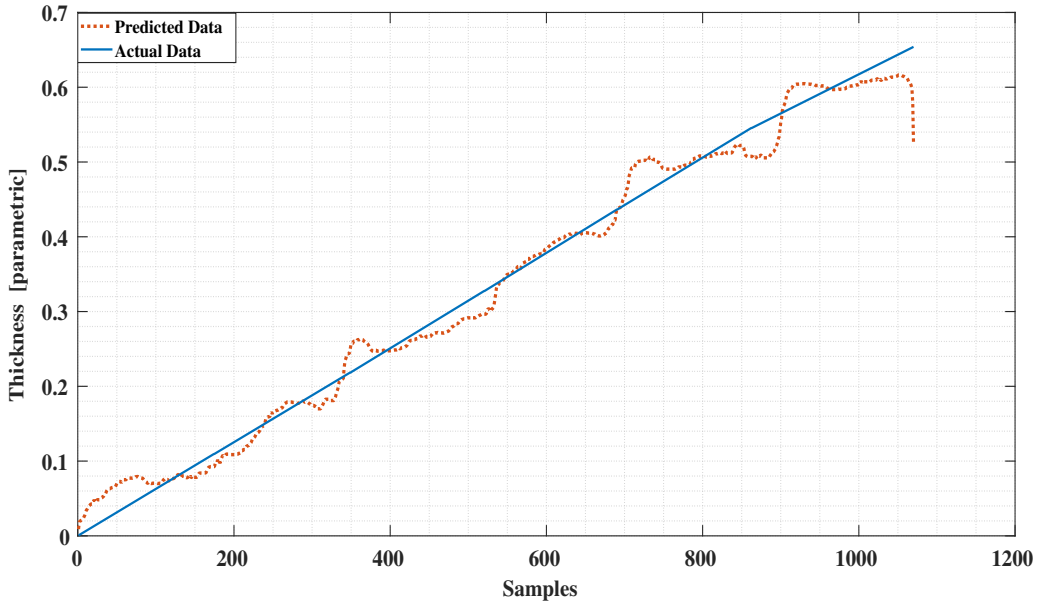

Figure 5.13: Detected Ice vs. Predictions using Neural Network.

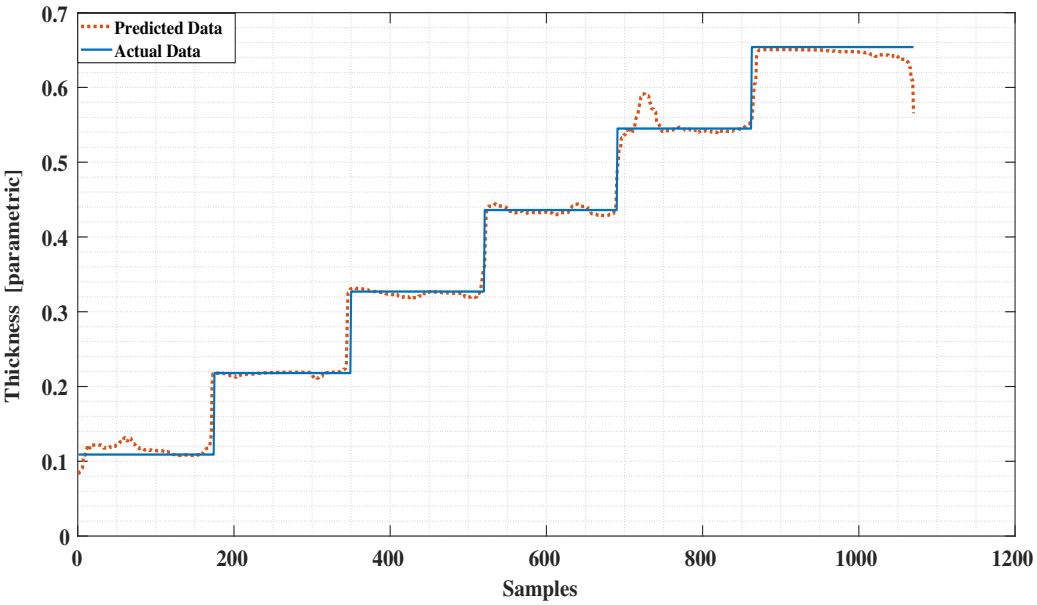

Figure 5.14: Detected Water vs. Predictions using Neural Network.

5.7 Conclusions

A novel sensor array has been developed to measure the marine icing accretion and to allow flexibility in deployment over curved surfaces. A new signal processing method based on a decision tree method has been applied to the array data. A theoretical analysis confirmed linearly decoupled signal characteristics that are critical in discriminating the water phase influence on the ice accretion measurement. An experimental analysis validated the high relevance of employing the decision tree method for signal processing. The ice accretion estimate obtained through the decision tree method demonstrates a significant improvement over the conventional least square method and a similar characteristic with the Neural Network method, however of a lesser computational overhead and a smaller footprint. Our three element capacitive array is easy to fabricate with off-the-shelf components and the 4 ch 28 bit signal processing interface circuit from TI is also aligned with a very low cost characteristics. The nature of our non-contact based design without any moving parts and the low cost characteristics promises a robust solution towards the marine icing measurement under the harsh environmental conditions.

Chapter 6

Conclusion and Future Work

6.1 Introduction

Accumulation of ice is a major problem for structures that operate in the arctic marine environment. It is important to know the rate of accumulation, or ice accretion, in the real time. This thesis proposed three variants of a low cost sensor that can detect the ice accretion with accuracy exceeding the previously proposed methods and in many cases also the commercially produced systems.

We have subjected our sensor systems to experimental evaluation at MUN Thermo-Fluid Laboratory. Two physical variants of capacitive sensor array have been built, tested and the data have been processed using three different signal processing algorithms. We first studied the array of variable gap sensors and used a multidimensional least-squares method (LSQ, Chapter 3) and then Artificial Neural Network method (ANN, Chapter 4) for the data processing. Later, we studied a new design of uniform gap array with variable surface insulation layer thickness (the bottom dielectric layer) using a decision tree algorithm.

The capacitive sensor array geometries have been first simulated and then manufactured using the common low-cost PCB technology. We used Ansys Maxwell finite elements method to simulate two-phase icing phenomena prior to the experimental verification. In Chapter 3 and 4, we also constructed our own design of capacitance to frequency converter for data acquisition based on analog oscillator array. Chapter 5 described a data acquisition method using a commercial system from Texas Instruments.

All three methods (Chapters 3-5) outperformed the existing systems due to the fact that the top water phase was accounted for in our approach. No comparative experimental study has been conducted though. The performance of our system has been compared to the performance of other systems based on the literature survey. Yet the absence of regard for the water phase layer and/or the marine icing specifics makes us believe that our proposed systems will provide the safety critical information about the icing accretion in the real time reliably and with a sufficient accuracy.

6.2 Contributions

Sensor systems for detection of ice accretion on marine structures have been designed, fabricated and tested. All our designs feature a planar spiral geometry that has been analyzed by the Electrostatics module in ANSYS Maxwell. The proposed sensors can detect both the thickness of ice layer and the thickness of water layer on marine structures simultaneously. When the marine icing is concerned, this is a new approach. The water layer information is not critical to collect data about however the water layer significantly influences the ice accretion measurement. This can be explained on the temperature compensation in other types of sensing methods in which case the ambient temperature effects have to be accounted for to increase the accuracy of the main measurement, not the temperature measurement.

Two journal papers (Chapter 3 and 5) and one full-paper peer-reviewed conference contribution (Chapter 4) have been published. Both publishers IEEE and MDPI are placed on top of the impact-factor scale.

The proposed methods do not just refer to the relatively narrow field of marine icing phenomena but have a broader impact as well. Our studies also make contributions to the wider sensor science and multiphase phenomena sensing in other industries like oil and gas, food or pharmaceutical. We outline methods that researchers can follow and further advance to suit their own specific field of multiphase or multivariable sensing.

The following are the itemized research contributions:

1. The study proposed experimentally verified methods for marine icing sensing.

2. The accuracy of marine icing sensing has been increased by accounting for the water phase.

3. FEM simulation was employed to pre-validate the initial hypothesis of multivariable sensing using the contour crossing graphs that has not been reported before.

4. In-house design of capacitance-to-frequency has been proposed, implemented and experimentally evaluated. Each oscillator in the array is isolated in a Faraday cage (both electrostatic and magnetic) and all oscillators track the same temperature. Since our method only evaluates the differences, potential temperature drift does not effect the result accuracy.

5. A low-cost design has been considered to allow deployment on curved surfaces which has not been reported before. This allows for use on curved blades of wind turbines for example.

6. Employing a multidimmensional Least Squares Method to the unique capacitive array data (Chapter 3)

7. Examining the effect of capacitance drifting on the results accuracy (Chapter 3)

8. Improving the LSQ method by using Artificial Neural Networks (Chapter 4).

9. Designing a new capacitive array sensor to match a novel machine learning algorithm based on the decision tree method. (Chapter 5)

10. All three methods proposed in this thesis are published in high-impact journals.

6.3 Future Work

The research discussed in this thesis is part of a large field of study in marine icing sensing and multiphase sensing in general. This work provides a starting point for the use of the capacitive sensing array in multivariable monitoring systems. This work further emphasizes the use of capacitive sensing array as a cost-effective and more reliable alternative to the other ice sensing methods designed primarily for terrestrial applications, homogeneous ice compositions and static deployment on stationary (non moving) objects.

One area I would like to see further development relates to the hardware of data acquisition system. If there is an opportunity, I propose to borrow a concept used in metal detectors where only the difference of two oscillators is detected. This would provide a higher quality signal data in my opinion.

We also designed the system being potentially deployed on curved surfaces but never conducted an extensive experimental work with such arrangement implemented. This is the area of primary focus in the offshore wind power generation using wing turbines. The future work shall conduct a series of experiments on different curvature surfaces.

Our experimental validation conditions were simulated in the laboratory conditions. In order for our methods to gain a broader acceptance and practical deployment, additional validation in the real field conditions is needed. This is an expensive proposition but a necessary one to raise the TRL (technical readiness level) to pre-commercial state.

Bibliography

[1] Saeed R. Dehghani et al, *A finite difference solution for freezing brine on cold substrates of spongy ice*, International Journal of Heat and Fluid Flow, pp 174-184, Feb 2018.

[2] Saeed R. Dehghani et al , *Analysis of ice accretion on vertical surfaces of marine vessels and structures in arctic conditions*, OMAE2015, St. John's, 2015

[3] S. Fikke, et al., *COST 727: Atmospheric Icing on Structures Measurements and data collection on icing: State of the Art*, Publication of MeteoSwiss, 2006

[4] René Cattin & Ulla Heikkilä, *Evaluation of Ice Detection Systems for Wind Turbines*, Weather Forecasts - Renewable Energies - Air and Climate - Environmental IT, METEOTEST 2016

[5] Kulyakhtin, A.Numerical Modelling and Experiments on Sea Spray Icing. PhD thesis, NTNU - Norwegian University of Science and Technology, 2014.

[6] Homola, M., Nicklasson P., and Sundsbø, P., 2006, "Ice sensors for wind turbines", Cold Regions Science and Technology, vol. 46, pp. 125-131

[7] Labkotec (2011), "LID-3300IP Ice Detector, Installation and Operating Instructions", Technical manual

[8] *T40 series of Icing Rate Sensors*; HoloOptics, User Guide. Katarinavägen 22, S116 45 Stockholm Sweden/Suede, 2010.

[9] Combitech, The Ice Load Surveillance Sensor IceMonitor, Product Sheet, 2013. Available online: `Http://www.rwis.net/res/pdffiles/IceMonitor_Product_Sheet.pdf` (accessed on 23 December 2020).

[10] Zhi, X.; Cho, H.C.; Wang, B.; Ahn, C.H.; Moon, H.S.; Go, J.S. Development of a Capacitive Ice Sensor to Measure Ice Growth in Real Time. *Sensors* **2015**, *15*, 6688–6698; ISSN 1424-8220.

[11] Ezeoru, C. Marine Icing Sensor Design Using Capacitive Techniques. Master's Thesis, Memorial University of Newfoundland, St. John's, NL A1B 3X5, Canada, August 2016.

[12] *Ice Meister Model 9734—Industrial Ice Detecting Sensor System*; New Avionics Corporation, Technical Data Sheet. 2501 East Commercial Blvd, Fort Lauderdale FL 33308 USA, 2016.

[13] *Goodrich Ice Detector Models 0871LH1*; UTC Aerospace Systems: Burnsville, MN, USA, 2013.

[14] Owusu KP, Kuhn DC, Bibeau EL. Capacitive probe for ice detection and accretion rate measurement: Proof of concept. Renewable energy. 2013 Feb 1;50:196-205.

[15] H. Semat and R. Katz, "Research Papers in Physics and Astronomy," in Capacitance and Dielectrics, Nebraska, Robert Katz, 1998, pp. 461-487.

[16] L. K. Baxter, *Capacitive sensors, design and applications*, in IEEE Press, New York, 1997

[17] C. Belmont and H.H. Girault. "Coplanar interdigitated band electrodes for synthesis Part I: Ohmic loss evaluation". In: Journal of Applied Electrochemistry 24.6 (1994), pp. 475–480.

[18] Bose, Neil. "Icing on a small horizontal-axis wind turbine—Part 1: Glaze ice profiles." Journal of wind engineering and industrial aerodynamics 45, no. 1 (1992): 75-85.

[19] Foder, Mogens H. "ISO 12494" Atmospheric Icing of Structures" and How to Use It." In The Eleventh International Offshore and Polar Engineering Conference. International Society of Offshore and Polar Engineers, 2001.

[20] Azam Fazelpour et al, *Ice Load Measurements on Known Structures Using Image Processing Methods*, World Academy of Science, Engineering and Technology International Journal of Electrical and Computer Engineering Vol:11, No:8, 2017

[21] Azam Fazelpour et al, *Effect of Ambient Conditions on Infrared Ice Thickness Measurement*, IEEE NECEC Conference 2016

[22] Azam Fazelpour et al, *Infrared Image Analysis for Estimation of Ice Load on Structures*, Offshore Technology Conference 2016

[23] Taimur Rashid et al., *Measuring thickness of marine ice using IR thermography*, Cold Regions Science and Technology, https://doi.org/10.1016/j.coldregions.2018.08.025

[24] Markus Neumayer, Thomas Bretterklieber, Matthias Flatscher, *Signal Processing for Capacitive Ice Sensing: Electrode Topology and Algorithm Design*, IEEE Trans on Instrumentation and Measurement, Vol. 68, No. 5, May 2019

[25] *IDS-20 Product Information*; SOMMER Messtechnik. Sommer GmbH, Strassenhaeuser 27, A-6842 Koblach,V-11/2016.

[26] Jeung Sang Go, Ice thickness measurement sensor. Patent No: US 10,066,923 B2. Date of Patent : 4 Sep. 2018. Available online: `Http://patentimages.storage.googleapis.com/bd/75/23/9016fcbfb5cbc2/US10066923.pdf` (accessed on 23 December 2020).

[27] Khalil I. Arshak, *Development of a Wireless Pressure Measurement System Using Interdigitated Capacitors*, IEEE Sensors Journal Vol 7 No 1, pp 122-129, Jan 2007

[28] Yu Gong et al, *Research on Coplanar Capacitive Sensor Design for Film Thickness Measurement*, Advanced Materials Research, Vols. 945-949, pp 2030-2036, 2014

[29] Tianming Chen, N. Bowler, *Analysis of a concentric coplanar capacitive sensor for nondestructive evaluation of multi-layered dielectric structures*, IEEE Transactions on Dielectrics and Electrical Insulation, 2010

[30] Shahid Malik et al, *Impedance-to-Time Converter Circuit for Leaky Capacitive Sensors With Small Offset Capacitance*, IEEE Sensors Letters, Vol.3, No. 7, July 2019

[31] Alex Risos et al, *A 3-D Faraday Shield for Interdigitated Dielectrometry Sensor and Its Effect on Capacitance*, MDPI Sensors, 2017, 17(1), 77

[32] Alex Risos et al , *Interdigitated Sensors: A Design Principle for Accurately Measuring the Permittivity of Industrial Oils*, IEEE Sensors Journal, Vol. 17, No. 19, October, 2017

[33] Alex Risos, *Interdigitated Sensors: The Next Generation Sensing Permittivity and Conductivity of Oils - Unaffected by Temperature*, IEEE Sensors Journal, Vol. 18, No. 9, May, 2018

[34] Alex Risos, Gideon Gouws, *In-situ aging monitoring of transformer oil via the relative permittivity and DC conductivity using novel interdigitated dielectrometry sensors (IDS)*, Elsevier Sensors and Actuators, B. Chemical 287, 2019

[35] Tianming Chen et al, *Analysis Of A Concentric Coplanar Capacitive Sensor Using A Spectral Domain Approach*, AIP Conference Proceedings 1335, 1647 (2011); 10.1063/1.3592126

[36] J. Ortiz, V. Masek *Cyclonic Capacitive Sensor for Multiphase Composition Measurement*, Sensors & Transducers, Vol. 191, Issue 8, pp. 1-11, 2015

[37] D. Wang, *FDC1004: Basics of Capacitive Sensing and Applications*, Texas Instruments, 2014

[38] N. Bowler, Tianming Chen *Concentric coplanar capacitive sensor system with quantitative model*, Patent: US8791707B2, July 2014

[39] Willem Chr. Heerens, *Application of Capacitance Techniques in Sensor Design*, J. Phys. E: Sci. Instrum., 19, 1986 pp.897-906

[40] Taimur Rashid, Hassan Abbas Khawaja & Kåre Edvardsen (2016) Review of marine icing and anti-/de-icing systems, Journal of Marine Engineering & Technology, 15:2, 79-87, DOI: 10.1080/20464177.2016.1216734

[41] Chokmani K, Khalil B, Ouarda TB, Bourdages R. Estimation of river ice thickness using artificial neural networks. InProc. 14th Workshop Hydraulics Ice Covered Rivers. CGU HS/CRIPE 2007 (p. 12).

[42] X. Zhi, H. C. Cho, B. Wang, C. H. Ahn, H. S. Moon, and J. S. Go, "Development of a capacitive ice sensor to measure ice growth in real time," Sensors, vol. 15, pp. 6688–6698, Mar. 2015.

[43] M. Neumayer, T. Bretterklieber, and M. Flatscher, "Signal processing for capacitive ice sensing: Electrode topology and algorithm design," IEEE Trans. Instrum. Meas., vol. 68, no. 5, pp. 1458–1466, May 2019

[44] A. Elzaidi, V. Masek and Y. Muzychka, "Phase Discrimination in Marine Icing Using a Coplanar Capacitive Array," in IEEE Sensors Journal. doi: 10.1109/JSEN.2019.2935616

[45] McComber, P., De Lafontaine, J., Laflamme, J.N., Druez, J. and Paradis, A., 1998. A neural network system to estimate transmission line icing.

[46] Larouche, E., Rouat, J., Bouchard, G. and Farzaneh, M., "Exploration of Static and Time Dependent Neural Network Technique for the Prediction of Ice Accretion on Overhead Line Conductors". 9th International Workshop on Atmospheric Icing of Structures. Chester, United Kingdom, 2000.session 2, 8.p.

[47] Ohta, H., et al. "Application of Disaster Warning System Due to Snow Accretion on Power Lines Using Neural Networks." Proc. 7th IWAIS, Chicoutimi (1996).

[48] Gantasala, S., Luneno, J.-C., & Aidanpää, J.-O. (2018). Identification of ice mass accumulated on wind turbine blades using its natural frequencies. Wind Engineering, 42(1), 66–84.

[49] Willem Chr. Heerens, *Application of Capacitance Techniques in Sensor Design*, J. Phys. E: Sci. Instrum., 19, 1986 pp.897-906

[50] Gregow, E.; Bernstein, B.; Wittmeyer, I.; Hirvonen, J. LAPS–LOWICE: A Real-Time System for the Assessment of Low-Level Icing Conditions and Their Effect on Wind Power. *J. Atmos. Ocean. Technol.* **2015**, *32*, 1447–1463.

[51] Dehghani-Sanij, A.R.; Dehghani, S.R.; Naterer, G.F.; Muzychka, Y.S. Marine icing phenomena on vessels and offshore structures: Prediction and analysis. *Ocean. Eng.* **2017**, *143*, 1–23.

[52] Elzaidi, A.; Masek, V.; Muzychka, Y. Phase Discrimination in Marine Icing Using a Coplanar Capacitive Array. *IEEE Sens. J.* **2019**, *19*, 11301–11308, doi:10.1109/JSEN.2019.2935616.

[53] Elzaidi, A.; Masek, V.; Bruneau, S. Water and Ice Detection in Marine Icing by Capacitive Sensor Array and the Artificial Neural Network Model. In Proceedings of the 2019 IEEE 10th Annual Information Technology, Electronics and Mobile Communication Conference (IEMCON), Vancouver, BC, Canada, 17–19 October 2019.

[54] Mosavi, A.; Ozturk, P.; Chau, K.-w. Flood prediction using machine learning models: Literature review. *Water* **2018**, *10*, 1536.

[55] Torabi, M.; Mosavi, A.; Ozturk, P.; Varkonyi-Koczy, A.; Istvan, V. A hybrid machine learning approach for daily prediction of solar radiation. In *Recent Advances in Technology Research and Education*; Springer: Cham, Switzerland, 2018; pp. 266–274.

[56] Jiménez, A.A.; Márquez, F.P.G.; Moraleda, V.B.; Muñoz, C.Q.G. Linear and nonlinear features and machine learning for wind turbine blade ice detection and diagnosis. *Renew. Energy* **2019**, *132*, 1034–1048.

[57] Mahmoud, T.; Dong, Z.Y.; Ma, J. An advanced approach for optimal wind power generation prediction intervals by using self-adaptive evolutionary extreme learning machine. *Renew. Energy* **2018**, *126*, 254–269.

[58] Alharbi, S.; Rodriguez, P.; Maharaja, R.; Iyer, P.; Subaschandrabose, N.; Ye, Z. Secure the internet of things with challenge response authentication in fog computing. In Proceedings of the 2017 IEEE 36th International Performance Computing and Communications Conference (IPCCC), San Diego, CA, USA, 10 –12 December 2017.

[59] Vanfretti, L.; Narasimham Arava, V.S. Decision tree-based classification of multiple operating conditions for power system voltage stability assessment. *Int. J. Electr. Power Energy Syst.* **2020**, *123*, 106251.

[60] Phiri, D.; Simwanda, M.; Nyirenda, V.; Murayama, Y.; Ranagalage, M. Decision Tree Algorithms for Developing Rulesets for Object-Based Land Cover Classification. *ISPRS Int. J. Geo-Inf.* **2020**, *9*, 329.

[61] Polat, K.; Güneş, S. Classification of epileptiform EEG using a hybrid system based on decision tree classifier and fast Fourier transform. *Appl. Math. Comput.* **2007**, *187*, 1017–1026.

[62] Knight, C.A. Curved growth of ice on surfaces. *J. Appl. Phys.* **1962**, *33*, 1808–1815.

[63] Texas Instruments, FDC2214 with Two Capacitive Sensors Evaluation Module. Available online: `Http://www.ti.com/tool/FDC2214EVM` (accessed on 23 December 2020).

[64] Song, Y.-Y.; Ying, L.U. Decision tree methods: Applications for classification and prediction. *Shanghai Arch. Psychiatry* **2015**, *27*, 130.

[65] Tan, P.-N.; Steinbach, M.; Kumar, V. *Introduction to Data Mining*; Pearson New International Edition PDF eBook. Pearson Schweiz Ag: London, UK, **2013**, *4*, 145–206.

[66] Han, J.; Pei, J.; Kamber, M. *Data Mining: Concepts and Techniques*; Elsevier: Amsterdam, The Netherlands, **2011**, *8*, 327–392.

[67] Gupta, D.L.; Malviya, A.K.; Singh, S. Performance analysis of classification tree learning algorithms. *Int. J. Comput. Appl.* **2012**, *55*, 39–44.

Appendix A

Appendix: A

A.1 OpenScad Software Equations

```
model Spiral()

r=0.1555;

loops=3;

slope1 =1/603;

slope2 =1/603;

thickness1 =0.1;

thickness2 =0.1;


linear extrude(height=0.1)

polygon(points= concat([for(t = [90:360*loops]) [(r-thickness1+slope1*t)*sin(t) ,

(r-thickness1+slope1*t)*cose(t)]

([for(t = [360*loops:-1:90]) [(r+slope1*t)*sin(t),(r+slope1*t)*cose(t)] )

polygon(points= concat([for(t = [90:360*loops]) [(r-thickness2+slope2*t)*sin(t) ,

(r-thickness2+slope2*t)*cose(t)]

([for(t = [360*loops:-1:90]) [(r+slope2*t)*sin(t),(r+slope2*t)*cose(t)] )
```

A.2 Circuit schematic diagram of the interfacing circuit

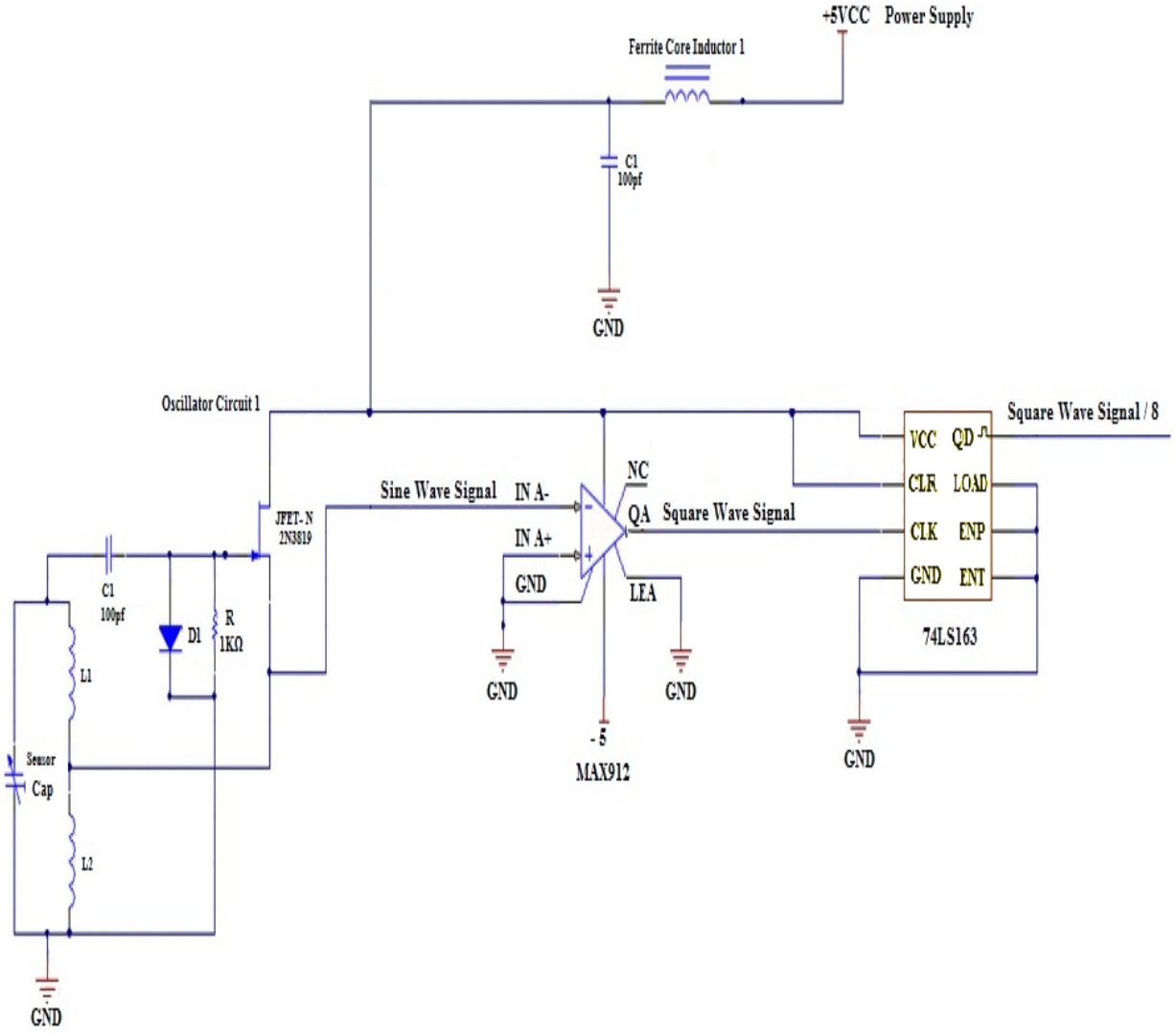

A.3 The four-level decision tree classifier output

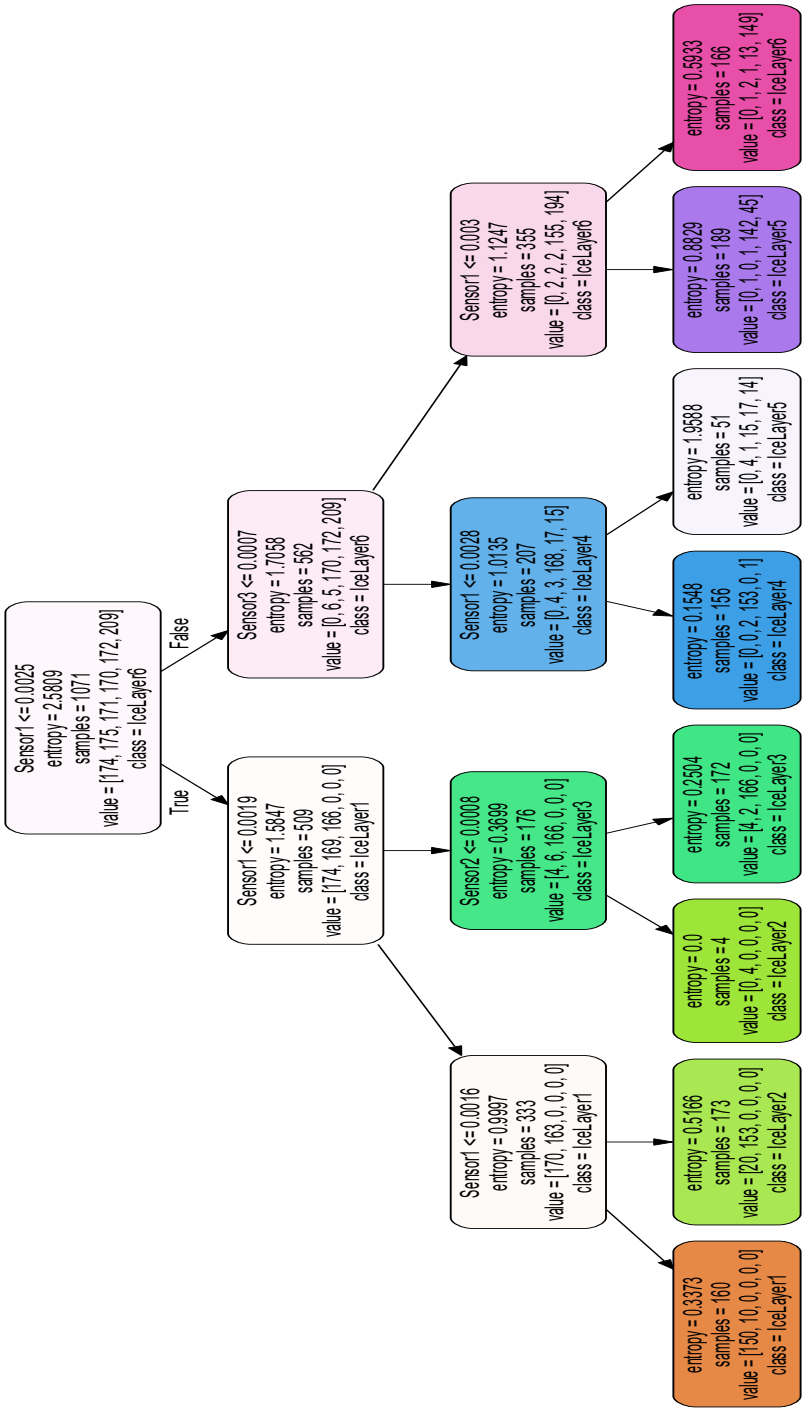

Water and Ice Detection in Marine Icing by Capacitive Sensor Array and the Artificial Neural Network Model with different Activation Functions

Abdulrazak Elzaidi, Vlastimil Masek, Stephen Bruneau
Faculty of Engineering and Applied Science
Memorial University of Newfoundland
St. John's NL A1B3X5, Canada
abdoeziedy@ieee.org, masek@mun.ca, sbruneau@mun.ca

***Abstract*—This work describes a capacitive sensor array for the measurement of marine ice accretion. Currently, all commercial icing detectors only track the ice phase disregarding the water phase. This approach is acceptable in many applications, mostly in the atmospheric icing domain however in the case of marine icing, the water phase creates a significant component of the measurement signal. The water phase cannot be disregarded and requires a novel methodology that takes into account the water-ice conditions simultaneously. A neural network approach is used to implement the signal-to-measurand mapping. Compared to the previous least-squares based mapping, the neural network method is more accurate and therefore becomes a preferred method of signal processing in capacitive array based marine icing sensing.**

***Index Terms*—Marine icing, Capacitive sensors, Coplanar PCB electrodes, Artificial Neural Network (ANN), Capacitance-to-frequency conversion, Multiphase Dielectrics**

I. Introduction

Marine icing monitoring provides the ice accumulation data in on/off-shore applications. Heavy icing conditions can cause severe operational challenges or can lead to severe safety hazards. Our main motivation is to develop a monitoring system which protects workers on vessels or ships [1]. Marine icing forms on a surface when the supercooled water turns into ice before the runoff time elapses. Chokmani [2], Zhi [3], and Ezeoru [4] developed a marine icing accretion monitoring system based on single phase assumption. Similarly, Sommer Messtechnik [5] is based on ice phase monitoring alone. Neumayer [6] and this work is focused on ice-water composition with a difference in the arrangement of the capacitive sensors.

Coplanar capacitive sensors are surface electrode structures which can be easily manufactured using a printed circuit board technology. Capacitive touch sensors replacing mechanical push buttons commonly used these days often employ this technology. The capacitance can be detected by numerous methods, however capacitance to time or frequency conversion gains wide popularity due to its digital nature and simple interface. Time or frequency signals are also less prone to interference. Neumayer [6] utilizes a capacitive array of constant spacing characteristics and applies Computer Tomography algorithm to detect the multiphase domains. In our research, we utilize an array of capacitive elements of varying spacing dimension, the inter-electrode gap. Each element features a different depth of 'penetration' and in the combination, the system provides linearly independent signals that can uniquely encode the ice accretion and water layer depth.

II. Experimental Platform

Our previous work [11] describes the experimental platform in more detail. Figure 1 & Figure 2 show the capacitive elements of varying spacing (3.5 mm, 3 mm, 2.5 mm, 2 mm, 1 mm, and 0.5 mm). A thin layer of insulation was also deposited on top of the PCB to insulate the electrodes from the external environment. This is a common practice in capacitance sensors to prevent the conductance to influence the measurement unless it is the part of the measurement method.

Hartley oscillator is used to detect the capacitance of each element. A comparator MAX 912 is used to convert the harmonic sine wave signals generated from the oscillator to square wave signals and consequently a counter 74LS163 divides the frequency 8x.

Prior to the experiment, the PCB was leveled in a deep cooler at $-20°C$. We used a paint roller to deposit a water layer over the PCB. A wet roller was rolled over the sensor plane in three runs separated by a few minutes each as shown in the data plot below. We assumed the entire PCB surface experiencing the same conditions and that each wetting cycle deposited an equal layer of water.

III. Signal Processing

Consistent water layers were created using a wet paint roller, and three wet cycles were applied across the sensor array PCB surface. The measured frequencies are shown in Figure 3. The plotted frequencies differed in a constant term as well as amplitude. Here the constant term corresponds to the case when no ice nor water is present, the initial condition.

While maintaining their linear independence, we normalized the acquired frequencies by the constant (initial) term in order to present them in one graph for comparative reasons. Figure 3 includes data for four elements with a slightly differnt duration

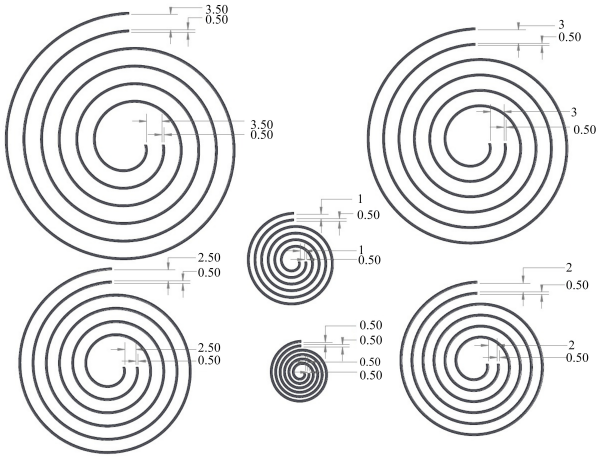

Fig. 1. Design of coplanar spiral electrodes of different air-gap spacing

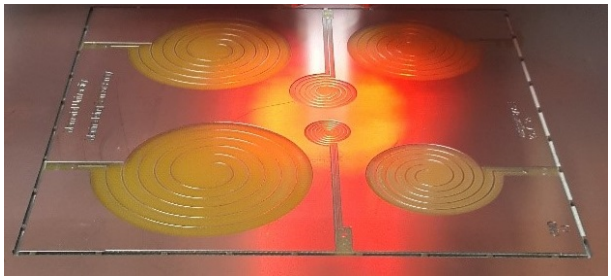

Fig. 2. Capacitive Sensor Array

of each wetting cycle. The cycles are getting shorter as thermal inertia of the built up ice is growing.

The frequency data were sampled at a rate of two samples per second using a DAQ card and Matlab was used to filter the noise off-line by Butterworth filter, Figure 4. Figure 5 shows the filtered data shifted back by 40 samples to align the characteristics with each wetting cycle instead of delaying the ice and water profiles by the filter's delay.

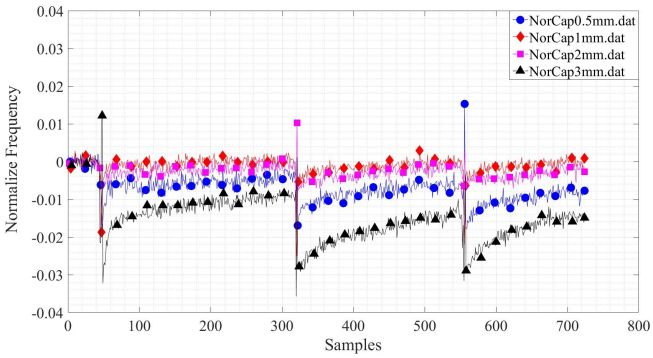

Fig. 3. Normalize Frequencies from Four Oscillators

Again we assume that each wetting cycle creates a uniform water film layer over the PCB. Figure 6 illustrates this assumption in a time profile for water and ice accretion. The profiles

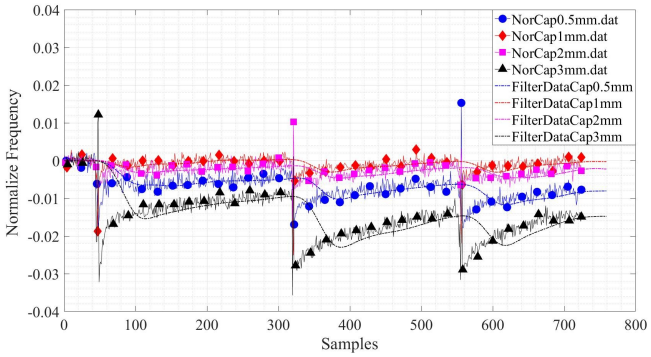

Fig. 4. Filter Data and Normalized Data for 0.5, 1.0, 2.0, and 3.0-mm Gap Sensors

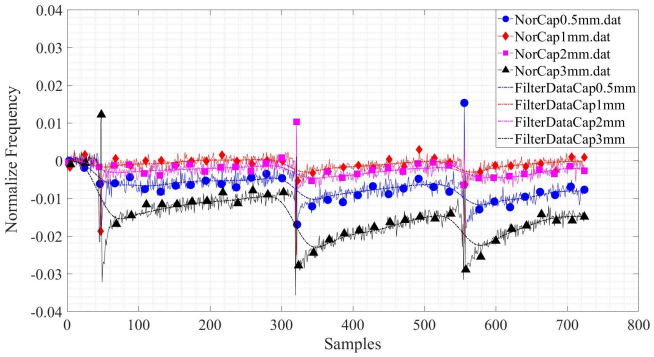

Fig. 5. Removed Delay Shift from Filter Data

are piecewise linear and their amplitude is not a concern in this study. In order to also determine the amplitudes, a more complex sensor calibration setup would be necessary where ice a water layer has to be measured accurately.

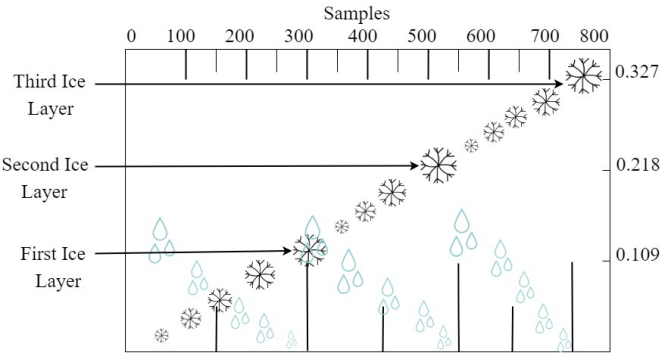

Fig. 6. Main Idea for the Model of Ice and Water Experiment Data

IV. Neural Network Mapping

Our previous work confirmed that an array of coplanar sensors of various spacing parameters has the ability to determine the ice phase and water phase individually. In this work we utilized an artificial neural network (ANN) to map the frequencies input to the ice accretion and water layer depth

output. This is a novel method also used in other studies by McComber [7], Larouche et al [8], and Ohta [9]. For example ANN was used to predict the icing condition based on the temperature, wind speed, and precipitation rate. Gantasala [10] used two parameter frequencies and wind speeds to determine ice mass through the ANN.

In this research, capacitive sensor frequencies were used as input and the water-ice profile as output. Input-Output training data set was then created across 740 time samples. Figure 7 shows the architecture of the used ANN model, which has four neurons in the input layer for the four frequencies, twenty neurons in the hidden layer and two neurons in the output layer for ice and water.

The ANN processes the input information in the following manner:

$$\begin{aligned}\mathbf{h_1} &= f1 * Wi1_1 + f2 * Wi2_1 + f3 * Wi3_1 \\ &\quad + f4 * Wi4_1 + Bi_1 \\ &\vdots \\ \mathbf{h_{20}} &= f1 * Wi1_{20} + f2 * Wi2_{20} + f3 * Wi3_{20} \\ &\quad + f4 * Wi4_{20} + Bi_{20} \\ \mathbf{h_n} &= f1 * Wi1_n + f2 * Wi2_n + f3 * Wi3_n + \\ &\quad f4 * Wi4_n + Bi_n \end{aligned} \tag{1}$$

Wi, ***Wo***, ***Bi***, and ***Bo*** represent input weights, output weights, input biases, and output biases respectively.

Initially, we applied the "Pure linear" activation function (Eq.5). As can be seen in Figure 8, the resulting characteristics for ice and water suffer from a large deviation from the expected characteristics. To overcome this limitation, we consequently tested two non-linear functions "Log-sigmoid" function (Eq.6) and the "tangent sigmoid" function (Eq.7). Figure 9 which corresponds to the "Log-sigmoid" activation function results in a nearly perfect match with the expected characteristics. Figure 10 resulting from the "tangent sigmoid" activation function also closely represents the ideal characteristics, however not as close as the Figure 9 case of the "Log-sigmoid" function.

$$\begin{aligned}\mathbf{O_{Water}} &= (h_1 * Wo1_1) + (h_2 * Wo2_1) \\ &\quad + ... + (h_{20} * Wo20_1) + Bo_1 \end{aligned} \tag{2}$$

$$\begin{aligned}\mathbf{O_{Ice}} &= (h_1 * Wo1_2) + (h_2 * Wo2_2) \\ &\quad + ... + (h_{20} * Wo20_2) + Bo_2 \end{aligned} \tag{3}$$

$$\mathbf{O_j} = \sum_{j=1}^{2}\sum_{k=1}^{20}[[h_k * Wok_j] + Bo_j] \tag{4}$$

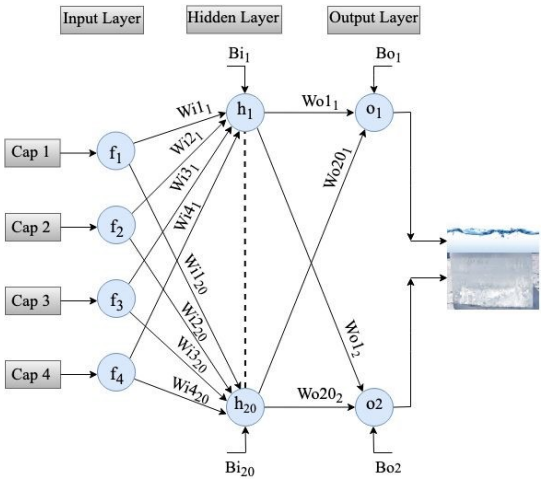

Fig. 7. Neural Network Prediction Model

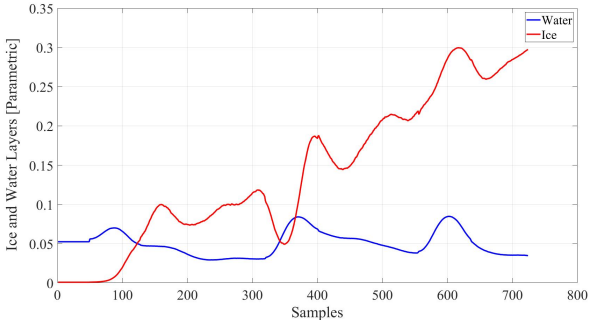

Fig. 8. Ice & Water layers Predicted by the ANN Model [Linear transfer function]

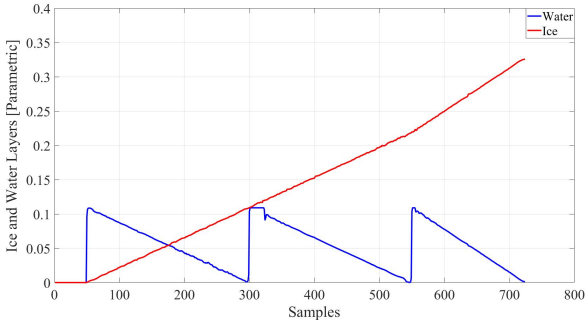

Fig. 9. Ice & water Layers Predicted by the ANN Model [Log-sigmoid transfer function]

Figures 9 & 10 show that the results from the ANN signal processing. Comparing these result to [11] shown in in Figure 11 without any detailed error analysis, one can observe the superiority of ANN algorithm over the least squares method in [11]. The nonlinear nature of Log-sigmoid neuron firing function in combination with the constant biases occurs to be a better fit to process the signals from linearly independent frequency data. Therefore we propose to use ANN over the least squares.

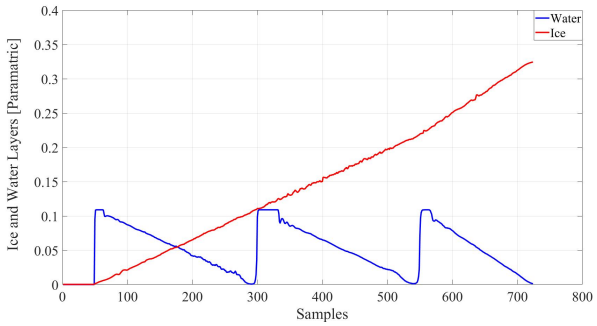

Fig. 10. Ice & Water layers Predicted by the ANN Model [Hyperbolic tangent sigmoid transfer function]

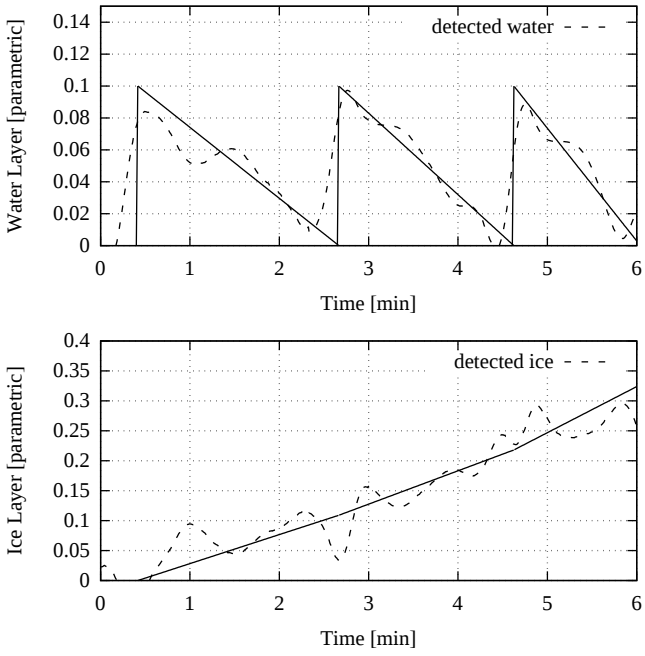

Fig. 11. Water and Ice Levels Predicted by Least-Squares method in [11]

the activation functions expressed as following:

$$\text{PureLin} \quad \mathbf{F}(n) = n \tag{5}$$

$$\text{LogSig} \quad \mathbf{F}(n) = \frac{1}{1 + exp(-n)} \tag{6}$$

$$\text{TanSig} \quad \mathbf{F}(n) = \frac{2}{1 + exp(-2n)} - 1 \tag{7}$$

V. Conclusion

Our previous research revealed that an array of coplanar capacitive sensors on a PCB surface can detect the ice accretion rate in presence of a significant water layer. This work followed up in the research and proposed using an artificial neural network for signal processing instead of previously used least-squares method. We adopted a three layer ANN to process frequencies from four sensors, previously normalized and low pass filtered. As a result, the accuracy of ANN derived ice accretion and water layer is superior to the least squares method. However more work is needed to validate the method's robustness under a presence of signal drifting or a low frequency noise.

Acknowledgment

The authors would like to gratefully thank the Libyan Ministry of Education for providing a postgraduate fellowship to the first author.

References

[1] Taimur Rashid, Hassan Abbas Khawaja & Kåre Edvardsen (2016) Review of marine icing and anti-/de-icing systems, Journal of Marine Engineering & Technology, 15:2, 79-87, DOI: 10.1080/20464177.2016.1216734

[2] Chokmani K, Khalil B, Ouarda TB, Bourdages R. Estimation of river ice thickness using artificial neural networks. InProc. 14th Workshop Hydraulics Ice Covered Rivers. CGU HS/CRIPE 2007 (p. 12).

[3] X. Zhi, H. C. Cho, B. Wang, C. H. Ahn, H. S. Moon, and J. S. Go, "Development of a capacitive ice sensor to measure ice growth in real time," Sensors, vol. 15, pp. 6688–6698, Mar. 2015.

[4] C. Ezeoru, "Marine icing sensor design using capacitive techniques," M.S. thesis, Memorial Univ. Newfoundland, St. John's, NL, Canada, Aug. 2016. Accessed: 03-Oct-2019.

[5] IDS-20 Product Information, SOMMER Messtechnik, Koblach, Austria,Nov. 2016. Accessed: 03-Oct-2019.

[6] M. Neumayer, T. Bretterklieber, and M. Flatscher, "Signal processing for capacitive ice sensing: Electrode topology and algorithm design," IEEE Trans. Instrum. Meas., vol. 68, no. 5, pp. 1458–1466, May 2019

[7] McComber, P., De Lafontaine, J., Laflamme, J.N., Druez, J. and Paradis, A., 1998. A neural network system to estimate transmission line icing.

[8] Larouche, E., Rouat, J., Bouchard, G. and Farzaneh, M., "Exploration of Static and Time Dependent Neural Network Technique for the Prediction of Ice Accretion on Overhead Line Conductors". 9th International Workshop on Atmospheric Icing of Structures. Chester, United Kingdom, 2000.session 2, 8.p.

[9] Ohta, H., et al. "Application of Disaster Warning System Due to Snow Accretion on Power Lines Using Neural Networks." Proc. 7th IWAIS, Chicoutimi (1996).

[10] Gantasala, S., Luneno, J.-C., & Aidanpää, J.-O. (2018). Identification of ice mass accumulated on wind turbine blades using its natural frequencies. Wind Engineering, 42(1), 66–84.

[11] A. Elzaidi, V. Masek and Y. Muzychka, "Phase Discrimination in Marine Icing Using a Coplanar Capacitive Array," in IEEE Sensors Journal. doi: 10.1109/JSEN.2019.2935616

Appendix B

Appendix: B

FDC2114 and FDC2214 EVM User's Guide

1 Overview

The FDC2114/2214 EVM demonstrates the use of capacitive sensing technology to sense and measure the presence or position of target objects. The EVM contains two example LC tank sensors that are connected to the FDC2114/2214 input channels. The latter is controlled by an MSP430, which interfaces to a host computer.

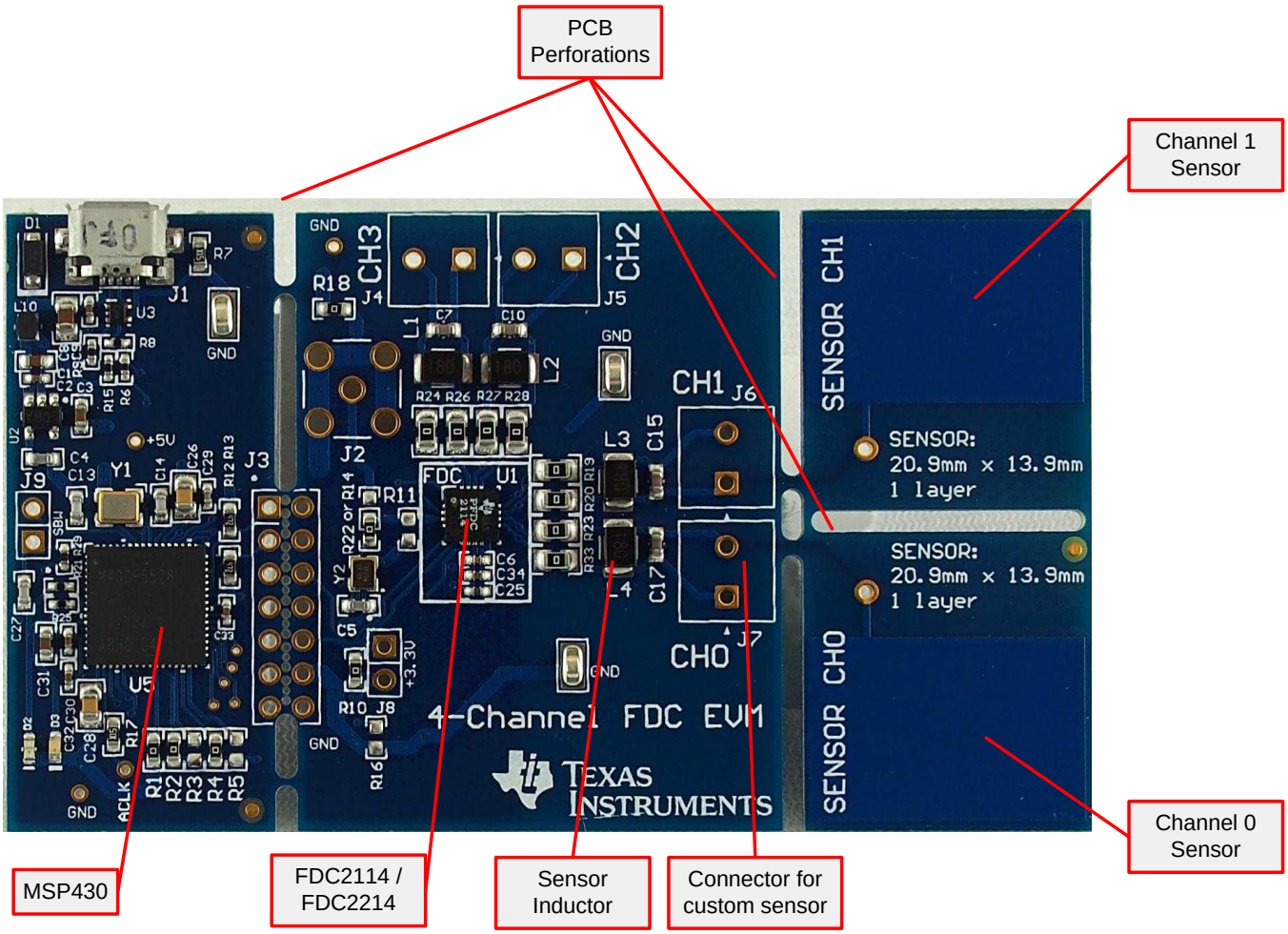

Figure 1. FDC2114/2214 Evaluation Module

The FDC2114/2214EVM includes two example PCB sensors. Each sensor consists of a single-layer capacitor plate, a 33pF 1% COG/NP0 capacitor, and a 18µH connected in parallel to form an LC tank.

PCB perforations allow separation of the sensor coils or the microcontroller, so that custom sensors or a different microcontroller can be connected.

2 Sensing Solutions EVM GUI

The Sensing Solutions EVM GUI provides direct device register access, user-friendly configuration, and data streaming.

2.1 System Requirements

The host machine is required for device configuration and data streaming. The following steps are necessary to prepare the EVM for the GUI:

- The GUI and EVM driver must be installed on a host computer
- - The EVM must be connected to a full speed USB port (USB 1.0 or above)

The Sensing Solutions EVM GUI supports the following operating systems (both 32-bit and 64-bit):

- Windows XP
- Windows 7
- Windows 8 and 8.1
- Windows 10

2.2 Installation Instructions

The Sensing Solutions GUI and EVM driver installer is packaged in a zip file. Follow these steps to install the software:

1. Download the software ZIP file from the EVM tool page
2. Extract the downloaded ZIP file
3. Run the included executable
4. If prompted by the User Account Control about making changes to the computer, click "Yes"

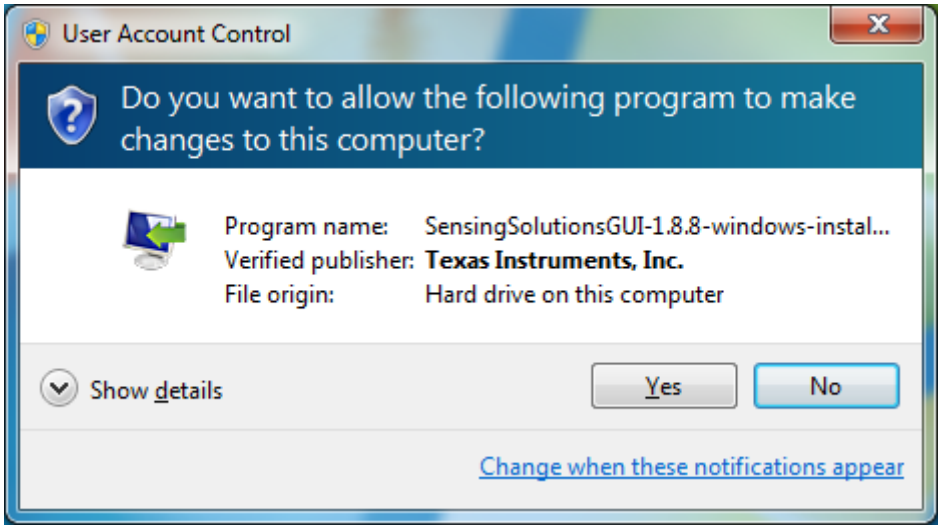

Figure 2. User Account Control Prompt

3 FDC2114/2214 EVM Schematics and Layout

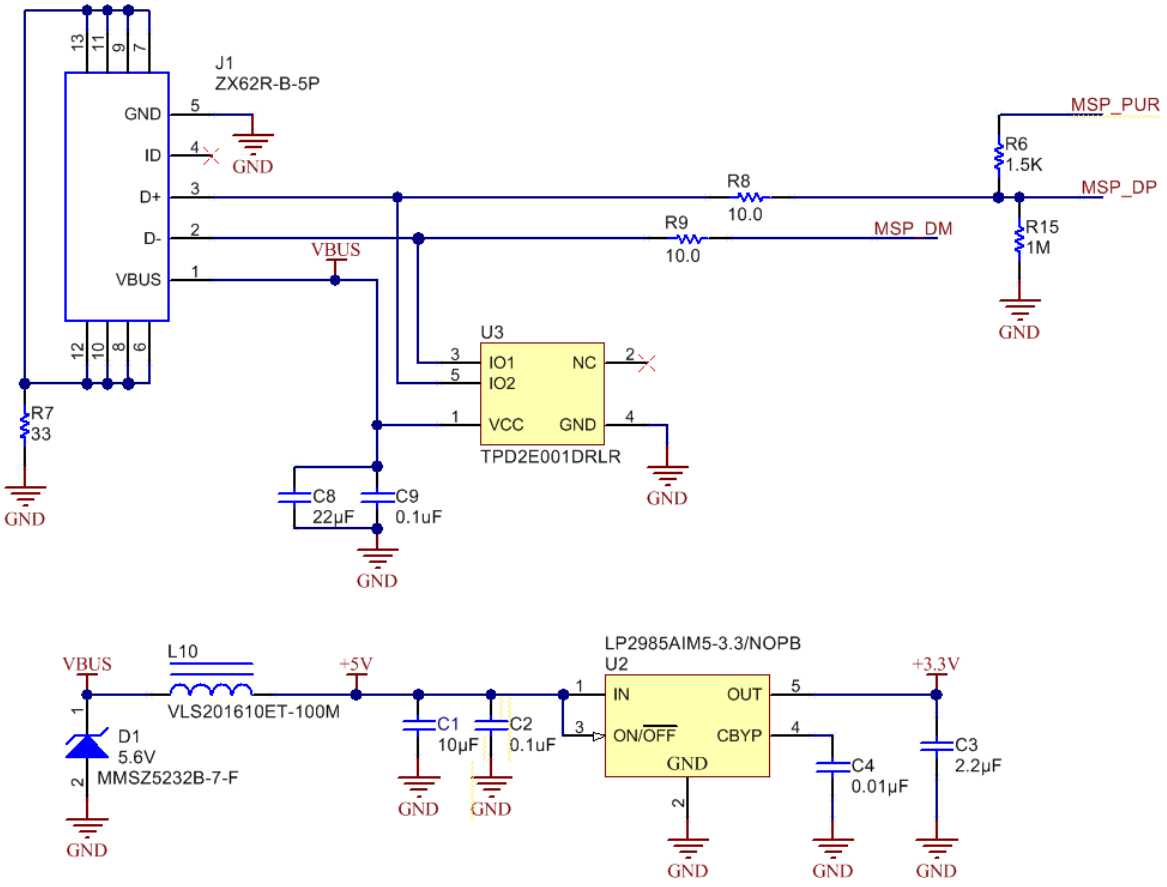

Figure 43. USB Connection and Power Circuit

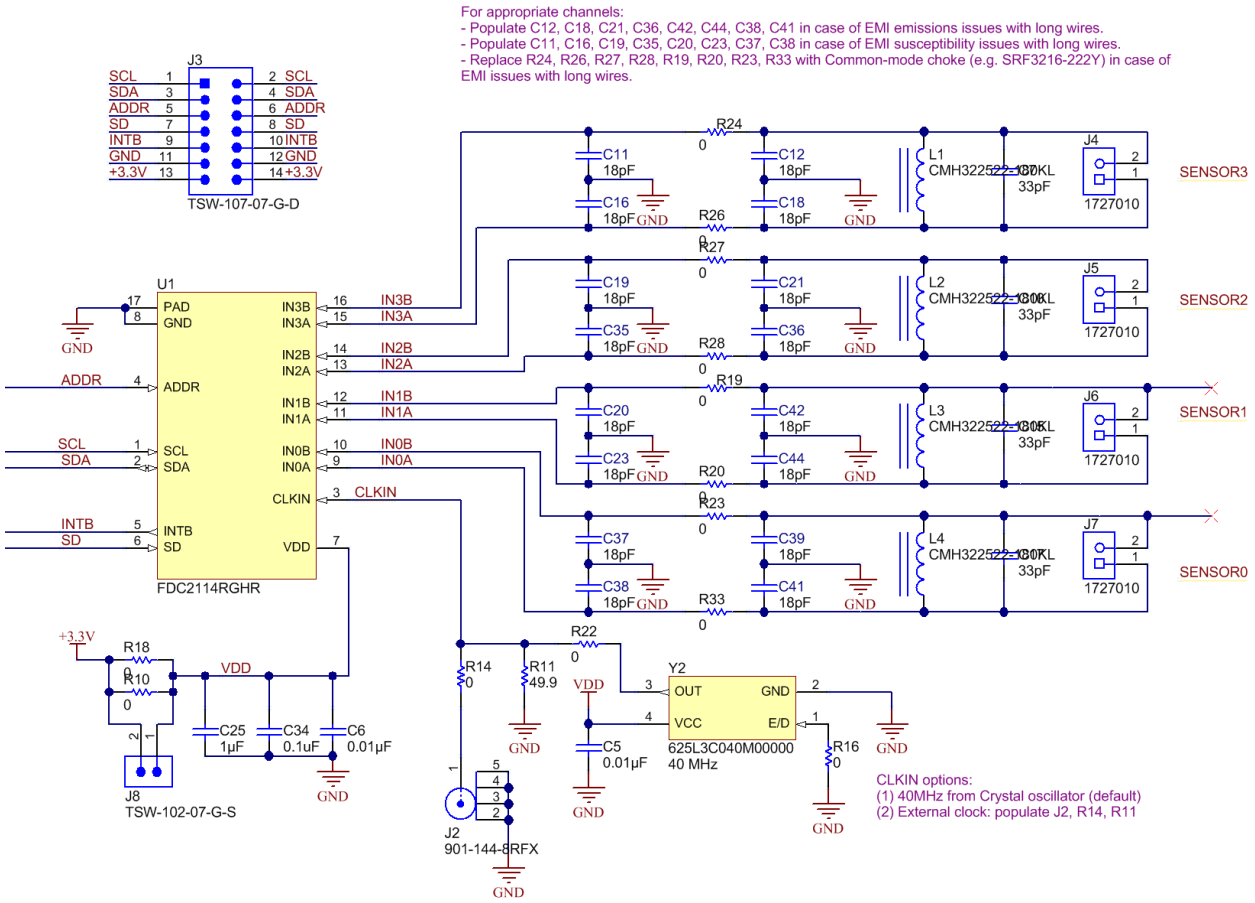

Figure 44. FDC2114/2214

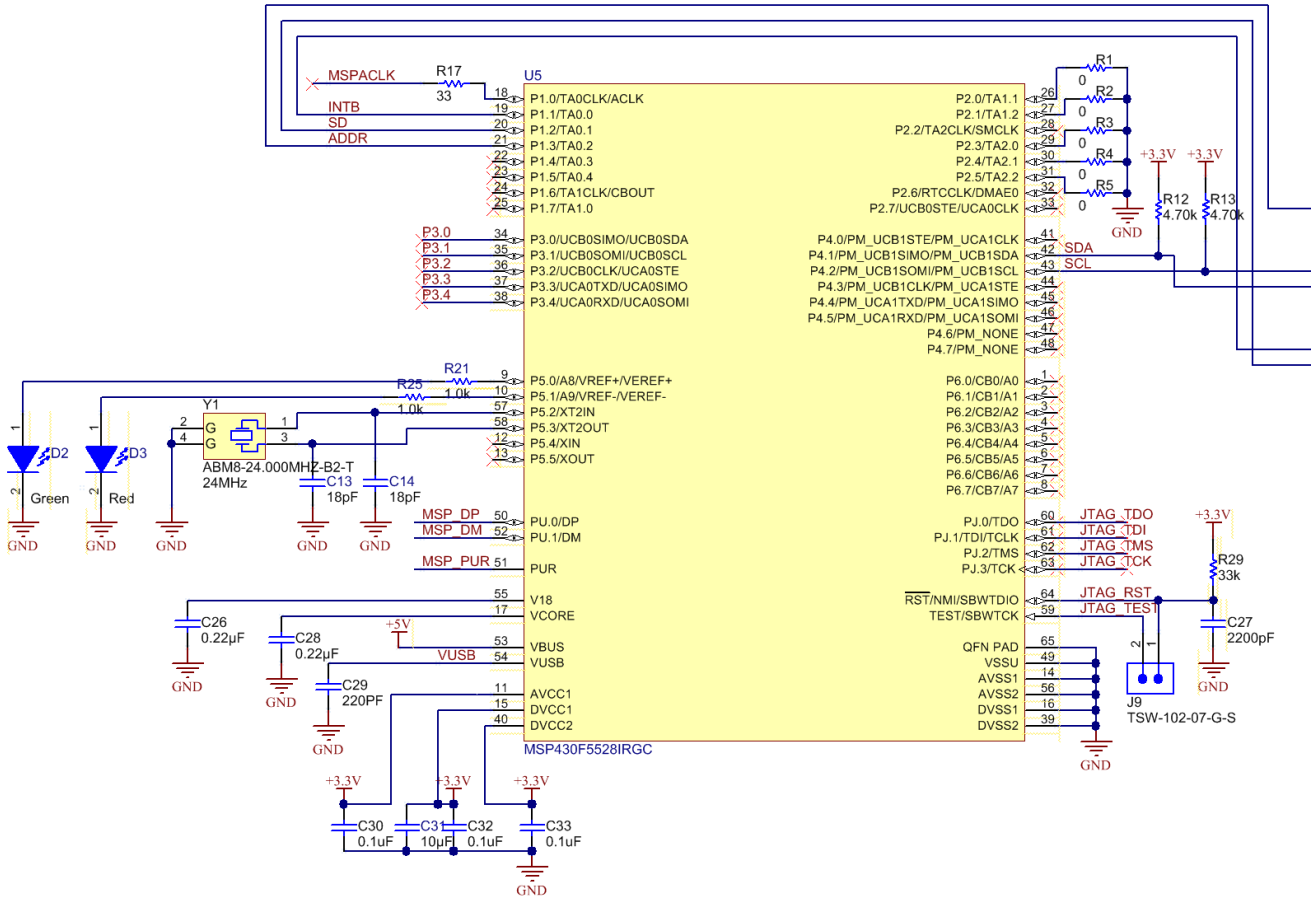

Figure 45. MSP430 Connections

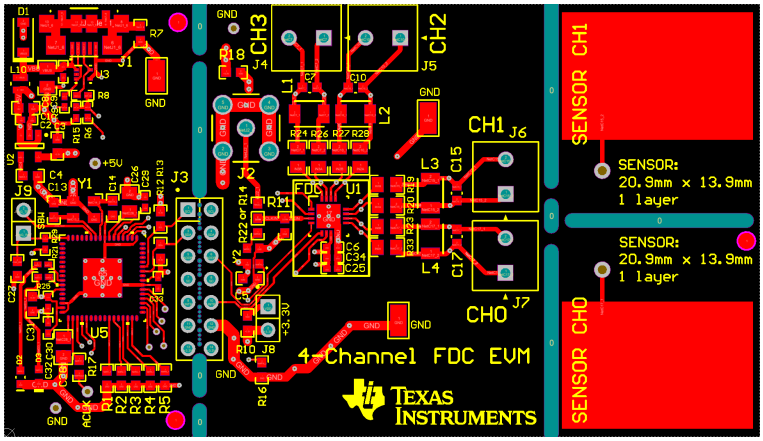

Figure 46. Layout Top Layer – Signals and Components

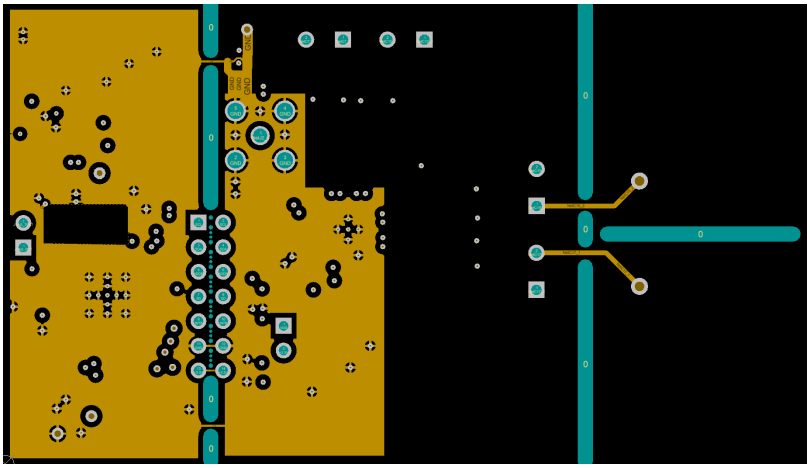

Figure 47. Layout Mid-Layer 1 – Ground Plane

Appendix C

Appendix: C

19-0157; Rev 2; 8/03

MAXIM

Single/Dual, Ultra-Fast, Low-Power Precision TTL Comparators

General Description

The MAX913 single and MAX912 dual, high-speed, low-power comparators have differential inputs and complementary TTL outputs. Fast propagation delay (10ns, typ), extremely low supply current, and a wide common-mode input range that includes the negative rail make the MAX912/MAX913 ideal for low-power, high-speed, single +5V (or ±5V) applications such as V/F converters or switching regulators.

The MAX912/MAX913 outputs remain stable through the linear region. This feature eliminates output instability common to high-speed comparators when driven with a slow-moving input signal.

The MAX912/MAX913 can be powered from a single +5V supply or a ±5V split supply. The MAX913 is an improved plug-in replacement for the LT1016. It provides significantly wider input voltage range and equivalent speed at a fraction of the power. The MAX912 dual comparator has equal performance to the MAX913 and includes independent latch controls.

Applications

Zero-Crossing Detectors

Ethernet Line Receivers

Switching Regulators

High-Speed Sampling Circuits

High-Speed Triggers

Extended Range V/F Converters

Fast Pulse Width/Height Discriminators

Features

- **Ultra Fast (10ns)**
- **Single +5V or Dual ±5V Supply Operation**
- **Input Range Extends Below Negative Supply**
- **Low Power: 6mA (+5V) Per Comparator**
- **No Minimum Input Signal Slew-Rate Requirement**
- **No Power-Supply Current Spiking**
- **Stable in the Linear Region**
- **Inputs Can Exceed Either Supply**
- **Low Offset Voltage: 0.8mV**
- **Now Available in a Small µMAX Package**

Ordering Information

PART	TEMP RANGE	PIN-PACKAGE
MAX912CPE	0°C to +70°C	16 Plastic DIP
MAX912CSE	0°C to +70°C	16 Narrow SO
MAX912EPE	-40°C to +85°C	16 Plastic DIP
MAX912ESE	-40°C to +85°C	16 Narrow SO
MAX913CPA	0°C to +70°C	8 Plastic DIP
MAX913CSA	0°C to +70°C	8 SO
MAX913EPA	-40°C to +85°C	8 Plastic DIP
MAX913ESA	-40°C to +85°C	8 SO
MAX913EUA	-40°C to +85°C	8 µMAX

Pin Configurations

TOP VIEW

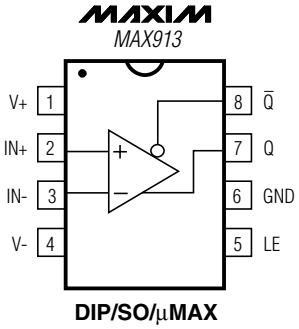

DIP/SO/µMAX

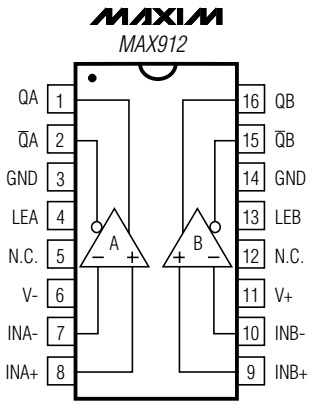

DIP/NARROW SO

Single/Dual, Ultra-Fast, Low-Power Precision TTL Comparators

ABSOLUTE MAXIMUM RATINGS

Positive Supply Voltage .....+7V
Negative Supply Voltage .....-7V
V+ to V- .....+13V
Differential Input Voltage .....+15V
Input Voltage (Referred to V-) .....-0.3V to +14V
Latch Pin Voltage .....Equal to Supplies
Continuous Output Current.....±20mA
Continuous Power Dissipation (T_A = +70°C)
8-Pin Plastic DIP (derate 9.09mW/°C above +70°C) ...727mW
8-Pin SO (derate 5.88mW/°C above +70°C).....471mW
8-Pin µMAX (derate 4.5mW/°C above +70°C) 362mW
16-Pin Plastic DIP (derate 10.53mW/°C above +70°C)842mW
16-Pin Narrow SO (derate 8.70mW/°C above +70°C) .696mW
Operating Temperature Ranges:
MAX91_C_ _ .....0°C to +70°C
MAX91_E_ _.....-40°C to +85°C
Storage Temperature Range .....-65°C to +150°C
Lead Temperature (soldering, 10s) .....+300°C

Stresses beyond those listed under "Absolute Maximum Ratings" may cause permanent damage to the device. These are stress ratings only, and functional operation of the device at these or any other conditions beyond those indicated in the operational sections of the specifications is not implied. Exposure to absolute maximum rating conditions for extended periods may affect device reliability.

ELECTRICAL CHARACTERISTICS

V+ = +5V, V- = -5V, V_Q = 1.4V, V_{LE} = 0V, T_A = T_{MIN} to T_{MAX}, unless otherwise noted. Typical values are at T_A = +25°C.) (Note 1)

PARAMETER	SYMBOL	CONDITIONS		MIN	TYP	MAX	UNITS
Input Offset Voltage (Note 2)	V_{OS}	$R_S \le 100\Omega$	T_A = +25°C		0.1	2	mV
			$T_A = T_{MIN\ TO}\ T_{MAX}$			3	
Offset Drift	TCV_{OS}				2		µV/°C
Input Offset Current (Note 2)	I_{OS}	T_A = +25°C			0.3	0.5	µA
		$T_A = T_{MIN\ TO}\ T_{MAX}$				1	
Input Bias Current	I_B	T_A = +25°C			2	5	µA
		C, E temperature ranges				8	
Input Voltage Range	V_{CM}	C, E temperature ranges		-5.2		+3.5	V
		Single +5V	C, E temperature ranges	-0.2		+3.5	
Common-Mode Rejection Ratio	CMRR	-5.0V ≤ V_{CM} ≤ +3.5V		80	110		dB
Power-Supply Rejection Ratio	PSRR	Positive supply; 4.5V ≤ V+ ≤ 5.5V		60	85		dB
		Negative supply; -2V ≥ V- ≥ -7V		80	100		
Small-Signal Voltage Gain	A_V	1V ≤ V_Q ≤ 2V, T_A = +25°C		1500	3500		V/V
Output Voltage	V_{OH}	V+ ≥ 4.5V	I_{OUT} = 1mA	2.7	3.4		V
			I_{OUT} = 10mA	2.4	3.0		
	V_{OL}	I_{SINK} = 4mA			0.3	0.5	
		T_A = +25°C, I_{SINK} = 10mA			0.4		
Positive Supply Current Per Comparator (Note 3)	I+	C, E temperature ranges			6	10	mA
Negative Supply Current Per Comparator (Note 3)	I-				1	2	mA
Latch-Pin High Input Voltage	V_{IH}			2.0			V
Latch-Pin Low Input Voltage	V_{IL}					0.8	V
Latch-Pin Current	I_{IL}	V_{LE} = 0V			-1	-20	µA

MOTOROLA

BCD DECADE COUNTERS/ 4-BIT BINARY COUNTERS

SN54/74LS160A
SN54/74LS161A
SN54/74LS162A
SN54/74LS163A

BCD DECADE COUNTERS/ 4-BIT BINARY COUNTERS

LOW POWER SCHOTTKY

The LS160A/161A/162A/163A are high-speed 4-bit synchronous counters. They are edge-triggered, synchronously presettable, and cascadable MSI building blocks for counting, memory addressing, frequency division and other applications. The LS160A and LS162A count modulo 10 (BCD). The LS161A and LS163A count modulo 16 (binary.)

The LS160A and LS161A have an asynchronous Master Reset (Clear) input that overrides, and is independent of, the clock and all other control inputs. The LS162A and LS163A have a Synchronous Reset (Clear) input that overrides all other control inputs, but is active only during the rising clock edge.

	BCD (Modulo 10)	Binary (Modulo 16)
Asynchronous Reset	LS160A	LS161A
Synchronous Reset	LS162A	LS163A

- Synchronous Counting and Loading
- Two Count Enable Inputs for High Speed Synchronous Expansion
- Terminal Count Fully Decoded
- Edge-Triggered Operation
- Typical Count Rate of 35 MHz
- ESD > 3500 Volts

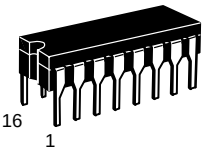
16
1

J SUFFIX
CERAMIC
CASE 620-09

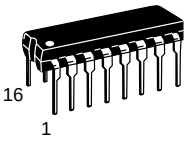
16
1

N SUFFIX
PLASTIC
CASE 648-08

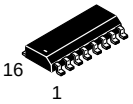
16
1

D SUFFIX
SOIC
CASE 751B-03

ORDERING INFORMATION

SN54LSXXXJ	Ceramic
SN74LSXXXN	Plastic
SN74LSXXXD	SOIC

CONNECTION DIAGRAM DIP (TOP VIEW)

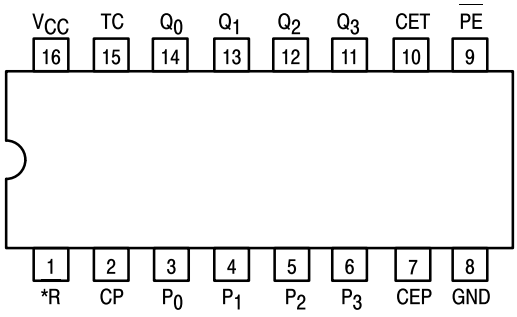

NOTE:
The Flatpak version has the same pinouts (Connection Diagram) as the Dual In-Line Package.

*MR for LS160A and LS161A
*SR for LS162A and LS163A

PIN NAMES

		LOADING (Note a) HIGH	LOW
$\overline{PE}$	Parallel Enable (Active LOW) Input	1.0 U.L.	0.5 U.L.
P_0-P_3	Parallel Inputs	0.5 U.L.	0.25 U.L.
CEP	Count Enable Parallel Input	0.5 U.L.	0.25 U.L.
CET	Count Enable Trickle Input	1.0 U.L.	0.5 U.L.
CP	Clock (Active HIGH Going Edge) Input	0.5 U.L.	0.25 U.L.
MR	Master Reset (Active LOW) Input	0.5 U.L.	0.25 U.L.
SR	Synchronous Reset (Active LOW) Input	1.0 U.L.	0.5 U.L.
Q_0-Q_3	Parallel Outputs (Note b)	10 U.L.	5 (2.5) U.L.
TC	Terminal Count Output (Note b)	10 U.L.	5 (2.5) U.L.

NOTES:
a) 1 TTL Unit Load (U.L.) = 40 μA HIGH/1.6 mA LOW.
b) The Output LOW drive factor is 2.5 U.L. for Military (54) and 5 U.L. for Commercial (74) Temperature Ranges.

LOGIC SYMBOL

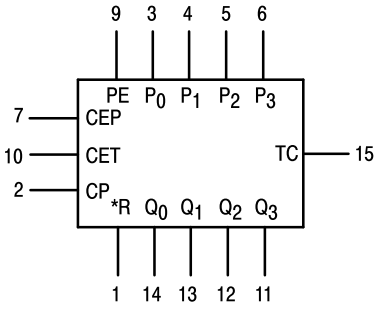

V_{CC} = PIN 16
GND = PIN 8

*MR for LS160A and LS161A
*SR for LS162A and LS163A

STATE DIAGRAM

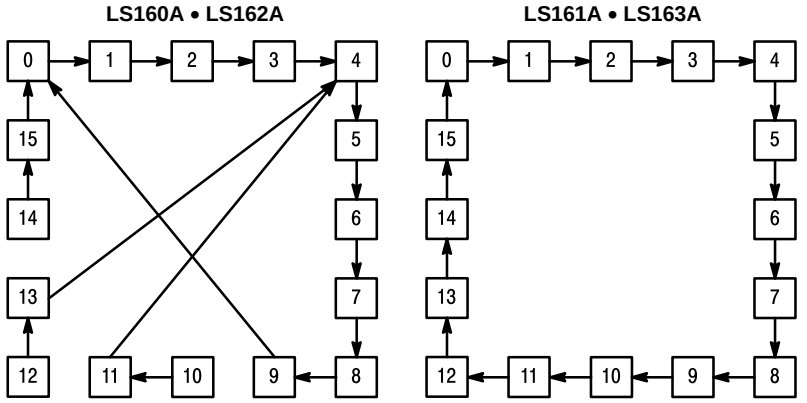

LOGIC EQUATIONS

Count Enable = CEP • CET • PE

TC for LS160A & LS162A = CET • Q_0 • $\overline{Q_1}$ • $\overline{Q_2}$ • $\overline{Q_3}$

TC for LS161A & LS163A = CET • Q_0 • $\overline{Q_1}$ • $\overline{Q_2}$ • $\overline{Q_3}$

Preset = $\overline{PE}$ • CP + (rising clock edge)

Reset = $\overline{MR}$ (LS160A & LS161A)

Reset = SR • CP + (rising clock edge)
(LS162A & LS163A)

NOTE:
The LS160A and LS162A can be preset to any state, but will not count beyond 9. If preset to state 10, 11, 12, 13, 14, or 15, it will return to its normal sequence within two clock pulses.

FUNCTIONAL DESCRIPTION

The LS160A/161A/162A/163A are 4-bit synchronous counters with a synchronous Parallel Enable (Load) feature. The counters consist of four edge-triggered D flip-flops with the appropriate data routing networks feeding the D inputs. All changes of the Q outputs (except due to the asynchronous Master Reset in the LS160A and LS161A) occur as a result of, and synchronous with, the LOW to HIGH transition of the Clock input (CP). As long as the set-up time requirements are met, there are no special timing or activity constraints on any of the mode control or data inputs.

Three control inputs — Parallel Enable ($\overline{PE}$), Count Enable Parallel (CEP) and Count Enable Trickle (CET) — select the mode of operation as shown in the tables below. The Count Mode is enabled when the CEP, CET, and PE inputs are HIGH. When the PE is LOW, the counters will synchronously load the data from the parallel inputs into the flip-flops on the LOW to HIGH transition of the clock. Either the CEP or CET can be used to inhibit the count sequence. With the PE held HIGH, a LOW on either the CEP or CET inputs at least one set-up time prior to the LOW to HIGH clock transition will cause the existing output states to be retained. The AND feature of the two Count Enable inputs (CET • CEP) allows synchronous cascading without external gating and without delay accumulation over any practical number of bits or digits.

The Terminal Count (TC) output is HIGH when the Count Enable Trickle (CET) input is HIGH while the counter is in its maximum count state (HLLH for the BCD counters, HHHH for the Binary counters). Note that TC is fully decoded and will, therefore, be HIGH only for one count state.

The LS160A and LS162A count modulo 10 following a binary coded decimal (BCD) sequence. They generate a TC output when the CET input is HIGH while the counter is in state 9 (HLLH). From this state they increment to state 0 (LLLL). If loaded with a code in excess of 9 they return to their legitimate sequence within two counts, as explained in the state diagram. States 10 through 15 do *not* generate a TC output.

The LS161A and LS163A count modulo 16 following a binary sequence. They generate a TC when the CET input is HIGH while the counter is in state 15 (HHHH). From this state they increment to state 0 (LLLL).

The Master Reset ($\overline{MR}$) of the LS160A and LS161A is asynchronous. When the MR is LOW, it overrides all other input conditions and sets the outputs LOW. The MR pin should never be left open. If not used, the MR pin should be tied through a resistor to V_{CC}, or to a gate output which is permanently set to a HIGH logic level.

The active LOW Synchronous Reset ($\overline{SR}$) input of the LS162A and LS163A acts as an edge-triggered control input, overriding CET, CEP and PE, and resetting the four counter flip-flops on the LOW to HIGH transition of the clock. This simplifies the design from race-free logic controlled reset circuits, e.g., to reset the counter synchronously after reaching a predetermined value.

MODE SELECT TABLE

*SR	PE	CET	CEP	Action on the Rising Clock Edge (⌐)
L	X	X	X	RESET (Clear)
H	L	X	X	LOAD (P_n Q_n)
H	H	H	H	COUNT (Increment)
H	H	L	X	NO CHANGE (Hold)
H	H	X	L	NO CHANGE (Hold)

*For the LS162A and LS163A only.

H = HIGH Voltage Level
L = LOW Voltage Level
X = Don't Care